Flexible neural probes with a fast bioresorbable shuttle : From in vitro to in vivo electrophysiological recordings

Jolien Pas

N°d'ordre NNT : 2017LYSEM040

THESE de DOCTORAT DE L'UNIVERSITE DE LYON

opérée au sein de

l'Ecole des Mines de Saint-Etienne

Ecole Doctorale N° 488

Sciences, Ingénierie, Santé

Spécialité de doctorat : Microélectronique

Discipline : Bioelectronique

Soutenue publiquement/à huis clos le 11/12/2017, par :

Jolien Pas

Flexible neural probes with a fast bioresorbable shuttle

From in vitro to in vivo electrophysiological recordings

Devant le jury composé de :

Lang, Jochen	Professeur	Université de Bordeaux	Président du Jury et Reporteur
Green, Rylie	Professeur associé	L'imperial College London	Reporteure
Minev, Ivan	Directeur de Recherche	Université Technique de Dresden	Examinateur
Bernard, Christophe	Directeur de Recherche	Aix Marseille Université	Examinateur
Malliaras, George	Professeur	Ecole des Mines de Saint-Etienne	Directeur de thèse
O'connor, Rodney	Maitre-Assistant	Ecole des Mines de Saint-Etienne	Co-encadrante de thèse

Official EMSE Page here

I truly hope that the 'neural interface' will, one day, help to restore the mobility to paralysis patients and help people who suffer from neurological disorders.

Let's make the science happen!

Jolien Pas, October 2017

École Nationale Supérieure des Mines

de Saint-Étienne

NNT : 2017LYSEM040

Jolien Pas

FLEXIBLE NEURAL PROBES WITH A FAST BIORESORBABLE SHUTTLE: From in vitro to in vivo electrophysiological recordings.

Speciality: Bioelectronics

Keywords: Organic electronics; Conducting polymer; Cortical cells; Bioresorbable polymers

Abstract

Neural interfaces are designed to unravel the mysteries of the brain and to restore the functions of paralyzed patients. Despite the success of traditional neural interfaces, these rigid devices are prone to failure within months after surgery. Mechanical mismatch with the soft neural tissue is believed to be one of the main causes. In this thesis, we studied the use of soft organic electronics to interface with neural tissue for both *in vitro* and *in vivo* applications. Parylene-based microelectrode arrays (MEAs) and depth probes were made, employing the conducting polymer poly(3,4-ethylene dioxythiophene):poly(styrene sulfonate) (PEDOT:PSS) to reduce the impedance at the cell-electrode interface. *In vitro*, we thereby showed how to enhance the recording yield of MEAs by creating a three-dimensional model of neurospheres. We further report on the fabrication of a new biodegradable polymer shuttle for flexible depth probes based on the combination of poly(vinyl alcohol) (PVA) and poly(lactic-co-glycolic) (PLGA). *In vivo*, the PVA/PLGA- shuttled probes were acutely tested in mice and revealed promising electrophysiological results. More research remains necessary to evaluate its long-term function *in vivo*. In conclusion, our results demonstrate that bioresorbable polymers are capable of providing the required stiffness to penetrate the brain, which shows much promise for future neural applications. This work thereby shows that a long-term functional neural interface is not far from being developed.

École Nationale Supérieure des Mines

de Saint-Étienne

NNT : 2017LYSEM040

Jolien Pas

SONDES NEURONALES FLEXIBLES AVEC UNE NAVETTE BIORESORBABLE RAPIDE: Des enregistrements électrophysiologiques in vitro à in vivo.

Spécialité: Bioélectronique

Mots clefs: électronique organique, polymères conducteurs, polymères biorésorbables, neuro-ingénierie

Résumé

Dans cette thèse, nous étudions l'utilisation de l'électronique organique à l'interface du tissu nerveux pour des applications *in vitro* et *in vivo*. Le principal objectif de ce travail est la fabrication d'interfaces neuronales flexibles pour enregistrer l'activité électrophysiologique de cellules neuronales sur de longues durées. À cette fin, nous utilisons du parylène-C ultra-fin comme matériau isolant et le polymère conducteur poly(3,4-éthylène dioxythiophène):poly(styrène sulfonate) pour réduire l'impédance de l'interface cellule/électrode. En utilisant nos matrices de microélectrodes, nous montrons comment améliorer le rendement d'enregistrement avec un modèle tridimensionnels *in vitro*. Nous constatons que la formation de clusters cellulaires 3D augmente considérablement le nombre d'enregistrementsde potentiels d'action unitaires. Ensuite, *in vivo*, nous démontrons la fabrication de sondes de support en polymères biodégradables sur nos capteurs flexibles en utilisant une combinaison de polymères alcool polyvinylique et poly(lactique-co-glycolique). Alors que notre support d'insertion en PVA fournit la rigidité nécessaire à la pénétration, le revêtement PLGA retarde la dissolution du support afin de placer précisément les capteurs à l'intérieur du cerveau. Cela nous permet d'enregistrer sur longue durée, en profondeur et, dans les conditions idéales, de minimiser les lésions cérébrales par rapport aux sondes traditionnelles rigides. Dans l'ensemble, nous avons réussi à effectuer des enregistrements électrophysiologiques avec nos propres microélectrodes et sondes invasives, améliorant de manière significative le rendement d'enregistrements *in vitro* et démontrant que nos supports d'insertion biodégradables pénètrent le cerveau. Ces résultats annoncent de prometteuses applications médicales futures.

Contents

Chapter 1. Introduction on neural interfaces

1.1 Introduction

'Bioelectronics is interfacing, what I like to say, nature's most advanced creation which is human beings and human kinds most advanced engineering venture which is electronics'

George Malliaras – August 2007

The human brain is by far the most complex organ of the human body. Scientists and engineers with multidisciplinary backgrounds have to join forces to unravel its structure and function. Why is there so much effort invested in understanding how the brain works? Millions of people in this world suffer from traumatic incidents (e.g. traffic accidents, war), neurodegenerative diseases or aging, which greatly affects quality of life [1]. Although basic communication principles from the brain are known, there is still much to learn about the connectivity and the exact functions of the brain.

The discovery of electrical sensitivity in living tissue, referred to as 'bioelectricity', dates back from the 17th century [2]. Swammerdam and Galvani were the first to report on this phenomenon, using frog legs to show the contraction of muscles by electrical stimulation using metal wires first and later the frog's sciatic nerve. Nowadays, there are multiple stimulating and recording devices available which interface with neural tissue. Stimulation examples include *cochlear implants* to improve hearing, *deep brain stimulators* for Parkinson's disease, *spinal cord stimulators* to suppress pain and *retinal implants* to improve vision. Examples of regularly used recording devices include the *electrocardiogram* (ECG) and the *electroencephalogram* (EEG) which measure heart and brain signals.

Two particularly interesting materials became of utmost importance for further development of the medical healthcare devices: *semiconductors* and *organic materials*. The semiconductor industry developed ways to fabricate custom-designed devices on microscale, whereas the rise of organic materials significantly improved the interaction with a living tissue. The advances resulted this last decade in a promising new research field for neuroscience, called *Organic Bioelectronics*.

This thesis involves multidisciplinary research where many aspects come together. To fully understand what needs to be done, an insight on the different aspects is provided in this chapter. First, the brain and its electrical properties are briefly introduced. Then, neural interfaces and the current challenges are discussed with a main focus on the foreign body

response. Finally, an overview on the existing compliant interfaces is given, which eventually brings the reader to the ultimate aim and scope of this thesis.

1.1.2 The brain

The central nervous system (CNS) is considered the most complex organ in the human body and is the part of the nervous system containing the brain and the spinal cord. The CNS continuously sends and receives signals to and from the rest of the body to control limb movement, regulate organs and coordinate cognitive functions. The information is transmitted through a large network of neurons, the electrochemically active cells in the nervous system (*Section Electrophysiology*). The CNS is in connection with the peripheral nervous system (PNS), which is the part of the nervous system with neurons which reach the limbs and organs. Structural changes in the CNS or PNS can lead to malfunction of the human body, greatly affect quality of life and result in neurological disorders.

The brain is a very well-protected organ. It is physically protected by multiple membrane layers, called the meninges, which include the pia mater, arachnoid mater and the dura mater *(Figure 1a)*. These membranes can undergo 10-20% tensile strain during normal postural movements [3]. Also, the cerebrospinal fluid (CSF), which is located between the arachnoid and pia mater, the skull (bone), the periosteum (connective tissue) and skin protect this vital organ from the outside world. Furthermore, a selective semipermeable membrane is present in the blood capillaries of the brain, called the blood-brain barrier (BBB) *(Figure 1b)*. Unlike other vessels in the body, the BBB has additional tight junctions between the endothelial cells in the vessels and astrocytes cell projections surrounding the endothelial cells. While water, glucose and hormones can pass the barrier through passive/active transport, neurotoxins or bacteria are not able to enter the brain due to the highly selective BBB.

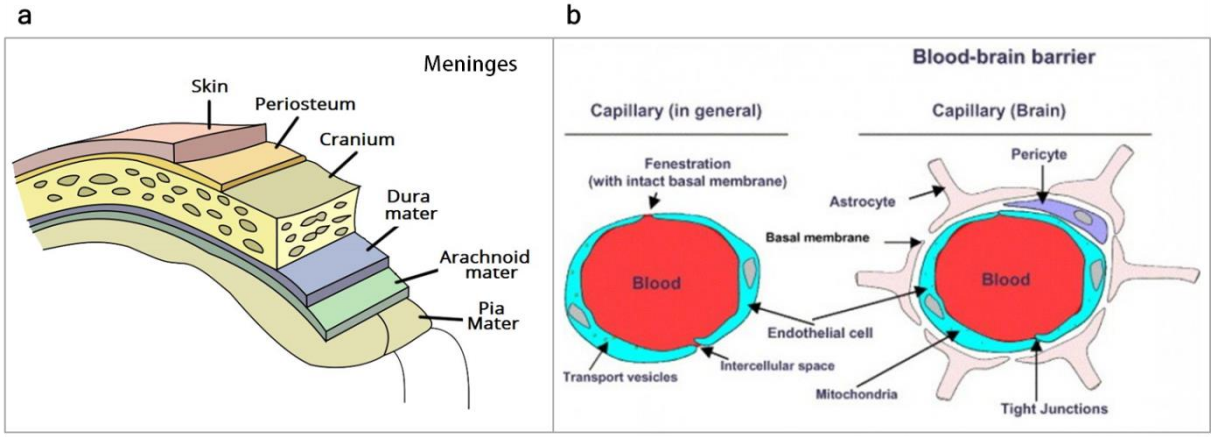

Figure 1. Protective systems of the brain. (a) Illustration of the different meninges layers. Adapted from [4] (b) A comparison of a normal capillary and a blood-brain barrier (BBB) capillary. The addition of tight junctions in between the endothelial cells and astrocyte processions around them, prevent the entering of neurotoxins or other dangerous species into the brain. Adapted from [5].

The human brain is a soft tissue, with a bulk elastic moduli between 0.1 to 10 kPa [3], [6]. It has a volume of approximately 1.3 liters and is mostly made up out of neurons, glial cells and extracellular matrix (ECM). The ECM is dense mesh of fibrous proteins, proteoglycans and glycosaminoglysancs located in between the cells in the interstitial space. Surprisingly, the CNS does not contain much collagen, which is normally the most abundant structural protein of the ECM elsewhere in the body. Despite the lack of the mechanically strong collagen, the ECM provides sufficient strength to keep the cells connected and prevent neural deformation.

1.1.3 Neurons and glial cells

The brain consists of billions of neurons that are the information messengers, transmitting electrical and chemical signals between different areas of the brain and the rest of the body. Although there are various types of neuron with different physical appearances, each neuron contains a cell body (soma) with up to nearly a thousand dendrites and a projection called the axon *(Figure 2)*. Basically, the dendrites receive incoming signals and the axon further transmits the signals to neighboring neurons. While the axon is only a few micrometers thick, it can vary in length up to 1 meter [3].

Neurons can be classified according to their function *(Figure 2b)*. Signals from the surrounding tissue or organs are received by *sensory neurons*, which transmit the signals to *interneurons*. These interneurons then transport and fine-tune the signals throughout the nervous system to eventually reach *motor neurons*. The motor neurons are connected to muscle fibers and transform the initially received information into a particular action.

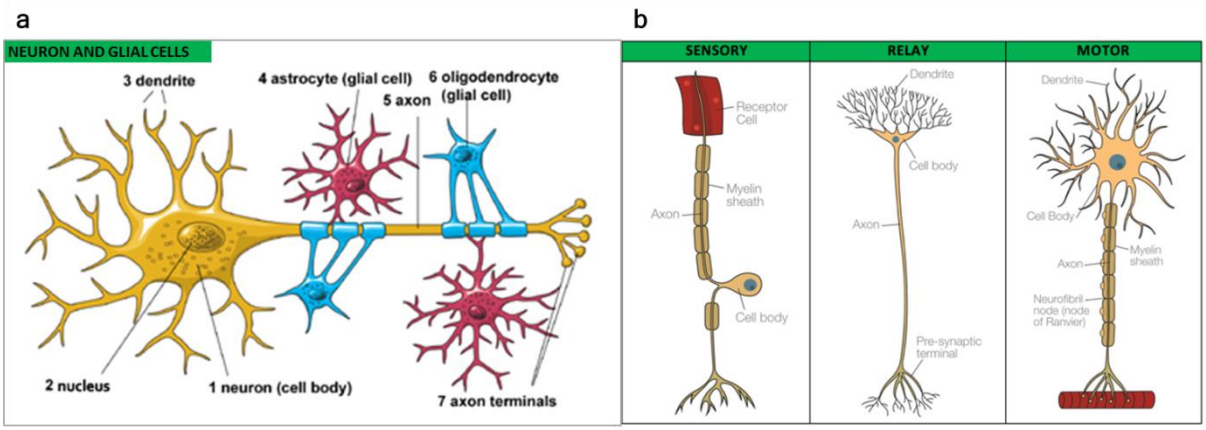

Figure 2. Presentation of brain cells. (a) Illustration of a neuron (yellow) supported by astrocytes (red) and oligodendrocytes. Adapted from [7]. (b) Illustration of the different neuron types. Sensory and motor neurons contain myelin sheaths, while the interneuron (relay neuron) does not. Adapted from [8].

Neurons need the support of glial cells to function correctly. There are three general types of glial cells, called astrocytes, oligodendrocytes and microglia *(Figure 2a)*. Astrocytes perform many vital functions, like for example provision of nutrients to the neurons, maintenance of extracellular ion balance, support of endothelial cells that from the blood-brain barrier (a highly selective membrane which accurately filters the blood before it enters the brain to

prevent any dangerous toxins from entering the brain), etc. Oligodendrocytes produce insulating myelin sheaths which wrap around the axon of the neuron to speed signal transmission. Microglia are the immune cells of the CNS and mediate the foreign body reaction by protecting the brain from any foreign material (*Section The main challenge: Foreign body response*).

1.1.4 Electrophysiology

Neurons communicate with one another through an electrochemical process. While impulses are conducted through electrical signals within the same neuron, communication between adjacent neurons is directed by the conversion of electrical signals into chemical signals. Hence, signal conduction through the nervous system requires constant transformation of electrical signals into chemical signals and vice versa. The neural signaling pathway is further elaborated below.

The special structure of the neuron allows for efficient transmission of the electrical signal. Dendrites integrate the activity other neurons and transmit the signal as electrical impulses to the cell body and axon of the neuron. This axon subsequently transmits the impulses away from the cell body towards synaptic terminals. This signal transmission along the axon proceeds at various speeds, depending on the diameter of the axon and whether they are insulated with myelin sheaths or not. In the case of myelinated axons, the signals are propagated from node to node as the sheaths themselves are electrical insulators.

The described signal transmission within a single neuron occurs by the movement of electrically charged ions through the neuron membrane *(Figure 3)*. During the resting period, a potential difference across the neuron's membrane is present. This bias is caused by the differences in concentration of ions between the interior and exterior of the cell. This gradient is maintained by various pumps, fueled by ATP (active transport). A membrane potential of -70 mV exists, with a negatively charged cell interior compared to the extracellular space. During synaptic transmission, neurotransmitters released by the presynaptic terminal, gate postsynaptic ion channels (passive transport).

Once the membrane potential reaches a threshold of approximately -50mV, voltage-gated sodium channels of the membrane briefly open and quickly inactivate. The influx of Na^+ into the cell depolarizes the membrane potential up to +30mV. During this phase, voltage-gated potassium channels open, causing intracellular potassium to leave the cell down the concentration gradient, finally repolarizing the membrane potential. The combination of opening and inactivating voltage-gated channels in the axon cause a depolarization wave enabling the propagation of the action potential.

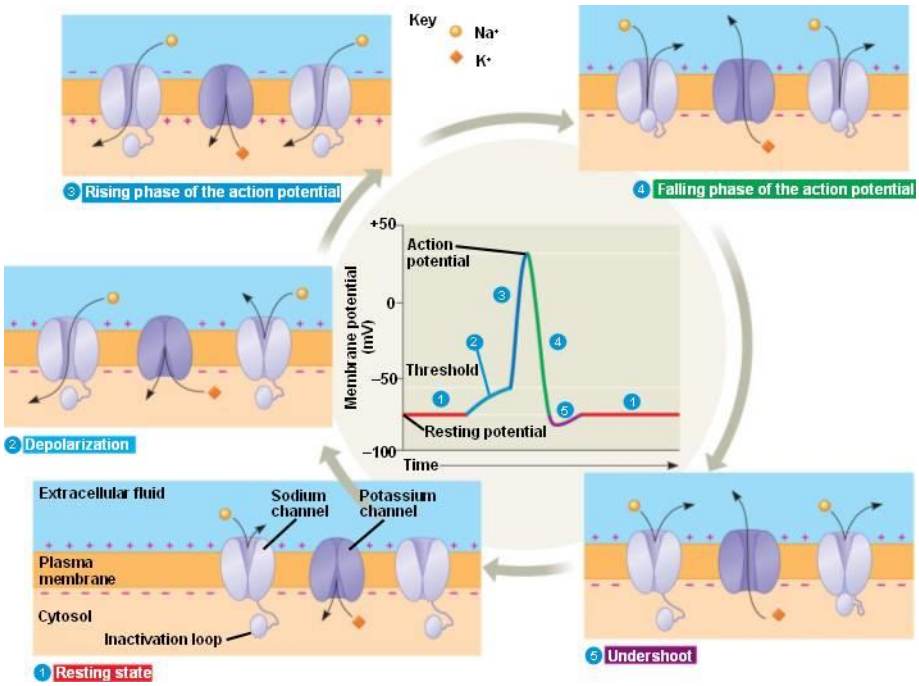

Figure 3. Illustration of the different stages during an action potential. Adapted from [9].

Once the electrical signals reach the nerve terminus (presynaptic terminal), the signals are transformed into chemical signals through *chemical synapses (Figure 4)*. Calcium ions enter into the pre-synaptic synapse, which causes the release of neurotransmitters across the synaptic cleft. The neurotransmitters in the cleft subsequently bind to the receptors of the adjacent neuron (postsynaptic neuron). The receptors then open a channel enabling the flux of ions, thus creating a current. The chemical signal is thus transformed back into an electrical signal changing the membrane potential of the post-synaptic neuron. The remaining neurotransmitters at the postsynaptic site are either quickly pumped back into the presynaptic nerve terminal, destroyed by enzymes near the receptors or left to diffuse into the surrounding area. Besides this relatively slow chemical transmission, the electrical signals can also be directly transmitted through *electrical synapses*. Such synapses contain pores, known as connexons, through which the ionic charge can flow from the presynaptic neuron to the postsynaptic neuron. Eventually, once the signals reach motor neurons, the electrical signal will be transferred to muscular cells to induce a tangible muscular response. By increasing the frequency of the action potentials and the number of muscular cells being activated, muscle contractions can be accelerated.

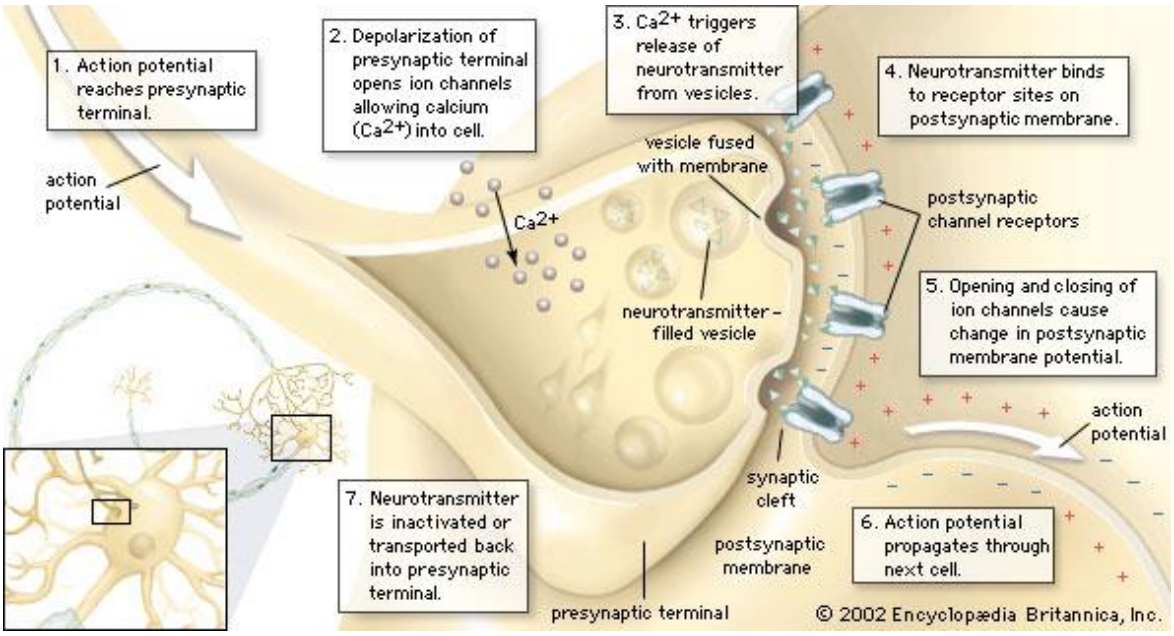

Figure 4. Illustration of the chemical transmission during an action potential. Adapted from [10].

1.2 Neural interfaces

A man-made connection between the nervous system and the outside world is a called a 'neural interface'.

> Neural interfaces are designed *"to create links between the nervous system and the outside world either by stimulating or by recording from neural tissue to treat or assist people with sensory, motor, or other disabilities of neural function"*
>
> *Hatsopoulos and Donoghue -- 2009* [11]

Today, the most successful neural interfaces used by humans are stimulating interfaces like *the cochlear implant*, which restores audition for deaf people and *deep brain stimulators* (DBS), which relieve symptoms of Parkinson disease. Recording interfaces have also already shown successful outcomes, like the impressive *BrainGate Systems* [12], [13]. For example, Cathy Hutchinson, a tetraplegic patient paralyzed from the neck down, was implanted with a 96-electrode intracortical silicon array (Utah array) in the motor cortex. Five years after the surgery, and many weekly practices with the *Brain Machine Interface* (BMI), she was able to control the movement of a robotic arm enabling her to drink from a bottle by herself using her thoughts. For safety reasons, such invasive devices are still removed after the clinical trials. Much more development is needed to reach the ultimate goal of permanently improving individuals with movement impairments for entire patient lifetimes [14].

Besides helping people with severe sensory and motor disabilities, this technology can also provide fundamental scientific knowledge about the still mysterious and complex central nervous system. There is still a need to understand basic brain functions, to study the

underlying physiological processes at cellular level and to also unravel the causes of neurological diseases. Depending on the desired neural information, various different neural interfaces can be used and are categorized according to their level of invasiveness [15]. These interfaces are explained in the next section.

1.2.1 Measurable neural signals

There are different types of electrical signals that can be recorded from the brain (*Figure 6b*). Besides the action potential which was previously introduced (*Section Electrophysiology*), there is also another type of potential to be measured from brain activity, the field potential (FP) [14].

- Action potential: signals which originate from a single neuron which is electrically excited. It can also happen that neurons are excited simultaneously, resulting in so-called multiunit activity.
- Field potentials: signals which are more complex as these contain information of all transmembrane currents of a small population of neurons, varying in size, frequency and spatial distribution. FP signals can be further classified into two groups:
    - Rhythmic signals: This is repetitive neural activity, which originates from the synchronized activity of large number of neurons and results in oscillations at different frequencies than the firing frequency of individual neurons. There are different types defined within this category:
        - Slow signals (< 1Hz)
        - Medium signals (δ rhythms, 1-4 Hz; θ rhythms 4-7 Hz; α rhythms, 8-15 Hz; β rhythms 16-31 Hz)
        - Fast signals (γ rhythms , >32 Hz)
    - Event-related potentials (ERPs): These are large potential shifts induced for example by an external event in a large neuronal group.

Besides these defined electrophysiological signals, there are many more electrical events taking place in the brain [16]. Examples are Ca^{2+} mediated spikes, back-propagation of an action potential, voltage-dependent membrane responses (some neurons resonate at a particular frequency), after hyperpolarizations or even membrane potential changes of glial cells [16]. All these transmembrane currents give rise to an extracellular field potential, which are measured using microelectrode arrays.

1.2.2 A neuron/electrode interface model

To understand the electrophysiological data that is recorded from the brain and find ways to improve the neural interface, models are made to electrically simulate what is measured. For example, *Figure 5a* shows such an equivalent circuit model, using three main components: a neuron, a cleft between the neuron and the electrode device and an electrode site. In this

model, the neural membrane facing the electrode site is referred to as *junctional membrane* and the membranes which are not facing the electrode site are called *non-junctional membranes*. Both membranes are represented by a resistance (R_{nj} and R_j) and a capacitance in parallel (C_{nj} and C_j). The cleft, which is filled with physiological solution, generates a so-called *seal resistance* (R_{seal}) and influences the current flow across the electrode site. Finally, the resulting current at the electrode site is represented with again both a resistance and a capacitance in parallel (R_e and C_e).

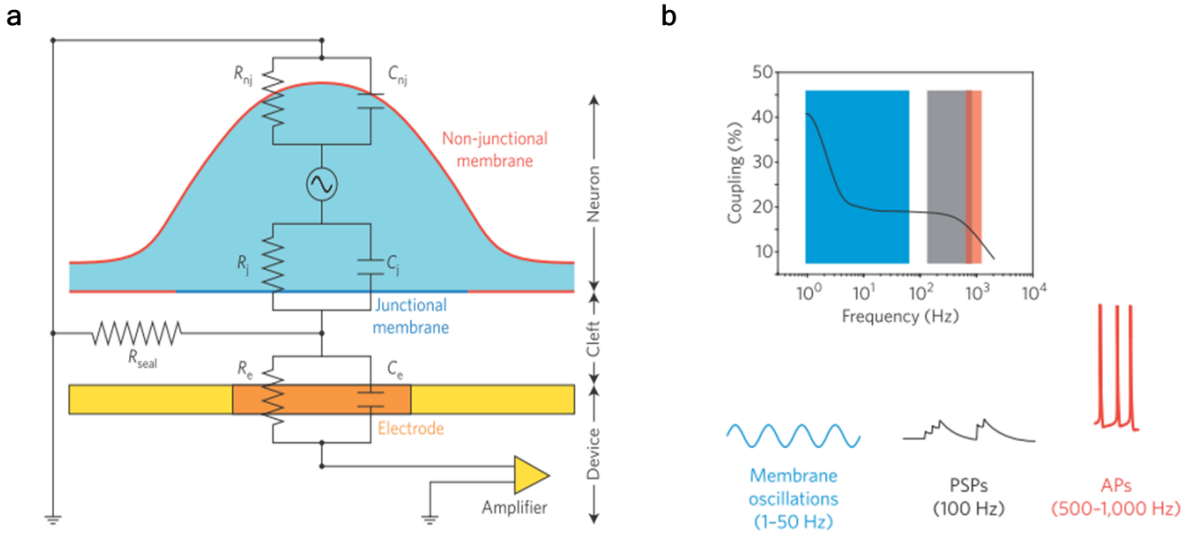

Figure 5. Equivalent circuit model to explain the measured extracellular brain signals. (a) The schematic shows a neuron (blue) present on an electrical recording device (yellow) with one electrode site (orange). The recorded signal originates from the transmembrane currents, which flows through a cleft with a seal resistance and results in a current flow at the electrode site. Abbreviations: R_{nj} and C_{nj}, non-junctional resistance and capacitance, R_j and C_j, junctional resistance and capacitance, R_{seal}, seal resistance and R_e and C_e electrode capacitance. (b) The efficiency of electrical coupling of recording devices in function of the frequency of the recorded signals and an illustration of slow membrane oscillations (blue), medium frequency signals (postsynaptic potentials (PSPs); black) and fast action potentials (red). Figures adapted from [17].

The electrical coupling between a neuron and a recording electrode can give insight on the efficiency of a neural interface. This parameter is defined as the ratio between the maximal recorded voltages of the device and the maximal voltage generated by the neuron. *Figure 5b* shows a simulation-based graph presenting this coupling percentage in function of the frequency signal, reported by [17]. It illustrates that the high frequency signals, such as the action potentials, are attenuated much more than the lower frequency dependent signals. One of the aims of this work was to record the action potentials despite this challenging fact.

Obviously, this model is a simplification of the actual measurable signal taking into account only a single neuron in close proximity of the electrode. In reality, a summation of all transmembrane currents in close proximity of the electrode can be measured. This is what makes the analysis of the recorded signal very complex. Luckily, there are programs developed to subtract single cell activity from the recorded signals by performing spike sorting analysis *(Chapter 4)*.

1.2.3 Non-invasive and invasive recording methods

While there are different ways to record neural activity from the brain (including intracellularly, extracellularly, optically, MRI based), the focus in this work is placed on extracellular measurements *in vivo*. The reader is referred to *Buzsaki et al.* or *Spira et al.* for information on other recording options [16], [17]. As previously explained, the invasiveness of the recording method will influence the amount of information attained from the brain (*Figure 6*). Below, we briefly describe various methods being used nowadays.

Functional information can be attained from the surface of the scalp using large non-invasive macro-electrodes, known by electroencephalography (EEG). The measured electrical signals originate from a large number of synchronous post-synaptic action potentials occurring deep within the brain. This activity results in local field potential (LFP) which can be measured at the skull, yet is largely attenuated being carried through different cerebral layers, the meninges and the scalp. Consequently, the amplitude of the signal is typically very low (25-100 uV) and within low frequency domain (<100 Hz).

Better spatial resolution is provided with more invasive recordings, such as electrocorticography (ECoG) and stereoencephalography (SEEG). In both cases, the scalp and skull are surgically removed (craniotomy) and the brain is exposed for the placement of the electrodes. For ECoG, the device is either placed on top (epidural) or below (subdural) the dura mater. Not penetrating the brain, mostly allows the capturing of LFP signals. The signals originate from superficial cortical neurons (with a maximum recording depth of about 1 cm) below a frequency of 200 Hz, ideal to accurately map epileptic zones during surgery. Interestingly, even the measurement of action potentials has been reported using this method [18]. Key to that success is the use of conducting polymer, PEDOT:PSS. More information is provided in the next chapter regarding this material *(Chapter 2)*.

The highest spatial and temporal resolution can be achieved through SEEG by using intracortical microelectrodes which are placed deep inside the brain. Examples of intracortical microelectrodes include a platform array with a substrate that remains on the cortical surface (like the Utah array), a depth probe which goes multiple millimeters deep into the brain, an assembly of microwires and a cone electrode, which is a microwire placed in a glass cone that is open at the end *(Figure 6a)* [14]. In general, the platform arrays and microwires have conductive tips through which is recorded, depth probes have multiple electrodes along the length of the shank and cellular elements grow into the cone for electrical transmission with the wire inside (*see also Section 1.2.4*). This most invasive interface provides the closest distance to the neurons and results thus in the highest signal resolution with potential to record both LFPs and action potentials *(Figure 6b)*. Frequencies up to 0.1 Hz can be measured, ideal for electrophysiological research, mapping of connectivity and brain machine interfaces [16].

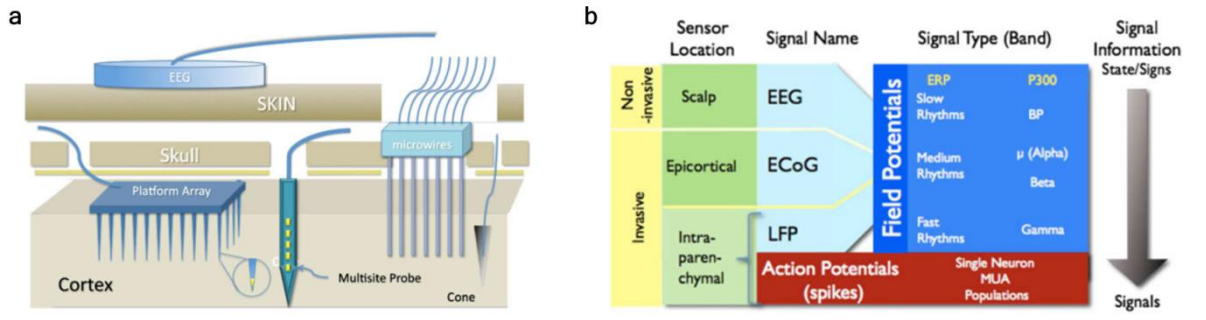

Figure 6. Recording methods for extracellular events. (A) Schematic of the EEG (less invasive) and intracortical microelectrodes, such as a platform array, a depth probe ('multisite probe'), a microwire assembly and a cone electrode. (b) Overview of electrical potentials to be measured with a neural interface (*Section 1.2.1*). Adapted from [14].

1.2.4 Invasive neural interfaces and their shortcomings

Neural interfaces have undergone significant evolution since the late 20th century. From the 1950's, electrical activity of the nervous system was investigated using microwires. In the late 1970's, patch-clamp techniques were developed which enabled the study of a single ion channel. This work led to the understanding of how charge is (selectively) transmitted through the membrane-proteins. Neher and Sakmann were rewarded for this revolutionary discovery with the Nobel Prize in Physiology in 1991. In the late 1980's, a new type of device was eventually developed with the advances made in the semiconductor microfabrication field: silicon-based microelectrodes [6], [19]. Well-known examples are the Michigan probes and Utah array, which are both metallic-based electrodes produced on silicon through lithography to interface, respectively, deep within or at the surface of the brain. Around the same time, stereotrodes and tetrodes were developed which are two or four polymer insulated micro-wires, electrochemically coated with gold. Multiple microwires bundled together allowed for a more accurate investigation of individual neural communication in large groups of neurons, identifying action-potentials to specific neurons via principle component analysis. The latest significant change that occurred in the development of penetrating neural probes (21st century) is the use of organic materials as substrate material [20]. The benefit of its softer nature could potentially improve the integration of the electronics with the soft brain *(Section 1.3)*.

Currently, platinum-iridium electrodes are used for DBS treatment and platform arrays (Utah array) and cone electrodes are being evaluated in human clinical trials [14]. The DBS system and the Utah array have been FDA approved and received the CE mark in Europe [19]. Other devices have not reached that stage yet or have been refused due to severe health consequences. The main issue with these interfaces is the *rigid nature* of the devices which excessively damage brain tissue and lose their function months after the surgery due to the foreign body response (*Section 1.2.5*). Academic investigators in the neuroscience field however try to solve fundamental questions mainly using tetrodes, due to their low costs, or

silicon-based probes, due to the vast amount of experience already obtained with these. Examples of commercially available silicon-based probes are shown in *Figure 7*.

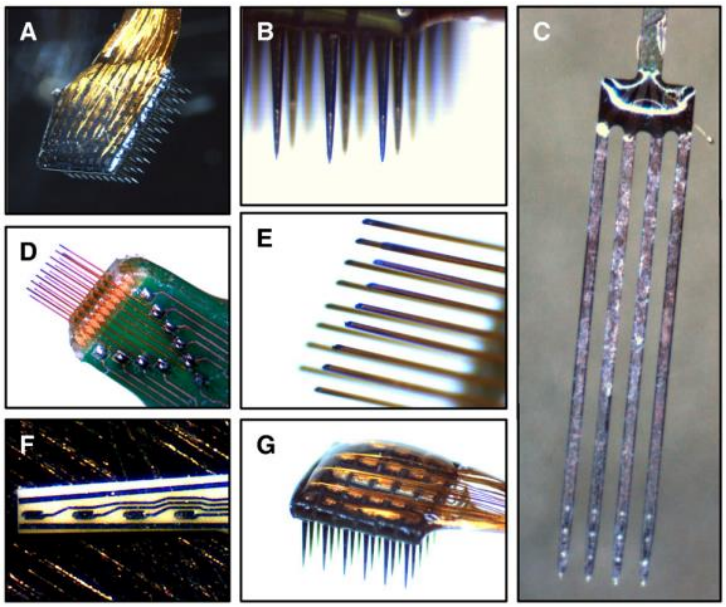

Figure 7. Examples of invasive neural probes. (A) Cyberkinetics Silicon-based 100-channel MEA. (B) View of recordings sites on the Cyberkinetics arrays (metallic portion on tip of each shank). (C) View of NeuroNexus Silicon-based MEA shanks (4 recording per shank). (D) Tucker-Davis Technologies Microwire MEA. (E) View of recording sites on the TDT microwire array. . (F) Moxon Thin-Film Ceramic-based MEA (G) View of bond pads on a 36-channel Cyberkinetics array. Adapted from [21].

These most commonly used invasive neural probes are far from being the ideal interface. In general, these rigid devices are prone to failure just a few weeks after implantation. There are many interplaying problems at the probe-brain interface that play a critical role [6], [19]. The failures can be classified into having either an engineering cause or biological cause and include problems such as direct mechanical damage, corrosion of electrical contacts, degradation of device layers and the foreign-body response resulting in electrical isolation of the probes *(Figure 8)*.

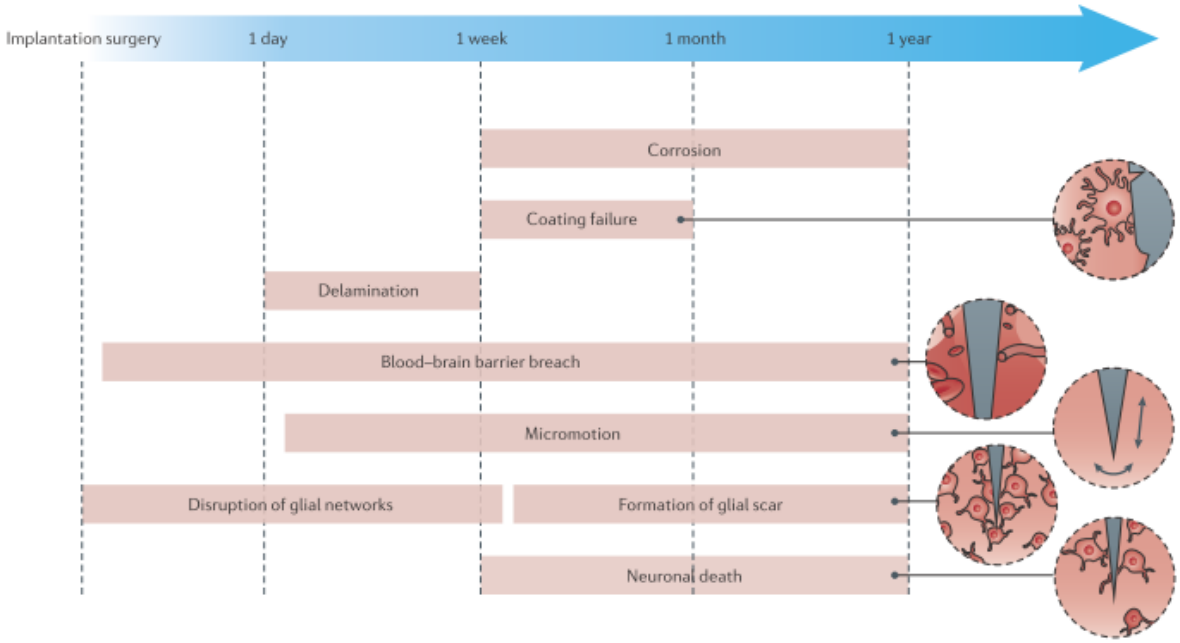

Figure 8. Failures of rigid neural probes in time. Adapted from [6].

1.2.5 Foreign body response as the main challenge

There main concern and challenge which still needs to be overcome is the ability to record signals over the long term. Although Braingate pilot trials have shown already very promising results to translate neural signals measured with the invasive Utah array for over five years now [13], a general decline in signal quality and decrease in the number of recording channels is observed within months after implantation [14]. The brain's response to any invasive intracortical microelectrodes is the same: rejection of the device due to the foreign-body response (FBR) with complete loss of electrode function as the ultimate result. To the best of our knowledge and irrespectively of the many differences in the type of device or microelectrodes, the sterilization method, the implantation method ([14]), there has not yet been the desired outcome of stable recording for more than months. Intracortical microelectrodes are prone to fail on long-term basis due to tissue reaction around the interface.

The FBR is a complex interplay of molecular and cellular responses to the penetrating probe inside the brain [19]. During probe implantation, vascular and cellular tissue is inevitably damaged followed by multiple systems to protect the brain from the foreign body *(Figure 9)*:

- A coagulation cascade is immediately initiated to restore the wound, during which tissue remodeling starts.
- The complement system is activated, which is a part of the immune system that enhances the ability of antibodies and macrophages to remove the damaged cells and pathogens at the injury site and promote inflammation.
- Reactive microglia and recruited macrophages release pro-inflammatory factors, like tumor necrosis factor-alpha (TNF-⊚⊚⊚⊚monocyte chemotactic protein-1 (MCP-1) and

Interleukines (IL-1,6 and 17). These factors further stimulate the immune response, by inducing more inflammation due to their toxic effect (also damaging the still healthy cells in the surrounding) or by attracting new macrophages to the injury site.

- Reactive oxygen species accumulate at the interface of the microelectrodes, leads to oxidative stress with damage to DNA, proteins and lipids as well as mitochrondrial dysfunction [22].
- Hypertophic astrocytes, fibroblasts and meningeal cells accumulate around the injury site, forming a dense scar-tissue to insulate the foreign body from the rest of the brain tissue.

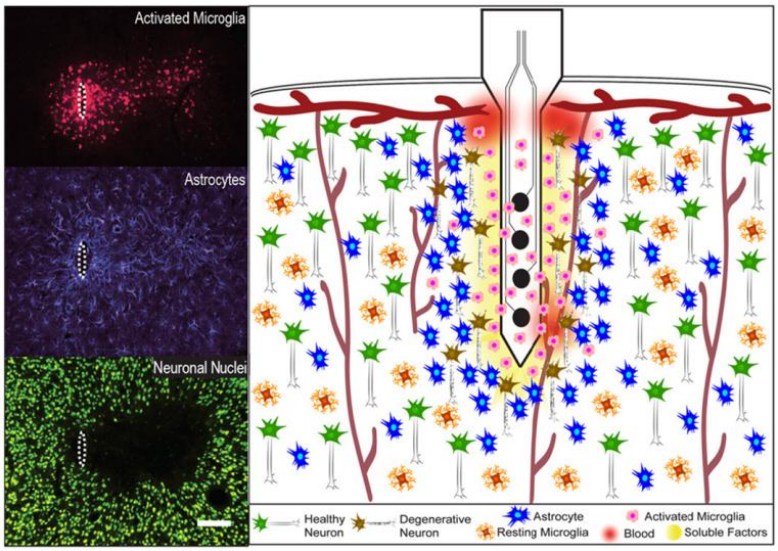

Figure 9. The effect of probe implantation inside the brain. (Left) Immunohistochemistry images of activated microglia, astrocytes and neural nuclei. (Right) Illustration of the probe/tissue interface. Briefly, activated microglia are primarily present at the electrode site, releasing pro-inflammatory factors. Astrocytes approach and eventually encapsulate the device (glial scar), while neurodegeneration persists at the interface. Adapted from [19].

There are several factors appointed to the extensive inflammation response [6], some of which are mentioned here below:

- The tissue damage during device implantation;
- The mechanical mismatch between the device and the neural tissue;
- Micro-motion of the implant relative to the brain;
- Disruption of the glial networks;
- Continuous rupture of the blood-brain barrier;
- And neurotoxicity of the materials.

The eventual consequence of this effective FBR is the complete loss of recording function. This function loss is partly since the blood-brain barrier remains impaired after penetration

with the invasive device and since inflammation remains chronically present at the electrode/tissue interface. Moreover, neuronal loss at the interface site was reported statistically significant at 2 weeks and 16 16 weeks after implantation [23]. A significant decrease in neurons was initially observed within a 50 um range, which decreased after 2 weeks to a 30 um range from the implant site. On average, a neuronal decrease of 40-60% is observed at the neural interface [19]. Although neurons remain observed near the interface, the loss of neurons does greatly limit recording performance. Ultimately, it is the thick scar-tissue which electrically isolates the entire probe from the remaining healthy neural tissue and results in the complete loss of recording function.

1.3 Efforts towards more compliant interfaces

The choice of material in the probe design has substantial influence on all above mentioned failures [3], [6], [24]. While the brain is a soft tissue with an elastic modulus ranging from 0.1-10 kPa, traditional probes have moduli even above 100 GPa [24]. This 7 orders of magnitude difference in stiffness creates an enormous mechanical mismatch with total failure of the device as result [19], [25]–[27]. Ever since this impact has been discovered, there has been put great effort to find ways to fabricate neural interfaces on more compliant materials or to make the intrinsic stiff materials much thinner, thereby also creating a more flexible substrate.

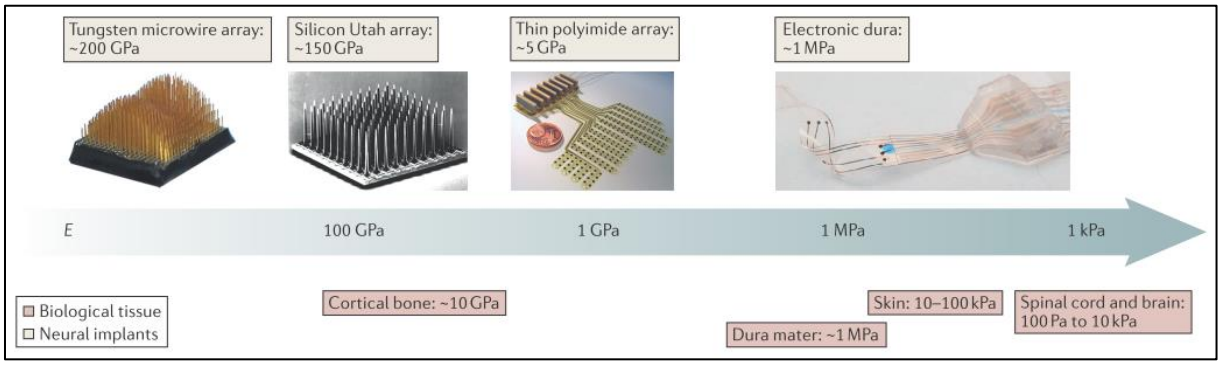

Figure 10. Mechanical mismatch between biological tissue and neural interfaces, adapted from [3].

1.3.1 Reported compliant materials

Multiple materials with various elastic moduli below the stiff traditional probes were investigated [19], [20]. Such materials include polyimide (PI), benzocyclobutene (BCB), polydimethylsiloxane (PDMS), SU-8 and parylene-C (Pc). Relevant properties, such as the elastic modulus and the tested biocompatibility, of these polymers are summarized in the table below *(Table 1).*

Table 1. Characteristics of reported compliant materials used for neural interfaces.

	Elastic modulus (GPa)	Biocompatible	Neural probe references	Limitation	Reported insertion aids
Silicon	200 [25]	-	[18]	Mechanically stiff	-
Parylene-C	3.2-3.8 [28] [29]	Yes [34]	[28], [19], [37]	Insertion system needed	-
BCB	3.1 [30]	Yes [30]	[30], [38], [39]	Insertion system needed	Additional silicon layer or a tungsten backbone [30], [38], [39].
SU8	2-3 [31]	Yes [35]	[40]–[43]	Toxic SU8 compounds can leach out [42], [51]	-
Polyimide	2.8 [32], [33]	Yes [36]	[44], [32], [45], [33], [46]	Moisture uptake: 4-6 wt% swelling [20], [38]	Scalpel or tungsten wire [32]; Needle [45]; additional silicon [33] or SU8 layer [46]
PDMS	0.001 [3]	Yes [34]	Spinal cord electronics [47], [48]; Retinal implants [49], [50].	Insertion system needed	Not relevant

The problem with the use of softer materials for penetration is the higher risk of buckling. *Buckling* occurs when the probe starts bending (*Figure 11a*), with the consequence of a more severe brain injury and a less accurate placement of the probe once it penetrates. Ideally, buckling should be prevented during insertion with the probe going straight down into the brain. The maximal force which a probe can withstand without buckling is called the *buckling force* [28] and is mathematically defined by:

$$\mathrm{F(buckling)} = \frac{\pi^2 \, \mathrm{E\,I}}{(K\,L)^2} \qquad with \qquad I = \frac{b\,h^3}{12}$$

With E the young's modulus; I the moment of inertia defined by the cross-section; K the effective length factor, with K=0.6999 for a probe that is fixed at one side ; L the length, b the width and h the thickness of the probe tip [28]. When taking this into account, the length of the probe tip can alter the buckling force significantly (being typically several millimeters, compared to the other parameters which are micrometer scale).

Besides the buckling force of the neural probe, one must also take into account the exerted insertion forces exerted on the penetrating probe to ensure successful penetration. The *insertion force* is defined by the minimum force required to penetrate the brain [19] and includes the axial tip force, the frictional forces originating from the penetrating surface and the clamping forces (*Figure 11b*). It was found that this force ranges between $1 - 30\ mN$ with the dura and pia layer still protecting the brain [29] (*Section 1.3.2*).

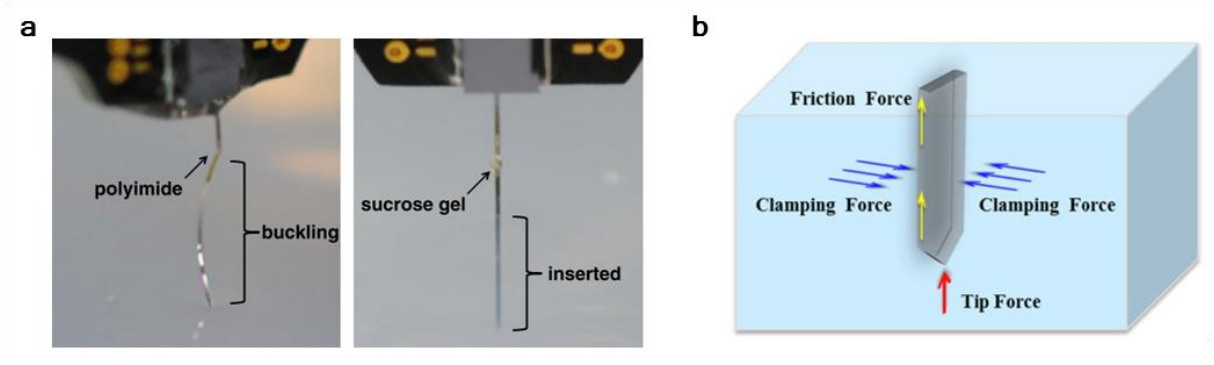

Figure 11. Forces exerted onto the neural probe. (a) Buckling of the flexible probe is observed as the probe bends, which is undesirable. A straight probe is necessary for accurate placement into the brain. Adapted from [30]. (b) Overview of the forces present onto the probe during insertion. Adapted from [19].

1.3.2 Design considerations

As previously mentioned, the main limitation of compliant polymeric substrates is that they do not provide the necessary stiffness to penetrate the brain. Although the device must have a certain flexibility to minimize motion-induced injury once positioned inside the brain, it still needs to have provide sufficient mechanical strength to insert into the brain. Although the brain is very soft (0.1-10 kPa [3]), the meninges around the brain have a higher mechanical strength and prevent in most cases the penetration of these probes. The dura is an especially tough membrane with an elastic modulus of 0.5-1.2 MPa [3].

When designing a new complaint neural probe, there are several factors to take into account to ensure successful penetration:

(1) The mechanical properties of the brain differ from rodent to human. For example, reported young's moduli of the dura for rat are 0.4-1.2 MPa, while humans' dura showed values of 32 and 62 MPa [20]. Moreover, a difference is observed between analogues brain structures, like the rat hippocampus (0.1-1.2 kPa) and the rat cerebellum (0.3-0.5 kPa) [20].

(2) The probe needs to withstand insertion forces of at least 0.5 - 1 mN (without the dura and pia layer) [31], [32] or 30 mN [29] to 50 mN [33] (with dura and pia).

(3) Insertion parameters such as speed and the location of brain will influence the success rate of penetration [31].

(4) Although decreasing the probe size is desired to minimize brain damage [34], the probe is more likely to undergo buckling [31], [35]. Buckling places undesired stress on the brain and limits insertion precision of the probe into the brain. However,

increasing the probe size will induce more brain damage due to the increased strain and compression placed on the tissue.

(5) Compression of the brain can be reduced by providing a sharp tip at the end of the probe [31]. Sharpness additionally lowers penetration forces and provides a more constant loading slope (force-displacement analysis) which minimizes stress placed on the brain.

Furthermore, once inside the brain, an implanted probe will continuously experience forces that tend to move the electrode [25], [35]–[37]. The brain itself continuously moves with respect to the skull, due to rotational accelerations of the head, intracranial pressure changes, respiration and vascular pulsations. If the probe is not flexible enough to accommodate the compression and tethering forces exerted on it, the device will inevitably deflect from its target location and even be pushed out of the brain [25], [36]. It is shown that tip deflections of approximately 10 um occur already solely due to brain-skull displacements (~1 mm) [35]. This small displacement most probably results in signals being lost in noise, due to fast exponential decay of a potential with distance [35]. The micro-motions of the probe should thus not be underestimated.

It remains unclear how soft and flexible a probe needs to be to maintain its function *in vivo* on a long-term basis. There is still a limited amount of studies done to investigate the tissue response of compliant probes in vivo [19]. In short, a balance is to be found looking at parameters such as the stiffness, flexibility, probe size and probe shape, to improve the life-time of depth probe *in vivo*.

1.4 Scope of the thesis

The current state-of-the art organic bioelectronics is a promising field to improve the long-term function of neural interfaces. The aim of this thesis is to present the fabrication of flexible neural interfaces designed to improve long-term signal recording for both in vitro as in vivo applications. In *Chapter 2*, the fabrication of parylene-coated microelectrode arrays (MEAs) and flexible parylene-based depth probes is discussed. Although parylene is intrinsically stiff (~3.2 GPa), the fabrication of thin parylene devices (< 10 μm) provides the desired flexibility to interface with soft brain tissue. Moreover, Poly(3,4-etheylenedioxy-thiophene):poly(styrenesulphonate) (PEDOT:PSS) is used on all of the devices as conducting polymer to significantly improve recording quality. The advantages of PEDOT:PSS are discussed in detail. *Chapter 3* then presents our findings on the in vitro experiments performed with primary rat cortical cell tissue on the MEAs. We show how to significantly improve single cell recordings through the use of high cell densities, the formation of 3D neural clusters (neurospheres) and the patterning of such neurospheres. Extensive spike sorting was performed to analyze all the electrophysiological data. In *Chapter 4,* a review is

given on the current state-of-the-art for inserting flexible probes and we report on a new bioresorbable polymer shuttle for flexible depth probes. The shuttle provides sufficient stiffness to enable brain penetration, yet dissolves fast enough to minimize mechanical mismatch at the interface. The depth probe is mechanically and electrically characterized and the first acute and chronic *in vivo* results are presented. To conclude, *Chapter 5* summarizes the efforts done in this multidisciplinary work and presents new challenges to be met for future investigations.

.

Chapter 2. Fabrication of PEDOT:PSS-based neural interfaces

2.1 Introduction

'Bioelectronics' is an exciting and growing research field focusing on the improvement of the interface between biology and electronics [38]. Since the 1960's, technology has undergone a tremendous boost due to the discoveries of two fascinating material types: semiconductors and conducting polymers.

The advances made in the semiconductor industry using *silicon* changed our world by enabling microscale circuit fabrication *(Figure 1a)*. Silicon is a semiconductor, which means it has an energy band gap that splits the valence and conduction band. This property makes the material special as it has the potential to conduct current depending on its environment and its purity: an external stimuli and/or the introduction of impurities ('doping') will render the material conductive. Silicon became the most used material to create integrated circuits (microchips) used in consumer electronics *(Figure 1b)*, due to its potential to be micro-patterned through photolithography. Microchips continue to decrease in size, making computers and other electronics, such as cameras, airbag control systems, cellular phones, etc. continuously smaller, cheaper and faster.

The use of photolithography has also enabled the development of state-of-the-art bioelectronics. This technique facilitates fabrication on the micrometer scale, which is essential for many biomedical applications. For example, the fabrication of lab-on-a-chip devices, which integrate laboratory functions on a single (micro)chip for automatic and high-throughput screening *(Figure 1c)* has been made possible. Additionally, to meet the needs of neuroscientists, photolithography has been employed to fabricate multiple silicon microelectrodes *(Figure 1d)* or polymer-supported metal microelectrodes (*Figure 1e)* on a single platform with the required spatial resolution to stimulate and record from brain tissue.

The second impressive turning point for bioelectronics was the discovery of conductive polymers in the late 1970's [39]. Fundamental research in both academia and industry have profited from the surprising finding that polymers can become conductive. The significance of this discovery was shown by granting the pioneers of conducting polymers, H. Shirakawa, A. Heeger and A. MacDiarmid, the Nobel Prize for their work in 2000 [40]. Conducting polymers are organic polymers with a conjugated backbone providing the potential property of conducting charge in the 'doped' state *(Section 2.2.2)*. The use of polymers is especially beneficial for industry, as they provide low-cost manufacturing for many applications. Through solution processing, thin polymer films can be useful for light displays, transistors in microchips, anti-static or microwave-absorbing screen coating, etc..

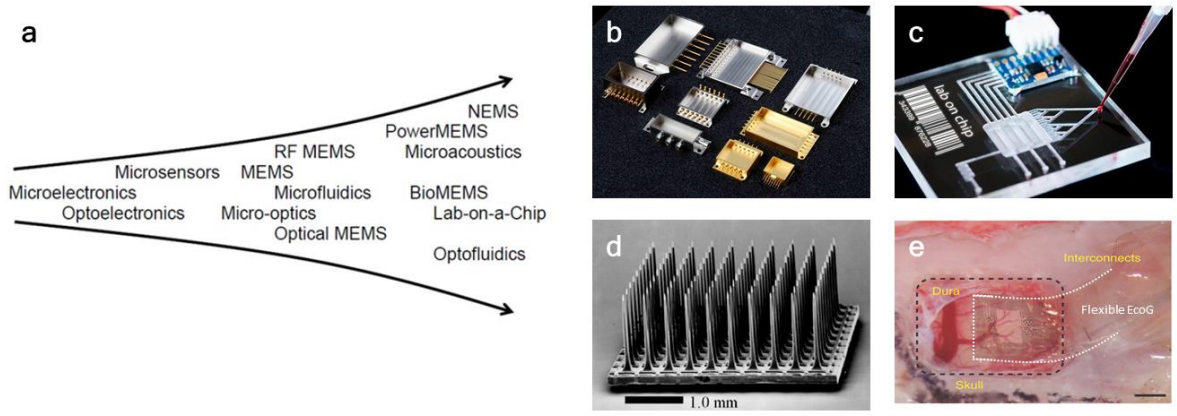

Figure 1. The growth in semiconductor industry. (a) A variety of fields have progressed as a result of applying microfabrication to (bio)electronics. Adapted from Aalto University in Finland. (b-e) Examples of integrated circuits (b), a lab-on-a-chip (adapted from Alamy) (c), the silicon-based Utah array (adapted from [41]) (d), and an organic-based EcoG (white dashed lines show the boundary of the EcoG) on top of a brain with the skull and dura removed (adapter from [18]).

The main advantages of organic electronics over inorganic electronics for bioelectronics applications are (1) the ability to conduct ions, in addition to electrons and holes, and (2) the soft nature of the material for a more conformable interface with living tissue [38]. Conductive polymers, such as polypyrrole [42], [43] and PEDOT:PSS [42], [44]–[47], have therefore extensively been studied in order to exploit these features for use in the neuroscience field.

In this chapter, the chosen materials are first introduced, along with the potential of these to enable the fabrication of *soft and organic bioelectronics*. The basic microfabrication steps are discussed, including photolithography and reactive ion etching. To conclude, a description of the fabrication of parylene-coated multi electrode arrays (MEAs) and flexible parylene probes will be given.

2.2 Choice of materials

The conformability of the final devices is obtained by the use of soft materials for both the substrate and the electronic interface. As explained in the previous chapter, a main goal of this work was to design flexible electronics to minimize (chronic) brain damage and enhance the recording performances of the electrodes. To this end, the main characteristics of the materials used during fabrication are presented here.

2.2.1 Parylene-C

Parylene-C (PaC) is used as the substrate and encapsulation material due to its remarkable properties for biomedical applications [48]. The polymer belongs to the poly(para-xyxylene) group and contains an additional chloride atom on the benzene ring, for which it has the additional letter C in its name *(Figure 2a-b)*. PaC is typically used as moisture diffusion barrier, as is chemically inert and it has a low dielectric constant ($\varepsilon \approx 3.1$ at 1 kHz [48], vs. 1 of

air and 78.2 for water). Moreover, the polymer is biocompatible and stable in physiological conditions, making it an attractive flexible electrical insulator.
Parylene is especially appealing due to its unique coating procedure of vapor deposition [48]. The polymer can be deposited on many different substrates, with sharp edges or on small areas, with a highly uniform thickness and is pinhole-free for films above at least 500 nm thickness [49]. Since the polymerization takes place through radical reactions *(Section 2.3)*, the polymer film is not chemically attached to the substrate below, nor does it contain any toxic components like catalysts or plasticizers. Moreover, the thickness of the film is proportional to the amount of loaded dimer at the start of the procedure, making it easy to variate the thicknesses according to the desired design [48].

Despite the potential to homogenously coat many different substrates, PaC does have the drawback of poor adhesion. Luckily, this problem has already been solved with the use of an adhesion promotor, such as silane A-174 [50]. Silane molecules, added to the deposition chamber, will chemically bind to the surface and provide a better adhesion surface for parylene. Furthermore, the use of oxygen plasma prior to the deposition further enhances adhesion, as it increases surfaces functionality and induces increased roughness [51]. Therefore, by employing these techniques, the problematic poor adhesion of parylene can be resolved.

Mechanically, PaC has shown great conformability to interface with soft tissue [18], [51] *(Figure 2d)*. With an appealing young's modulus of 3.7 GPa [52], it has shown its capabilities during both in vitro [47], [50] and in vivo applications [18], [46], [51]–[53]. While this compliancy is beneficial to potentially minimize chronic brain inflammation, the material requires an additional insertion system to position the microelectronics. To accomplish this, *Takeuchi et al.* reported for example on the fabrication of a parylene-based microfluidic system filled with PEG [53] and *Williamson et al.* used an SU8 shank to implant the flexible parylene probe into the brain [54]. Although these methods successfully positioned the microelectronics, a more tissue-friendly method is proposed and elaborated in Chapter 4.

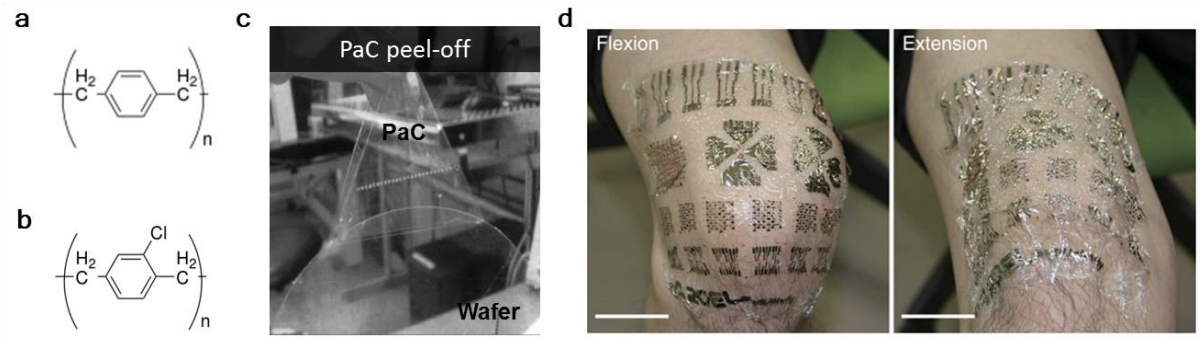

Figure 2. Presentation of parylene. (a-b) Structural formula of parylene (a) and parylene-C (PaC) (b). (c-d) Illustration of the conformability of a PaC-based device (c) during peel-off from a glass wafer, adapted from [46], and (d) on a human knee, adapted from [51].

2.2.2 Conducting polymer PEDOT:PSS

The discovery of conducting polymers (CPs) in 1977 led to an exciting new era of polymer-based electronics. Although it was initially thought that polymers ('plastics') were all insulators (i.e. non-conducting materials), this changed when polyacetylene showed to be highly conductive when 'doped' through the oxidation with a halogen (chlorine, bromine or iodine) [40]. A conductivity of 10^5 Siemens per meter (S/m) was achieved, which is in between that of an insulator such as Teflon (10^{-16} S/m) and that of a conductor such as copper (10^8 S/m). This led to the investigation of other polymers, including polypyrrole, polyaniline and polythiophenes *(Figure 3a)*, which all showed the same conductive behavior when doped. It was seen that CPs appeared to have a conductivity comparable to that of semiconductors *(Figure 3b)*.

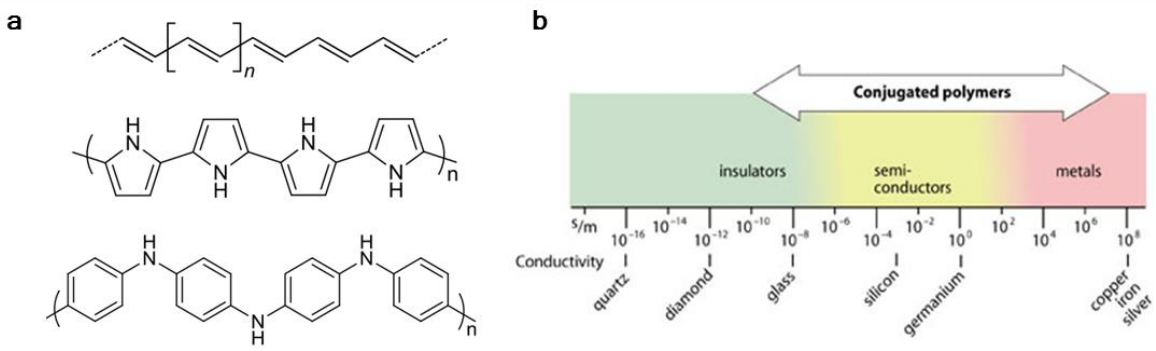

Figure 3. Presentation of conducting polymers. (a) Structural formula of polyacetylene, polypyrrole and polyaniline. (b) conductivity of conducting polymers compared to other materials, ranging from insulators (quartz) to conductors (metals). Adapted from [40].

What makes a CP conductive? Conductivity in a CP is induced by doping the polymer. A CP has conjugated bonds in its backbone, which are alternating single and double bonds. The single bond (σ–bond) is a strong chemical bond with localized electrons and the double bond (π–bond) is a weaker bond with delocalized electrons. By injecting extra electrons (via reduction, n-doped) or removing electrons, creating so-called 'holes' (via oxidation, p-type), the material is doped and allows the transport of charge across its backbone (i.e. conduction).

Why are CPs so important for the field of bioelectronics? Researchers strive towards improving the signal resolution of neural recordings with the ultimate aim to map and understand the connectivity of small neurons inside the brain. A high signal resolution can be achieved by making electrodes small. However, the reduction in electrode area results in a decrease of capacitance (ability to store electrical charge), an increase of impedance (effective resistance to the current flow) and thus a decreased signal resolution at the electronic/tissue interface. This is where CPs show their potential, as these polymer films have shown to decrease the impedance while maintaining a small electrode area [42], [55], [56]. CPs significantly increase the surface roughness of the metal electrode it is coated on, thereby providing a larger area of interaction with the soft neural tissue [57]. In addition to increase the effective surface area, these polymers have a mixed electronic/ionic conductivity. By not only transporting

electrons and holes, but also taking up biologically relevant ions, the entire volume of CP films is utilized, allowing for a more efficient transduction of biological signals [56].

Among various CPs, poly(3,4-ethylenedioxythiophene) doped with poly(styrene sulfonate) (PEDOT:PSS) is considered one of the most promising candidates for neural interfacing. PEDOT:PSS is a p-type doped semiconductor with sulfonate groups of PSS entangled in the PEDOT region *(Figure 4)*. The conducting polymer has been described as having a 'pancake-like' morphology with PEDOT-rich (blue) domains in a supported matrix of PSS (grey) [58]. PEDOT oligomers are believed to polymerize along the PSS chain, which is present in large excess and stabilizes the material in aqueous environment. The CP is particularly interesting due to its commercial availability as dispersion for solution processing, its relatively high conductivity (~1000 S/cm), and its electrical and chemical stability in an wet environment [58], [59]. Additionally, this CP provides a soft interface (40 MPa when hydrated) which reduces the mechanical mismatch of metals used below the polymer coating [21].

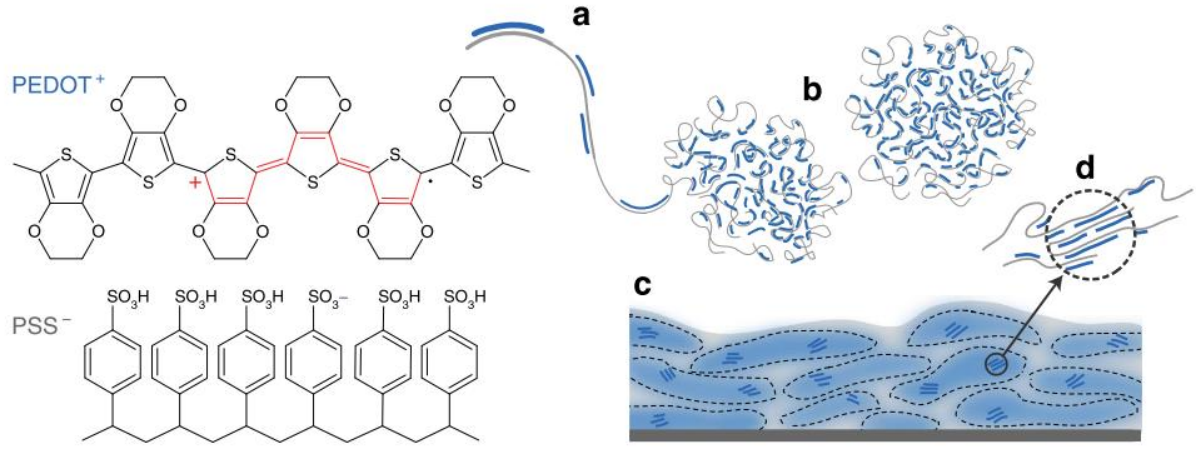

Figure 4. PEDOT :PSS structure and morphology. The structural formula of PSS-doped PEDOT along with a schematic of the micro- and macrostructure of PEDOT:PSS. (a) Short chains of PEDOT (blue) polymerize along the long PSS chains (grey). (b) Gel-like particles are formed in dispersion. (c) The resulting film with PEDOT:PSS (blue) and PSS (grey) regions in a pancake-like organization. (d) Well-organized (crystallite) regions within the PEDOT:PSS region. Adapted from [58].

PEDOT is rendered conductive through either vapor-phase chemical or electrochemical polymerization [61]. During *chemical synthesis*, oxidants like iron(III)sulfate or potassium peroxodisulfate are added to the monomeric EDOT solution, which polymerize the PEDOT into short chains. PSS is added as the counter-ion to stabilize the entire complex. Chemically polymerized PEDOT:PSS is commercially available in aqueous solution. This stable dispersion is usually spin-coated to generate a thin polymer film, dried and further patterned through photolithography [46]. PEDOT:PSS can also be obtained through *electrochemical deposition* by dissolving the monomeric unit EDOT in aqueous solution with

PSSNA and applying galvanostatic (constant current) or potentiostatic (constant voltage) procedures [61], [62]. Electrochemical polymerization allows for the introduction of a wider range of counter-ions, like perchlorate (ClO^{4-}) or small biomolecules such as the neuron binding peptide YIGSR [62]. Interestingly, the two different techniques for PEDOT:PSS have recently been compared by our group in collaboration with D.C. Martin and despite the different physical appearances of the films observed with scanning electron microscopy (SEM) *(Figure 5)*, the study essentially showed very similar and low impedances [61].

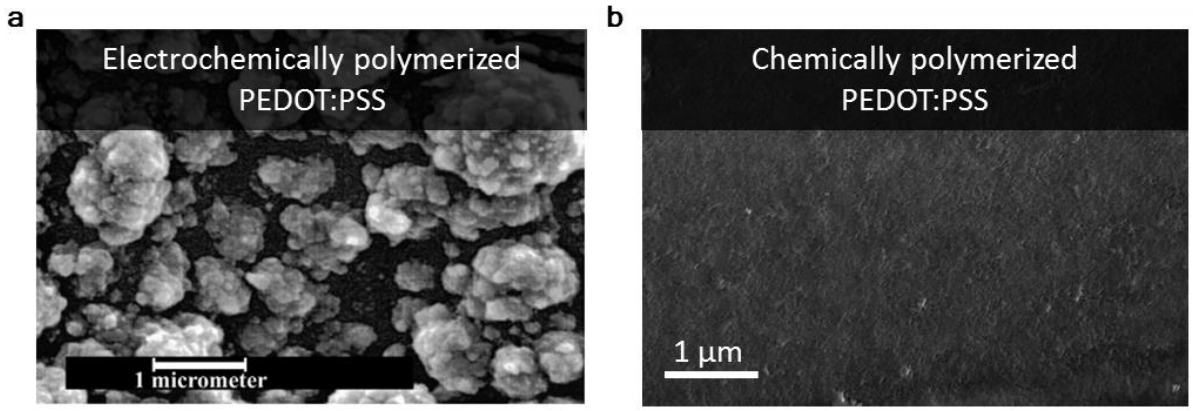

Figure 5. The difference in polymerized PEDOT :PSS film on top of golden electrodes using SEM. (a) Electrochemically polymerized (adapted from [62]) and (b) chemically polymerized PEDOT:PSS films (SEM made by M. Donahue).

Although conductive PEDOT:PSS is commercially available aqueous solution (Clevios PH1000, Hereaeus), there are several methods to further improve the thin film coating properties. The standard formulation utilized throughout this work contains a mixture of 95% Clevios PH1000 with 5% v/v ethylene glycol (EG), 0.25% v/v dodecylbenzenesulfonic acid (DBSA) and 1% of 3-glycidoxypropyltrimethoxysilane (GOPS) *(Figure 6)*. Each component has a particular influence on the final conductive film, which has shown on average a conductivity of 850 S/cm [58]:

- EG: This co-solvent has a significant effect on both charge transports (ionic and electronic) inside the bulk of the material [58]. Various concentrations of ethylene glycol were investigated in the aqueous solution. Ultimately, 5 % v/v showed the most promising result with high conductivity (800 S/cm) and reasonable ion mobility (1.7 $cm^2 V^{-1}s^{-1}$).

- DBSA: This surfactant improves the wettability of the PEDOT:PSS film, to enable better film formation [50]. Moreover, there are data showing that the addition of 2 % v/v improves the electrical conductivity of the film [63]. However, such large concentrations resulted in poor film quality, counteracting the initial reason for this addition. Thus, a minimal amount of DBSA is sufficient to ensure proper film formation.

- GOPS: This is a common surface adhesion promoter and cross-linker, which enhances the stability of PEDOT:PSS films on various substrates [50].

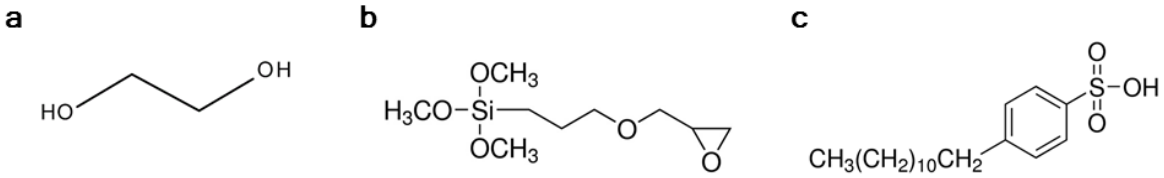

Figure 6. The structural formula of the additional components used to enhance the conductivity and stability of Clevios PH100. (a) Ethylene glycol (EG), (b) Dodecylbenzenesulfonic acid (DBSA) and (c) 3-glycidoxypropyltrimethoxy-silane (GOPS).

2.3 Microfabrication of organic materials

In the 1950's, Bell Laboratories was the first industrial enterprise to use photolithography to pattern silicon-based devices. Analogous patterning techniques are also applicable to organic materials, as demonstrated by *DeFranco and colleagues* [49]. These techniques were applied to both the in vitro and in vivo devices in this work, which will be discussed in the following sections. Before proceeding to those details, a short description is given here on the techniques used during fabrication.

Microfabrication must be performed in a so-called cleanroom to ensure the accurate, microscale patterning of the devices without contamination. A cleanroom is a tightly controlled environment which continuous regulates the number and sizes of pollutants (such as dust, airborn microbes, aerosol particles, etc.), the humidity and the temperature. The work presented here was performed in a cleanroom facility with a minimum level of 100 particles of size 0.5 μm per cubic foot ('S100' - i.e. no more than 2.83 particles of 0.5 μm per cubic meter, compared to an outside urban environment which contains 35,000,000 particles of 0.5 um or larger per cubic meter).

Chemical vapor deposition Parylene-C is deposited through chemical vapor deposition (CVD). The raw material consists of a dimer with two para-xyxylene moieties as shown in *Figure 7*. It is first vaporized in an evacuated chamber (around 175 °C) and then pyrolyzed at high temperature (above 550 °C) to become radical monomers. These reactive monomers enter the deposition chamber which remains at room temperature and condense on the surfaces. The radical terminals thereby polymerize and form long, randomly orientated polymer chains.

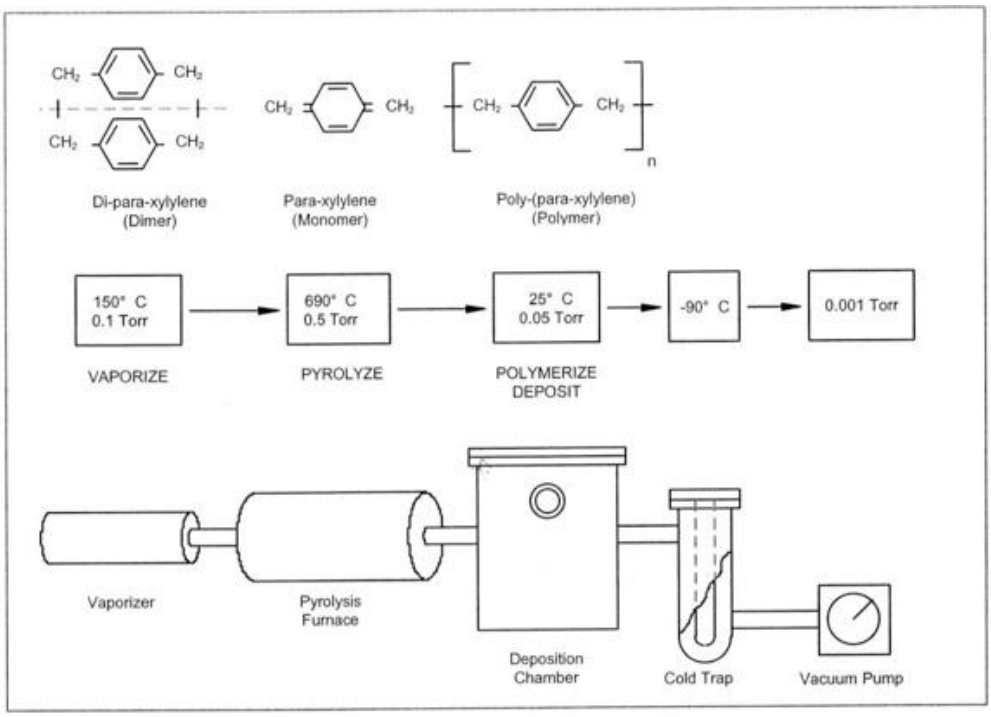

Figure 7. The process of chemical vapor deposition (CVD) of parylene.

Photolithography Micro-patterning of (inorganic or organic) material is carried out through the use of photosensitive materials, a photoresist (or simply 'resist'), which is deposited by spin coating *(Figure 8)*. The resist is exposed to UV-light through a photomask which contains the pattern to be transferred. After treatment with a developer, the pattern becomes visible in the resist film. The developer either removes the exposed resist parts (positive resist) or the unexposed parts (negative resist). This development is typically performed in an alkaline solution, as the resins of the resist are hydrophilic and the photosensitive compounds becomes hydrophilic after exposure (positive resist) or crosslink and remain present on the wafer while the unexposed resist areas are washed away (negative resist).

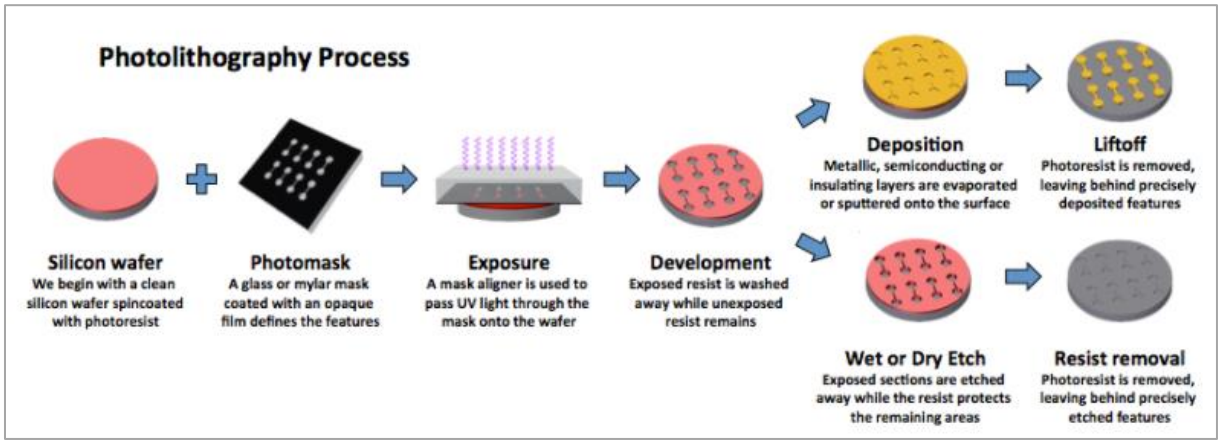

Figure 8. Illustration of a photolithography process using a silicon wafer. Adapted from the University of California Santa Cruz (UCSC).

Reactive ion etching This procedures enables the removal of material not protected by a photoresist using chemically reactive plasma *(Figure 9a)*. Substrates are placed into a vacuum chamber, where a gas is ionized by a radiofrequency electromagnetic field. This creates reactive plasma, which chemically and physically removes the unprotected (organic) material. Volatile products removed from the substrate are extracted through a pump system. Besides this described dry etching technique, wet etching is the alternative approach for a more isotropic removal by the immersion of the substrate in an etching solution *(Figure 8)*. Note: wet etching was not used during this work.

Strip-, lift and peel-off Once the pattern is physically transferred onto the (organic) material, the resist has served its purpose and can be removed (‘*stripped off*’) by the use of an appropriate solvent. Similarly, *lift-off* represents a process which does not require any etching as the desired pattern is directly transferred by the resist. In this case, the to-be patterned material (such as metal) is deposited after the resist is spin-coated and patterned *(Figure 8)*. After *lift-off* in an appropriate solvent, the deposited material remains in the areas not protected by the resist, while the protected areas are removed, taking away the deposited material. *Peel-off* is another patterning method which is used to selectively coat microelectrodes with PEDOT:PSS. It involves the use of a sacrificial parylene layer on top of the insulating layer, which are both etched through reactive ion etching. Subsequently the sacrificially layer is physically peeled-off after spin-coating PEDOT:PSS across the entire wafer.

Metal evaporation This technique allows the deposition of thin metal layers (with nanometer precision) in a vacuum chamber *(Figure 9b)*. The metal is placed on a crucible (a container which withstands very high temperature), thermally evaporated and condenses on the substrates placed at the top of the chamber. The evaporation requires vacuum with a typical pressure of 10^{-4} Pa, to prevent any contamination of other vapors and to allow the metal vapor particles to travel directly to the substrate.

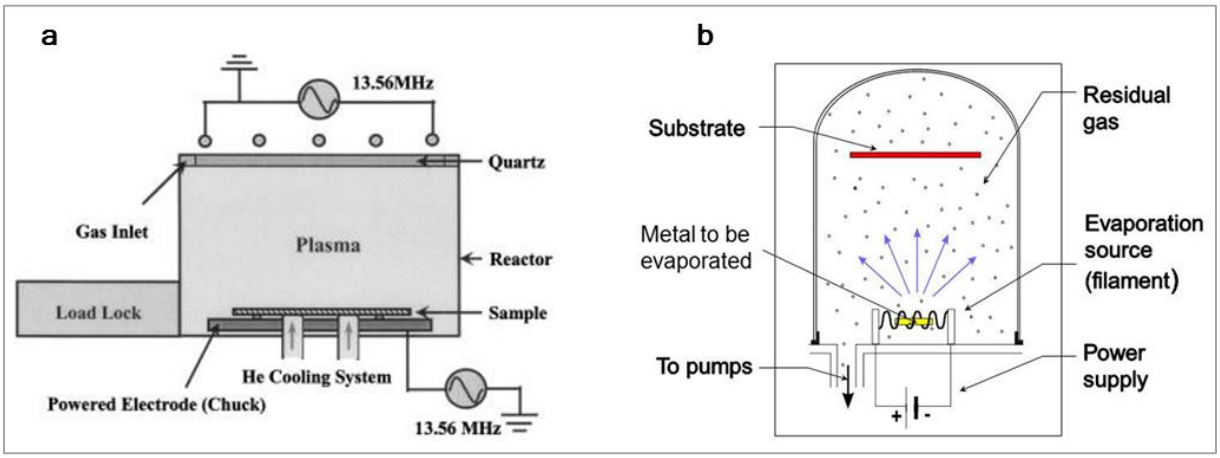

Figure 9. Presentation of a (a) dry etching machine and (b) metal evaporator.

2.4 Microelectrode array fabrication

The MEAs consist of glass slides which are patterned with chromium and gold contact lines and insulated with parylene-C to create a soft interface. The microelectrodes are patterned with PEDOT:PSS to decrease the impedance for a better signal-to-noise ratio. While the exact parameters are reported in the protocol shown in *Figure 10*, a brief explanation is given below to guide the reader through the fabrication process with some additional remarks.

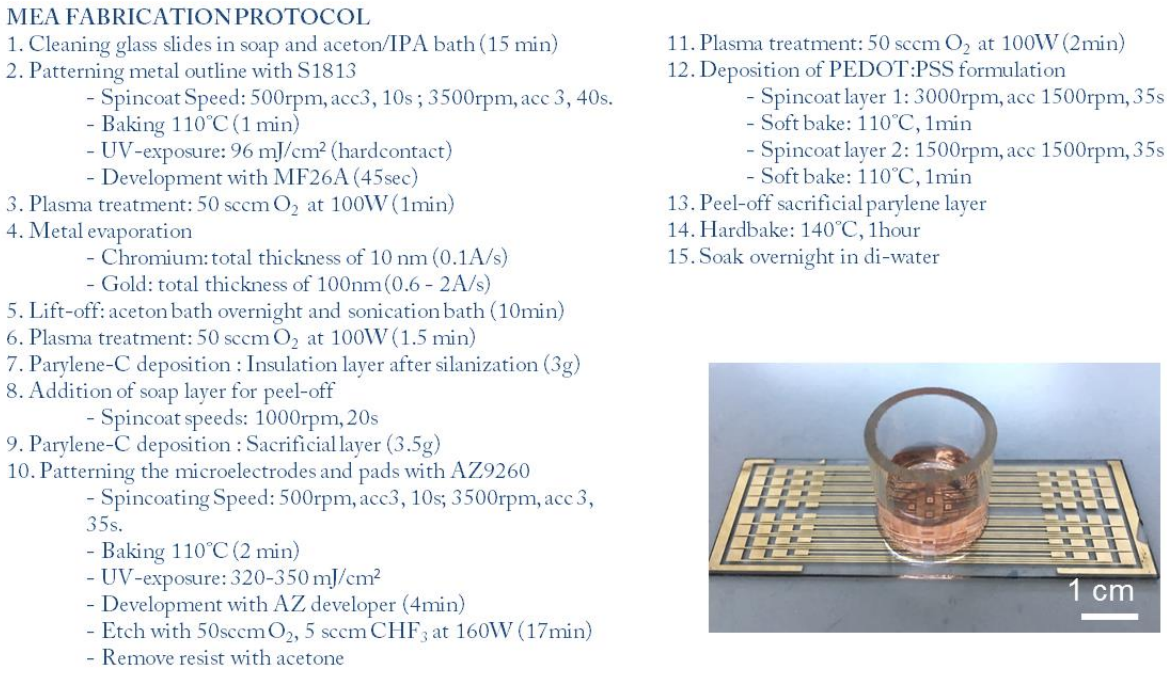

Figure 10. The fabrication protocol of MEAs and a picture of a final MEA device ready for cell-culture.

Before any procedure is performed on the glass substrates, a thorough washing should take place to remove any contamination which could interfere during the fabrication process. The glass slides are first manually cleaned with a tissue and soap, followed by sonication for 15 min in a soap bath and an acetone/isopropanol bath for another 15 min. The substrates are rinsed with deionized water (DI water) and dried with a nitrogen gun. The metal outline is then patterned on the substrate, using the positive photoresist S1813. The resist is spin-coated, baked for dehydration, exposed to UV light and developed in MF26A. To ensure a good adhesion of the metal on the substrate, a plasma treatment is followed which removes any photoresist residue within the pattern. During metal evaporation, chromium is first evaporated to a thickness of ~10 nm. Chromium serves as adhesion promotor for gold, which is evaporated with a minimal thickness of 100 nm. Next, the glass slides are placed in an acetone bath overnight for lift-off. To aid the lift-off process, sonication may be employed along with the use of cue-tips to manually remove the remaining undesired chromium/gold. The device is kept wet with isopropanol to inspect the pattern under the microscope.

Subsequently, the insulating PaC layer of the MEA is deposited. To ensure good adhesion, oxygen plasma treatment is again performed and silane is added to the CVD chamber where the substrates are placed. The final thickness of the parylene layer is dependent on the amount of PaC dimer loaded for deposition, with 2 grams resulting in approximately a 1 μm thick layer. Before patterning and etching the insulation layer to open the connector pads and microelectrodes, a second sacrificial layer of parylene is deposited. Prior to this deposition, a 2% soap solution is spin-coated onto the substrates to ensure smooth final peel-off. The contact pads and microelectrode openings can subsequently be patterned, using a viscous AZ resist as an etch mask. This resist allows for a thicker and more resilient protective layer, necessary to allow etching through the two parylene layers. The remaining resist is removed with acetone.

Finally, the microelectrodes can be coated with the previously described PEDOT:PSS formulation: 95% Clevios PH1000 with 5% EG, 0.25% of DBSA and 1% of GOPS (v/v) *(Section 2.2.2)*. The solution is spin-coated and shortly baked to remove most of the solvent. A second spin-coating is performed to increase the thickness of the PEDOT film further, which has shown to scale with the capacitance of the electrodes [64], [65]. Since the electrodes and connector pads are etched at the same time, the pads will also be covered in PEDOT during this deposition step. This excess of PEDOT can still mechanically be removed with a wet cue-tip, without placing too much force on the device to not damage the underlying insulation layer. The sacrificial parylene layer is then peeled off and the devices are placed on a hotplate for a final hard-bake. This step ensures the crosslinking of the GOPS inside the PEDOT film, which improves the adhesion of the conducting polymer and the film stability. Before cell culture, the devices are soaked in deionized (DI) water overnight which allows the removal of excessive low molecular weight compounds from the PEDOT film and a glass well is attached on top.

Figure 11 shows an overview of the microelectrodes on the MEA device. Each MEA contains 64 electrodes *(Figure 11a)*. Various spacing's were used in the design, with respectively 100 μm and 150 μm in between the electrodes in the same row and column and 200 μm of spacing in between the 4th and 5th row. The electrodes had a metal area of 20 x 20 um^2, which was mostly covered with PEDOT:PSS (14 x 14 um^2). The darker blue color on the microelectrodes originates from the conducting polymer PEDOT:PSS. A cross-section of an electrode made shows the full coverage of the gold with PEDOT:PSS and the tight insulation layer of parylene around *(Figure 11c)*. This was accomplished by focused ion beam-scanning electron microscopy (FIB-SEM) with collaborator *F. Santoro* [66].

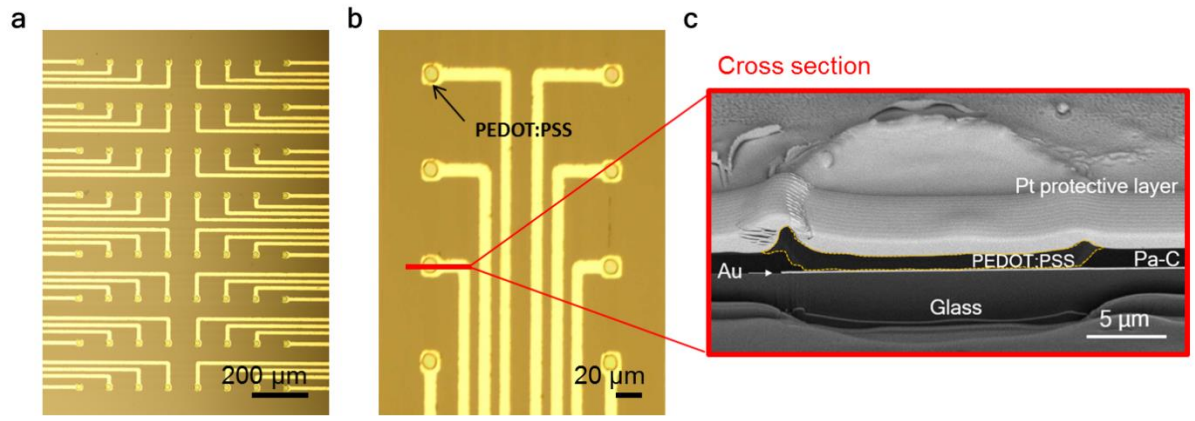

Figure 11. Microelectrode array overview. (a) Overview of the 64 electrodes on the custom-made MEAs. (b) Zoomed-in view of PEDOT:PSS-coated electrodes. The red line indicates the location of the cut performed with FIB. (c) FIB-SEM image of the cross-section. The MEA consists of a glass substrate, with a metal pattern, electrode openings covered with PEDOT:PSS and insulated with Parylene-C. A platinum protection layer is added to perform the FIB cut and image with SEM. Abbreviations used: PaC, Parylene-C. Au, gold.

2.5 Flexible depth probe fabrication

The fabrication of the flexible depth probes is similar to the process described above, with the exception of having an additional parylene layer deposited initially to act as the final substrate. Thus, a multi-stack parylene design is used, which makes the fabrication slightly more sensitive to defects in the layers and can result in complete delamination if not careful. To avoid repetition of previously explained steps, only the additional steps will be discussed in this section. The reader is referred to the *Figure 12* below for the entire procedure.

Flexible Probe Fabrication

1. Cleaning glass wafers in soap and acetone/IPA bath (15 min)
2. Plasma treatment: 50 sccm O_2 at 100W (1 min)
3. Parylene-C deposition: substrate material (4.2 g)
4. Patterning metal outline with LOR/S1813
   - Spincoating Speed LOR: 500rpm, acc. 5, 10 s; 3000 rpm, acc. 1, 40s.
   - Baking 200˚C (5 min)
   - Spincoating Speed S1813: 500rpm, acc 5, 10s; 5000rpm, acc 1, 40s
   - Baking 115˚C (2 min)
   - UV-exposure: 96 mJ/cm² (hardcontact)
   - Development 1 in MF26A (45 s)
   - **Hard-bake: 125˚C, 5min**
   - -Development 2 in MF26A (1 min)
5. Plasma treatment: 50 sccm O_2 at 100W (1 min)
6. Metal evaporation
   - Chromium: total thickness of 10 nm (0.1A/s)
   - Gold: total thickness of 100nm (0.6 - 2A/s)
7. Lift-off overnight in NMP
8. Plasma treatment: 50 sccm O_2 at 100W (1 min)
9. Parylene-C deposition: Insulation layer after silanization (3 g)
10. Patterning probe outline with AZ9260
    - Spincoat speeds: 500 rpm, acc. 5, 10 s; 3000 rpm, acc. 1, 40 s
    - Baking 110˚C (2 min)
    - UV-exposure: 65-90 mJ/cm² (hardcontact)
    - Development in AZ developer (4min)
    - Etch with 50sccm O_2, 5 sccm CHF_3, 160W (15 min)
    - Remove resist with acetone
11. Addition of soap layer for peel-off
    - Spincoat speed: 1000rpm, 20s
12. Parylene-C deposition : Sacrificial layer (3g)
13. Patterning the microelectrodes and pads with AZ9260
    - See step 10.
    - UV-exposure: 65-90 mJ/cm² (hardcontact)
    - Development with AZ developer (4min)
    - Etch with 50 sccm O_2, 5 sccm CHF_3 at 160W (17 min)
    - Remove resist with aceton
14. Plasma treatment: 50 sccm O_2 at 100W (1 min)
15. Deposition of PEDOT:PSS formulation
    - Spincoat layer 1: 3000rpm, acc 1500rpm, 35s
    - Soft bake: 110˚C, 1min
    - Spincoat layer 2: 1500rpm, acc 1500rpm, 35s
    - Soft bake: 110˚C, 1min
16. Peel-off sacrificial parylene layer
17. Hardbake: 140˚C, 1hour
18. Soak overnight in di-water

Figure 12. Fabrication protocol of flexible neural probes.

During this microfabrication process, glass wafers were used to fabricate multiple probes simultaneously. After the cleaning step, parylene is deposited to function as substrate material for the probes (S*tep 2 and 3*). The patterning of the metal outline is carried out using an additional lift-off resist (LoR) before depositing S1813 (*Step 4*). This photoresist results in an undercut profile, which facilitates the lift-off by preventing sidewall coverage of the subsequently deposited metal interconnects. Lift-off is carried out by leaving the wafers in N-methylpyrrolidon (NMP) overnight to remove all the remaining resists (*Step 7*).

Following deposition of the insulating PaC layer and before the deposition of the 2% soap solution (*Step 11*), the outline of the probe is to be etched. This cannot be done simultaneously with the etching of the pads and electrodes (*Step 13*) as this would prevent the possibility to perform the sacrificial peel-off. As previously explained, AZ9260 resist is utilized as an etch-mask for the parylene. The following steps (soap deposition, sacrificial PaC deposition, RIE etching and PEDOT:PSS deposition) have been explained in *Section 2.4*. Note, that the deposition and spin-coating of the 2% soap solution should be done as quickly as possible. Prolonged contact to the aqueous solution may cause the probes to detach slightly and the alignment of the microelectrodes will not be accurate.

The final result is a glass wafer which contains multiple probes with a final thickness of only 4 μm that were simultaneously fabricated *(Figure 13a)*. The probe tip, which is the part that penetrates the mouse brain, is designed to be either 2.5 or 3 mm long with a tip width of the tip 180 μm *(Figure 13b)*. The connector pads (illustrated with white dashed lines on one side) are relatively long, to facilitate handling during electronic connection steps. There are 6 microelectrodes at the end of each tip, which have a diameter of ~15 um and are slightly colored blue from the PEDOT:PSS coating *(Figure 13c)*. The electrodes are separated from each other by 90 μm (center to center) and the tip has a sharpness angle of 20°.

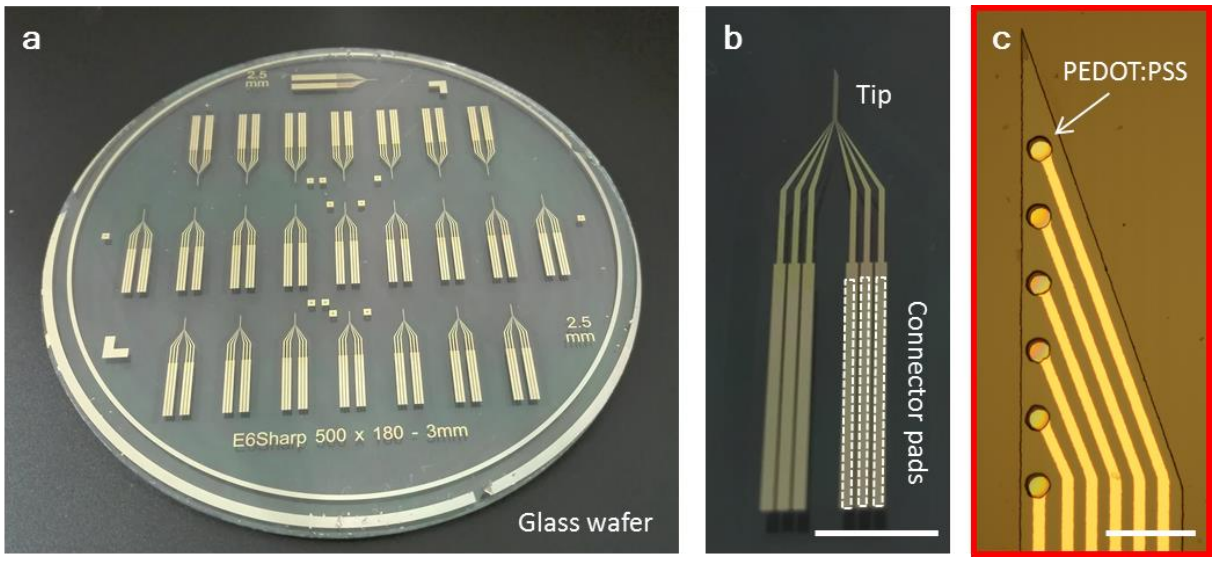

Figure 13. Presentation of the parylene-based depth probes. (a) A glass wafer with 24 probes attached to it. The tips have a length of 2.5 or 3 mm. (b) A picture of a single probe. The connector pads are illustrated on the right side of the probe with white dashed lines. The tip is the upper part which will penetrate the brain. *Scale*

bar: 4.8 mm. **(c) A microscope picture of the tip, showing the 6 microelectrodes with a PEDOT:PSS coating (blueish) on top. The width of the probe tip is 180 μm and the tip has an angle of 20°.** ***Scale bar: 100 μm.***

2.6 Electrical characterization

The MEAs and flexible probes were electrically characterized before use through electrochemical impedance spectroscopy (EIS). This is a well-known characterization method to study charge transfer processes at the electrode/electrolyte interface. The impedance measurements were performed with an Autolab potentiostat (PGSTAT128N) in a three electrode configuration. An Ag/AgCl reference electrode and Pt counter electrode were used, along with the recoding electrode of the MEA as the working electrode. The characterization was performed in DPBS solution by applying a 10 mV root mean square (RMS) sine wave over a large frequency range of 1 Hz to 100 kHz. The impedance amplitude at 1 kHz is a key value typically used to compare neural interfacing electrodes as single neural activity occurs at this frequency.

2.6.1 PEDOT:PSS MEAs

The EIS impedance spectrum of our PEDOT:PSS-coated microelectrodes is shown in *Figure 14a* and is similar to previously reported data on conducting polymer coated electrodes [50], [61], [67]. At high frequency the impedance is relatively low, while this significantly increases towards lower frequencies. There are generally three frequency regions defined [67], based on the equivalent circuit model describes earlier in this thesis *(Chapter 1, Section 1.2.2)*.

(1) High frequency region: A resistive behavior is observed, corresponding to the resistance of the phosphate solution between the working and reference electrode. The resistance is low and the phase angle is near zero.
(2) Middle frequency region: A linear relationship between the impedance modulus and the log frequency. This corresponds to the capacitance of the electrode/electrolyte interface. The impedances increases from high to low frequency and the phase angle decreases to – 90° (Note: The minus sign in the Y-axes title of the phase (*Figure 14a*)).
(3) Low frequency region: The impedance continues to increase, while the phase angle has reached its maximum and increases slightly again.

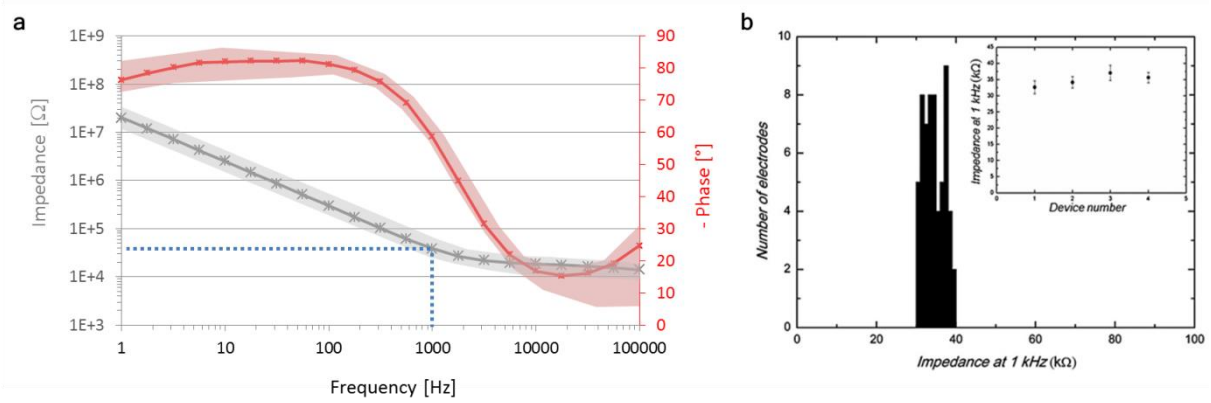

Figure 14. The impedance responses of PEDOT :PSS coated microelectrodes. (a) Electrochemical impedance spectrum with the impedance and frequency axes in logarithmic scale. The impedance modulus is shown in grey and the phase angles in red. The area colored around the measured data points show the observed variations between multiple measurements (n=20). The low impedance at the biologically relevant 1 kHz is emphasized with the blue dotted line. (b) The variation in impedance at 1 kHz of 60 microelectrodes from 4 different MEAs (n=60). An average of 34.6 ± 0.3 kΩ was measured at 1 kHz. Inset: The variation in average impedance at 1 kHz between the 4 MEA devices. Adapted from *Koutsouras, Hama, Pas, et al.* [47]. Data is presented as mean ±SD.

Although the impedance at 1 kHz is a delicate boundary due to the sudden increase of impedance, the addition of PEDOT:PSS keeps the impedance sufficiently low. On average, an impedance of 34.6 ± 0.3 kΩ was observed at this biologically relevant frequency (n=60) (*Figure 14b)*. The impedance of 12 x 12 μm² microelectrodes coated with PEDOT:PSS show an impedance distribution mainly between 30 to 40 kΩ. Only a small variation was observed between different MEA devices *(Inset of Figure 14b).*

2.6.2 PEDOT:PSS coated probes

To improve the electrical connection during in vivo recordings with a 4 μm thin parylene probe, a ZIF connection (Mouser™) attached to the probe. This is accomplished by using an anisotropic conductive paste (ACP, Kyocera™), which is an interconnection adhesive consisting of a polymer matrix with small conductive beads [68]. A conductive pathway is formed from one metal contact (ZIF cable) to the other metal contact (connector pad of probe) via the conductive beads which are put in place under pressure and heat. The beads have nanometer sizes with insulating polymeric matrix in between to prevent cross-talk between the different contact pads.

Figure 15 shows how the ACP is applied between the parylene probe and the ZIF cable. A soldering machine is used to accurately align the two substrates *(Figure 15 a)*. ACP is applied on the cable, which is attached with kapton tape in the middle of a glass slide *(Figure 15 b)*. To ensure homogeneous pressure, a ZIF cable is cut in two and attached on both sides of the ZIF cable of interest *(Figure 15 d)*. The ZIF-glass slide is held upside down by applying vacuum and the probe is placed on a kapton sheet on a glass holder below with the connector pads upwards *(Figure 15 e)*. After the alignment is performed using a camera (screen, *Figure 15*a), the ZIF-glass slide is lowered onto the probe to make contact and apply sufficient pressure. A temperature profile is executed, heating the sample for 4.5 min at 75 °C

and 95°C *(Figure 15 e-f)*. The complex is then lifted up from the holder, removed from the glass slide and the result is a ZIF-cabled flexible probe on a kapton sheet *(Figure 15i)*.

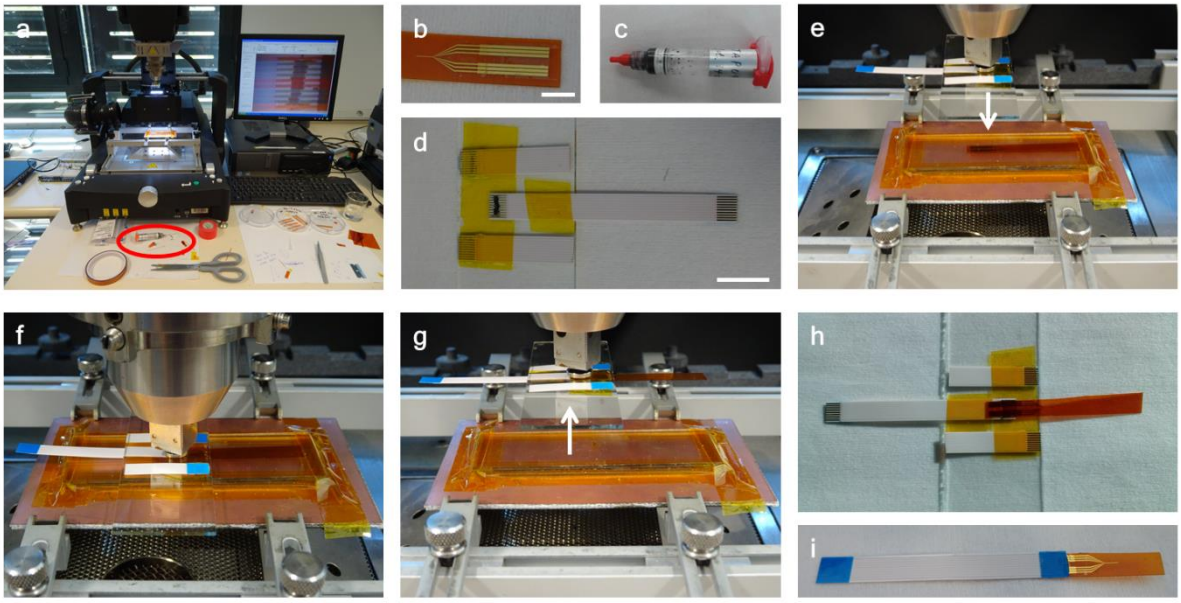

Figure 15. Illustration of the ZIF cable attachment to a parylene probe. (a) Soldering machine with camera connected to the computer to follow the alignment of the ZIF cable to the probe. (b) Parylene probe on a kapton sheet (orange). (c) anisotropic conductive paste (ACP). (d) ZIF cable attached to glass substrate with ACP on top of metal contacts. (e-g) soldering of ZIF to probe, by lowering the cable onto the probe, heating up the sample under pressure and lifting the ZIF-probe complex up. (h) The probe attached to (d) after soldering. (i) The result: the probe on a kapton sheet attached to a ZIF cable.

Not surprisingly, the same frequency-dependent impedance trend is observed during EIS measurements *(Figure 16)*. There is however a larger variation in impedance compared to the MEAs, as shown in *Figure 16b*. This is explainable due to various fabrication challenges, such as the variations in PEDOT:PSS thickness dependent on the probe location on the glass wafer during spin-coating and the mechanical stress placed on the probe for removal of the wafer. Nevertheless, the impedance remains low with an average 36.0 ± 14.2 kΩ (n=28), and occasionally one or two electrodes on a device showing an impedance above 1 MΩ. The MΩ values were not taken into account when calculating the average *(Figure 16b)*, as these are considered as outliers (<7% of electrodes).

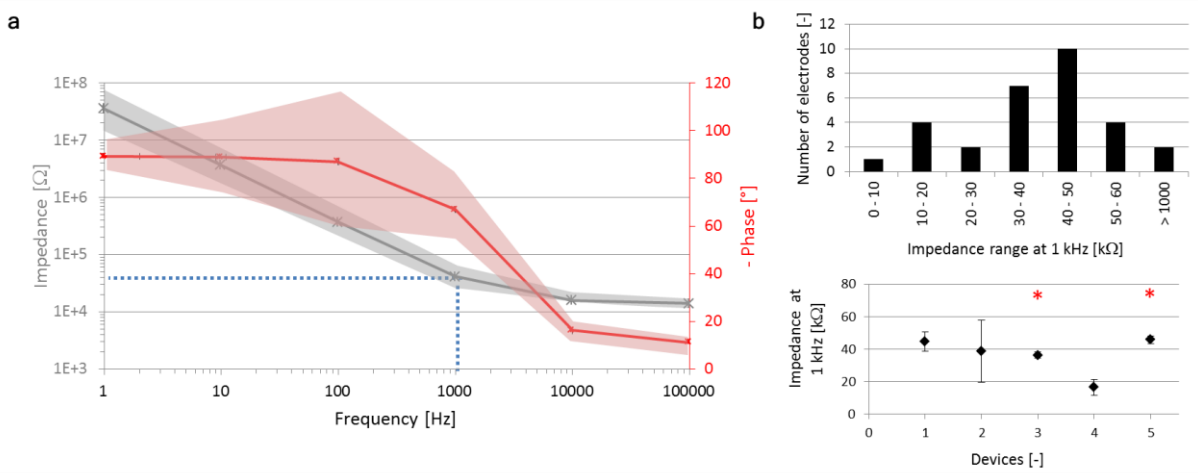

Figure 16. The impedance responses of PEDOT:PSS coated microelectrodes on flexible probes. (a) Electrochemical impedance spectrum. The impedance modulus is shown in grey and the phase angles in red. The area colored around the measured data points show the standard deviation of the measured electrodes (n=30 electrodes, 5 probes). The low impedance at the biologically relevant 1 kHz is emphasized with the blue dotted line. (b) The variation in impedance at 1 kHz of 30 microelectrodes from 5 different probes (n=30), shown by classifying the measured impedances in a particular impedance range and per device. An average of 36.0 ± 14.2 kΩ was measured at 1 kHz. Data is presented as mean ±SD.

2.7 Conclusion

In this Chapter, the microfabrication procedures of PEDOT:PSS-coated MEAs and flexible depth probes has been introduced. Parylene-C and PEDOT:PSS were chosen as substrate and coating materials to provide a flexible and low-impedance neural interface. The ease of deposition with a guaranteed homogenous layer and the highly conformable character of parylene make the biocompatible polymer an ideal substrate material to interface with soft brain. Moreover, the impedance of our small microelectrodes was lowered with the use of conducting polymer PEDOT:PSS. This is important to eventually improve the recording capability during the *in vitro (Chapter 3)* and *in vivo* experiments *(Chapter 4)*.

Chapter 3. In vitro: Enhancement of single unit recordings

This Chapter is based on the publication:

"Neurospheres on patterned PEDOT:PSS microelectrode arrays enhance electrophysiology recordings.", J. Pas, C. Pitsalidis, D.A. Koutsouras, P. Quilichini, F. Santoro, B. Cui, L. Gallais, R.P. O'Connor, G.G. Malliaras and R.M. Owens (2017) *Adv. Biosystems.* DOI: 10.1002/adbi.201700164.

3.1 A challenge: Single cell recordings on microelectrode arrays

The brain is continuously processing electrochemically transduced information via an entangled yet organized network of billions of neurons. As the most complex organ in the human body, subtle changes in its structure and function can greatly affect the quality of life. Almost 2% of the total world's population suffers from neurological disorders, a number that is expected to grow substantially in the future [1]. There is thus a great need to understand the nature of disorders of the central nervous system in general to diagnose them and develop therapies.

One way to systematically study the electrophysiology of neural systems is through in vitro recording of neural activity using microelectrode arrays (MEAs) [69]. MEAs provide a non-invasive way to record changes in the extracellular field generated by cells cultured on the device. The electric field is caused by the ionic currents flowing through the cell membranes and include the fast action potentials of individual neurons (i.e. unit activity), subthreshold synaptic potentials and even slow glial potentials [15], [16]. The extracellular detection of those signals in vitro, can be modeled using an electronic circuit (reviewed and detailed by Spira et al. [17]) and depends mostly on the magnitude, sign and distance of the neurons from the electrode site [15], [16]. In a successful recording, the extracellular signal is in the range of tens to hundreds of microvolts and is measured within some milliseconds. In 1980, Pine was the first to report MEA recordings from dissociated neuronal cultures [70]. Since then, this in vitro method has been widely explored and a diverse catalogue of MEAs have been developed for different applications [15], [17], [69]. Essential for in vitro recording are: (1) an accurate and sensitive recording system and (2) an electrically active neural network. To this end, various device designs and neural cell culture optimizations have been explored to improve the success of microelectrode studies, as briefly described below.

On the device side, two- and three-dimensional designs have been investigated to improve electrical coupling between neurons and recording sites [15], [17], [71]. Microelectrodes are typically made of metallic conductors, such as gold, titanium nitride, platinum, etc. Generally, the electrode size, number and inter-electrode spacing vary between 5 to 50 μm, 32 to 60 and 100 to 250 μm, respectively [71]. The recording performance of the microelectrodes can be improved by increasing their effective surface area by surface modification with nanostructures or other electrode coatings, thereby reducing the electrode impedance. Examples of such modifiications include porous platinum black, golden nanoflakes or -pillars, carbon nanotubes, conducting polymers such as polypyrrole and poly(3,4-ethylenedioxythiophene):poly (styrenesulfonate) (PEDOT:PSS) [47], [50], [55], [71], [72]. To further improve MEA recordings, recent efforts have focused on creating three dimensional microelectrodes to interface intracellularly with cells [17]. However, the main limitation of this approach is that long-term recording is not yet possible, most probably due to their invasive nature, as only multiple day experiments have been reported.

On the biology side, the culture of primary neural cells on top of MEAs remains a challenge. Most importantly, neurons need to survive for long periods on the substrates (preferentially several weeks) and they need to be as close as possible to the electrode site and within the recording distance (<140 μm) [73]. However, their tendency to adhere randomly to the substrate after cell seeding renders this rather challenging, unless there is a particular cell-pattern designed on the device. Thus, a plethora of patterning techniques have been developed aiming to make the surface either cell-adhesive and/or cell-refractive, including micro-contact printing, surface modifications or the use of physical structures (reviewed by Kim et al. [71]). The most commonly used coatings as cell adhesion promoters on MEAs include collagen, poly-lysine and laminin [74]. Notably, a primary cell culture contains multiple cell types apart from the neurons, such as astrocytes, oligodendrocytes and microglia. While mature neurons do not undergo cell division, the other supporting cells in the brain (particularly astrocytes) do not have that restriction. Continuous proliferation and migration of astrocytes can push neurons away from the electrode site by positioning themselves below the neural somas [75]. The presence of glial cells is nevertheless important for neuronal communication [76], [77]. The use of serum-free media can be used as a simple way to prevent overgrowth of glial cells in vitro [74]. However, the growth of cells in vitro, being a rather dynamic process, can affect the performance of the microelectrodes due to the continuous deposition of proteins from the media and the extracellular matrix of the cells resulting in the so called biofouling of the microelectrodes within days [74].

Despite the abovementioned efforts to optimize in vitro MEA recordings, the overall recording yield of MEAs remains sparse [17], [78]. While the whole reason for developing MEAs is to record action potentials from multiple neurons simultaneously, the probability of recording such small signals is very low. This challenge is difficult to quantify, as numerous parameters play a role herein, including for example electrode density and surface treatment,

the type of neurons and their cell density, etc. It is nevertheless a well-known problem in the in vitro neuroengineering field.

Here, we demonstrate an enhancement of recording spontaneous single units through the formation of neurospheres on planar, custom-made MEAs. We initially found that a high cell density (HCD) on our PEDOT:PSS coated MEAs significantly increased the number of recording electrodes. The presence of even higher local cell densities in the form of 3D clusters, known as neurospheres, further improved MEA recording performance. This more natural cellular organization of CNS (central nervous system) cells in vitro increased the success rate of recording single unit activity per microelectrode to 42.2%**.** We demonstrate this through the analysis of multiple MEA recordings using semi-automated spike sorting algorithms. Finally, we demonstrate how to confine neurospheres on MEAs through laser patterning of polyethylene glycol diacrylate (PEGDA). This approach provides a way to control the location of neurospheres on the MEA to further maximize their recording yield.

3.2 MEA design and growth of cortical cells

Figure 1a shows a PEDOT:PSS coated MEA device fabricated on a glass substrate. The metal electrodes were patterned by photolithography and insulated with parylene-C. Each MEA contains 64 electrodes, spaced 100 μm from center to center and with an active area of 12 x 12 μm^2 (*Chapter 2, Section 2.4*). All the electrodes were coated with the conducting polymer PEDOT:PSS via a peel-off technique, as previously reported [47], [50]. The addition of the conducting polymer significantly lowered the impedance, resulting in an average impedance of 38.5 ± 2.4 kΩ at 1kHz. A glass well was placed around the electrode area and used as container of cell media. Prior to cell seeding, the MEA was coated with the polypeptide poly-D-lysine (PDL) and the extracellular matrix (ECM) protein laminin, known to improve both cell adhesion and neurite outgrowth [77], [79]–[81]. Without any coating, cells did not survive past 5 days in vitro (DIV5) (Supplementary Figure 2).

Rat embryonic day 18 (E18) primary cortical cells grew a complex network within a couple of weeks in culture. The cells adhered within 1 hour on the MEAs and as shown in the scanning electron microscopy (SEM) images, they also attached to the PEDOT:PSS coated microelectrodes (Figure 1b-c). The images show the top (Figure 1b) and cross-section (Figure 1c) view of a microelectrode with a single cell on top (indicated in blue) and a complex network of neurites and ECM around. The cross-section was performed as presented in [66] using a focused-ion beam (FIB) prepared sample (see Experimental Section). The image demonstrates the coverage of PEDOT:PSS on gold, the encapsulation of parylene around it and most importantly, the tight attachment of the cell on the microelectrode. The development of a complex network of neurites within 3 weeks of culture is shown in Figure 1d. After DIV21, the number of synapses at the dendrites and soma are known to have

reached saturation [15]. Recording of spontaneous activity was consequently performed after DIV21.

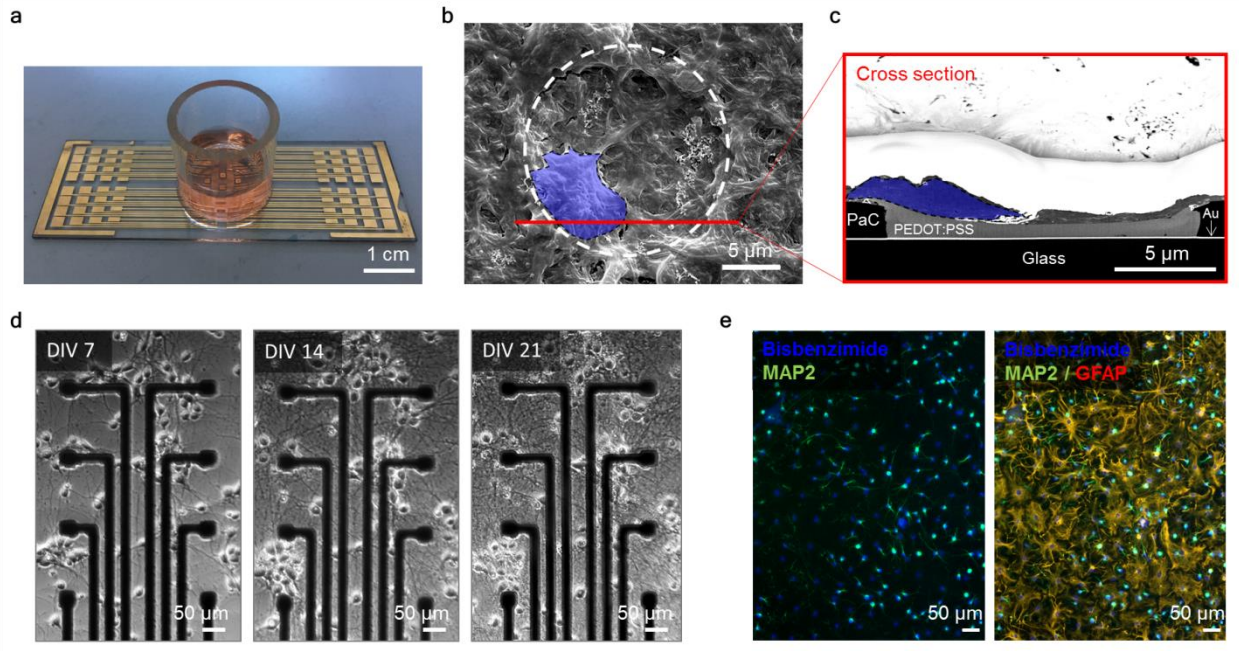

Figure 1. Presentation of the MEA device and primary cell culture thereon. (a) Photograph of the parylene-insulated and PEDOT:PSS-coated MEA. A glass well is attached as container for the cell culture. (b) SEM image of a top view of a microelectrode with a single cell adhered to the PEDOT:PSS. The white dashed circle shows the boundary of the microelectrode, the blue area indicates the single cell and the red line points out the location of the cut performed with FIB for the cross-section in (c). (c) FIB-SEM image of a cross-section indicated in (b). The cell tightly adhered to the PEDOT:PSS coated microelectrode. (d) Phase contrast images of the cortical cell culture at DIV 7, 14 and 21 showing the growth of the cells on the MEA. (e) Immunofluorescence analysis of rat E18 primary cortical cells on parylene-C coated glass substrates. Neurons were stained for MAP2 (green), astrocytes for GFAP (orange) and cell nuclei with Bisbenzimide (blue). Abbreviations used: PaC, Parylene-C. Au, gold.

The presence of neurons and astrocytes in the cell culture was confirmed at DIV21 through an immunofluorescence analysis (Figure 1e). Neurons were stained for the neuronal marker MAP2 (green), astrocytes for the glial marker GFAP (orange) and all cell nuclei for Bisbenzimide (blue). Both cell types were homogeneously spread on the surface. The astrocytes were clearly visible in between the smaller cell-bodied neurons, playing their essential role of neuronal support [76], [77]. A serum-free media was used without any growth factors to prevent astrocytes from further proliferation. The cells showed a very high survival rate at DIV21 on the PDL- and laminin-coated MEAs (Supplementary Figure 2e).

3.3 Comparison of low vs. high cell density

The difference in recording yield between MEAs seeded with a low cell density (500 cells/mm^2, LCD) and a high cell density (900cells/mm^2, HCD) were compared. Figure 2a shows phase contrast images and scatter plots based on a Principle Component Analysis (PCA) of the two different cell density experimental groups. The scatter plots show a two-

dimensional view of the sorted single units done via the PCA (See Experimental Section). The classification of units is based on spike amplitude and waveform variability within the recorded electrophysiological data [83], [84]. In short, data recorded from one electrode can contain single unit activity from multiple neurons. Identified units were isolated from the data and classical techniques of spike sorting were used to group the recorded spikes into individual neurons, called "clusters" [83], [85]. Each unit cluster (i.e. activity originating from one given neuron) is subsequently shown in one particular color. In Figure 2a, this means that three different neurons were detected at LCD and twelve neurons were detected at HCD. HCD on MEAs therefore resulted in the recording of significantly more neurons.

To show more clearly the difference between the recordings of LCD and HCD, recordings from single electrodes of both experimental groups are shown in Figure 2b. The recording graphs present the amplitude of the recorded signal in voltage as a function of time. Raster plots are shown just below, which indicate the occurrence of single units in time from one or more neurons detected in that given signal. There are several observations from this result. First, the average recorded unit activity is higher in amplitude at HCD (Supplementary Figure 2). It is well known that unit activity is mostly the extracellular summation of recorded signals from the neural somas and proximal dendrites [73]. Moreover, the voltage amplitude mostly depends on the proximity of the neural soma to the electrode sites, decreasing rapidly with increasing distance from the electrode [73], [86]. The highest amplitudes were found at higher cell density, which implies that those cells were more likely to be located proximal to the electrodes. This can be explained by the larger number of cells that is present on the MEA, increasing the probability of cell bodies positioned closer to the electrode site. Secondly, the recorded activity of single electrodes at HCD contained activity of multiple neurons, unlike the recordings at low cell density (Figure 2b, *Raster plots*). This means that a single electrode can pick up more signals at HCD compared to LCD, which stands to reason as the probability of their location near a given recording site would increase. The capability of recording from cultures with higher density is important as it moves the device performance in the direction of the higher density packing of neurons observed in tissue in the brain.

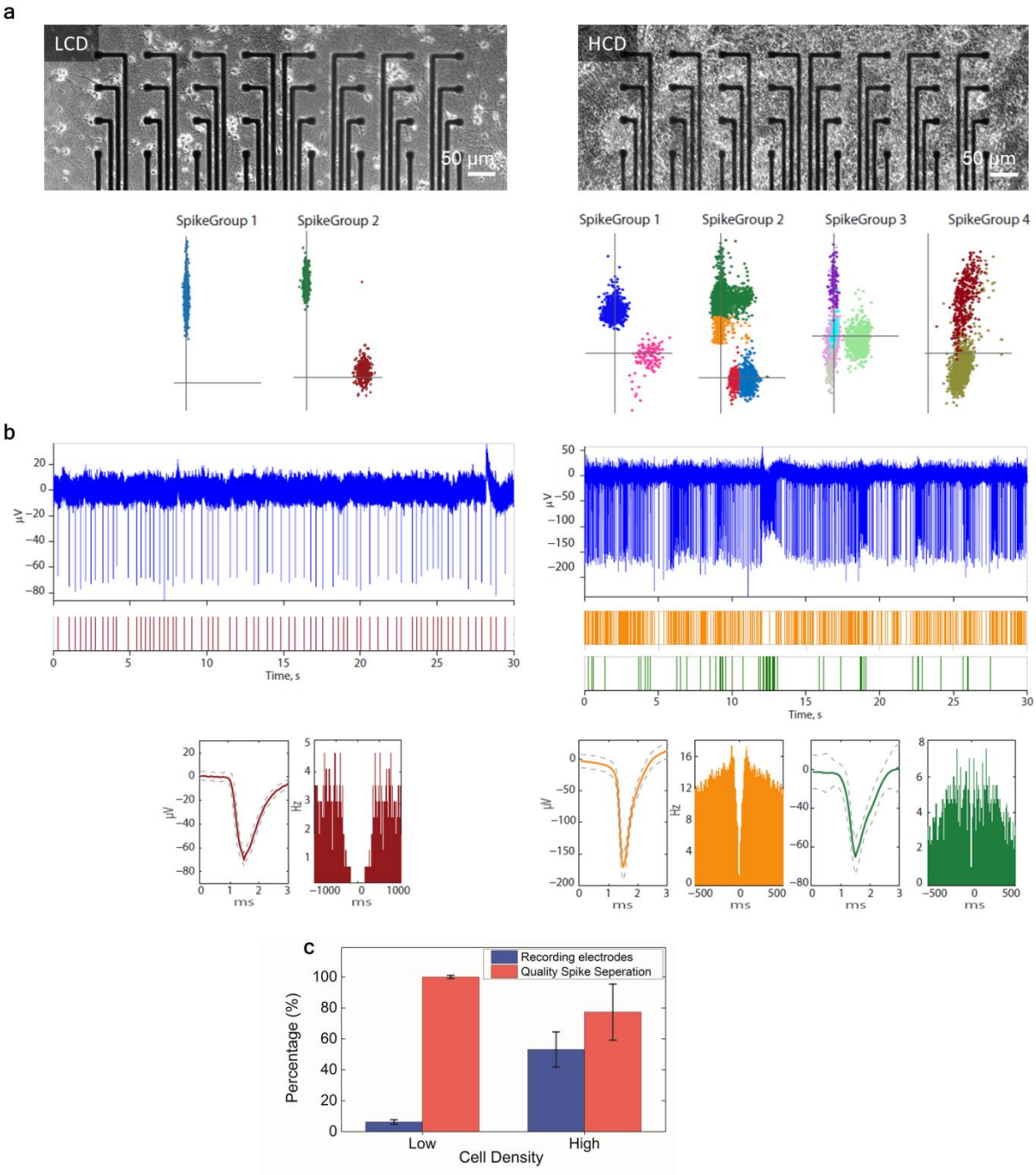

Figure 2. The influence of cell density on MEA recordings. (a) Phase contrast images and PCA-based scatter plots of (left) low cell density (500 cells/mm^2, LCD) and (right) high cell density (900 cell/mm^2, HCD). The scatter plots display the "clustering" of the single units into isolated clusters (individual neurons) in the Principle Component space, which are represented by different colors. More single unit activity was recorded at HCD compared to LCD. (b) Example of electrophysiological recordings with corresponding raster plot, unit waveforms and auto-correlograms (ACGs) per cell density group. (c) Percentage of recorded electrodes and the quality of spike separation per cell density group. Data is presented as mean ± SD (n=2 per experimental group).

Despite a clear increase in unit recordings at HCD in vitro, the complexity of spike sorting increased (Figure 2b and 2c). Below the recordings of Figure 2b, an example is given of detected waveforms of single units and their auto-correlograms (ACG). These graphs show the voltage amplitude and frequency of the signal as a function of time, respectively. A clear

refractory period was observed in the ACG of low cell density groups, which means that the probability that the sorted units belongs to a single neuron is very high. This was however not always the case for HCD ACGs. This is a plausible consequence of having many more cells on or near the electrode sites at HCD emitting units simultaneously. Thus, there is a small trade-off between number of recording electrodes and spike separation quality. However, the increase in recording electrodes at HCD (53.10 ± 11.31% at HCD vs. 6.25 ± 1.41% at LCD) by far outweighed the small decrease of signal separation (77.30 ± 18.00% vs. 100 ± 0.00%).

3.3.1 The formation of neurospheres

The significant enhancement of recordings at HCD led us to consider a more 3D organization of the primary cell culture on MEAs. Since a more compact cell culture increased the probability of recordings, we reasoned that it might be beneficial to engineer highly local clusters in cell density, commonly known as neurospheres [87]. Previous work has reported stimulation of neurospheres [88] and the network bursting activity of neurospheres [89]–[91]. However, in this work we focus on single unit activity and do not use any surrounding scaffold or supporting structure to facilitate 3D tissue formation [92]. We anticipated that this would result in more electrophysiological recordings as more cells are expected in closer proximity to the microelectrodes, especially in the z-direction. Moreover, cells would be positioned closer to other cells, forcing them to form neurites in many more directions.

The formation of neurospheres with primary E18 cortical cells was observed at HCD using NbActiv4^{R} media (provided by Brainbits^{R}, which is a variation on the standard Neurobasal^{TM}/B27^{TM} media). Figure 3a shows that neurons are present in the neurosphere on parylene-coated glass slides used as control samples. As previously mentioned, neurons, astrocytes and cell nuclei were stained for MAP2 (green), GFAP (orange) and bisbenzimide (blue), respectively. A live/dead assay was performed on DIV21 to show the survival of cells within the neurosphere (Figure 3b). The same neurosphere formations were subsequently observed on MEAs and some clusters fortuitously developed on top of microelectrodes (Figure 3c).

As anticipated, neurospheres on top of the microelectrodes significantly increased single unit recordings. The PCA-based scatter plot in Figure 3c gives an example of the units recorded from a single electrode, unlike previously shown, on the MEA covered with a neurosphere. The six different colors show the unit activities of six different neurons. The unit waveforms and ACGs of these detected neurons are shown in Figure 3d. Detection of up to 7 neurons with a single microelectrode was achieved. This multi-neuron recording with a single electrode had not previously been observed. In total, 76 different neurons were detected with 45 microelectrodes containing neurospheres on top. Moreover, the overall chance of recording increased with the presence of neurospheres. While only 3 microelectrodes with single cells on and around microelectrodes resulted in successful recordings (2.4 ± 0.7% out

of 123 microelectrodes recorded on a total of 5 MEAs), 45 microelectrodes with neurospheres on top successfully measured single unit activity (44.6 ± 8.5% recorded of 101 microelectrodes on a total of 5 MEAs). The success rate of recording single unit activity per microelectrode has thereby increased with more than 40%.

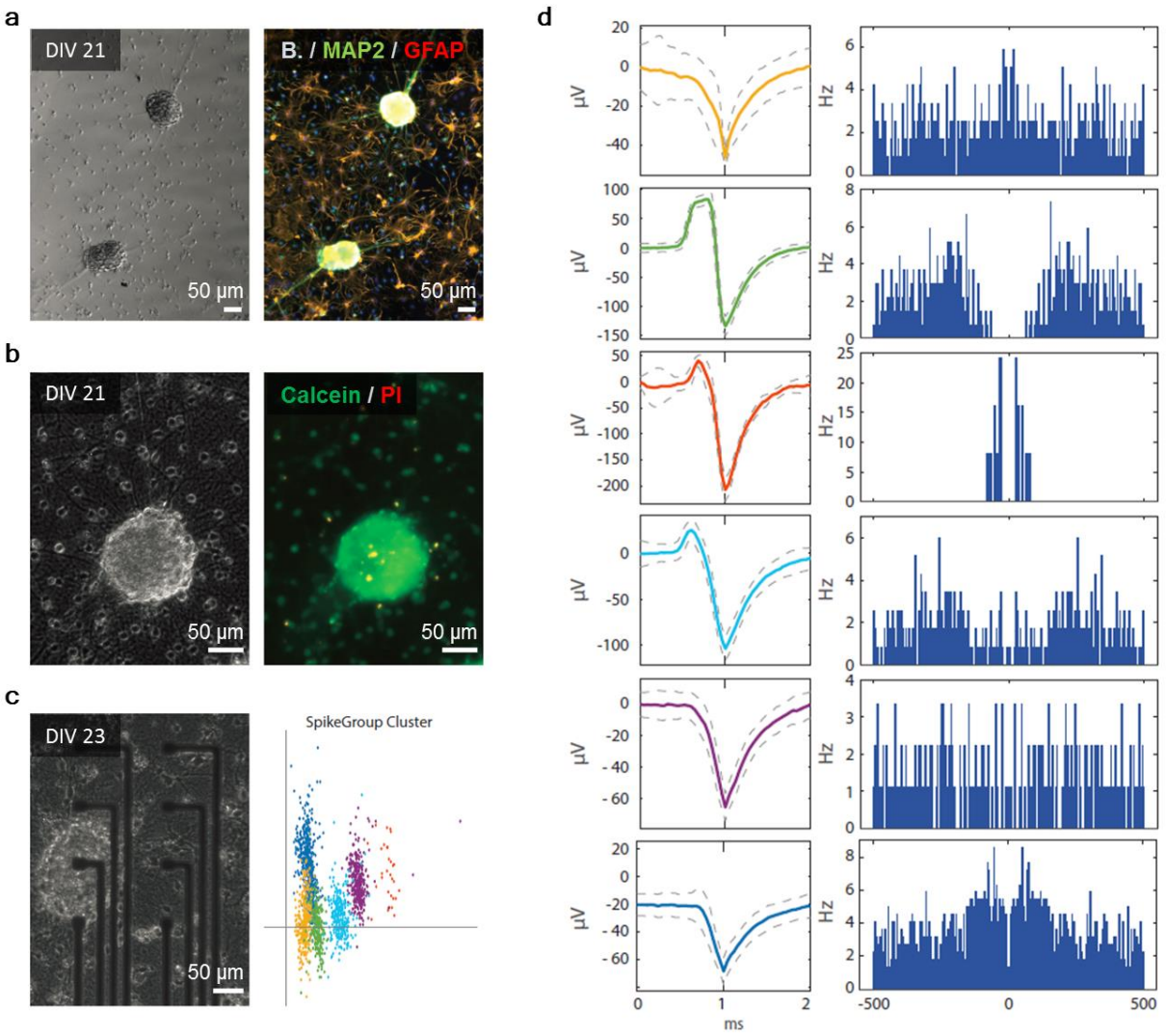

Figure 3. Neurospheres increase the number of single unit recordings on a single microelectrode. (a) Phase contrast image and fluorescence image of cells on DIV21 seeded on parylene-covered glass slides (control samples) at HCD, cultured in NbActiv4. (b) Phase contrast image and corresponding fluorescence image of live/dead staining on DIV21. Green cells are alive (Calcein) and dead cells are orange (Propidium Iodide). (c) Phase contrast image of a neurosphere on top of a microelectrode at DIV23 and the PCA-based scatter plot, showing the unit detection of 6 different neurons from the recorded electrophysiology on that single electrode. (d) The corresponding single unit waveforms and ACGs of the 6 different neurons. Abbreviations used: B., Bisbenzimide. PI, Propidium Iodide.

A high level of interconnectivity was observed between the neurospheres on the MEAs (Figure 4). The cell distribution was investigated at DIV21 on a parylene-coated glass slide to avoid limitation from the metal MEA pattern. While neurons seem to predominate in the neurosphere (Figure 4a-c), a selection of z-stack images showed that astrocytes were also located within (Figure 4d). Interestingly, despite the 3D organization of the cells on a 2D device, neurons above the plane of the MEA managed to extend processes down to make connections with the substrate surface (Figure 4e-g). The neurospheres were aggregations of cells with heights of up to at least 100 µm. Thick bundles of neurites from various orientations on the sphere were observed radiating out to connect with neighboring neurospheres and attached at different points on the MEA. This observation could indicate that recordings were not necessarily limited to the cells in direct contact with the electrode site, but also from neurons located at higher positions on neurospheres.

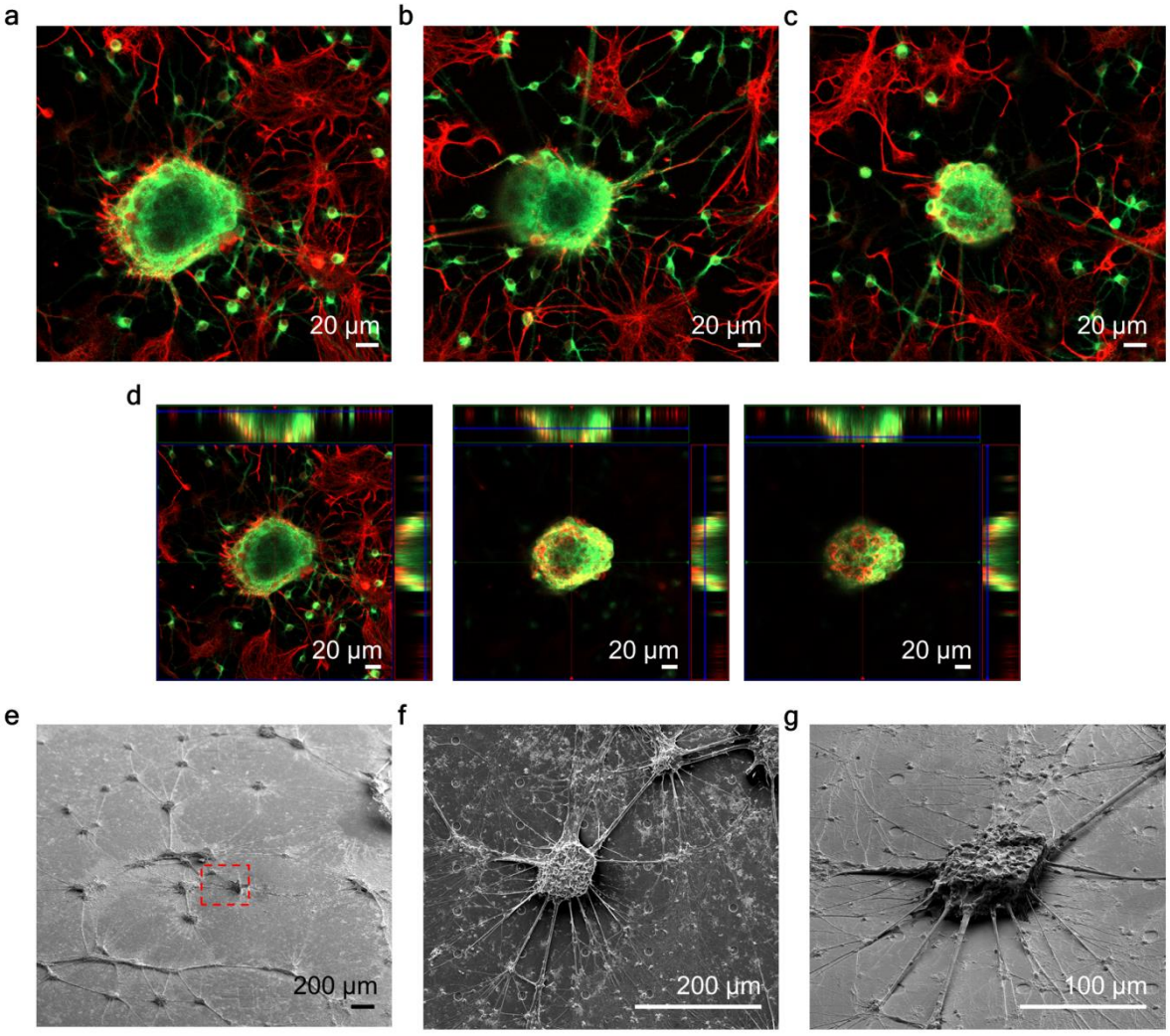

Figure 4. Optical characterization of the neurospheres. (a-c) Confocal fluoresence images of neurons (MAP2, green) and astrocytes (GFAP, red) of various neurospheres on parylene-coated glass slides. Neurons were observed within the neurosphere, closely surrounded by astrocytes. (d) A selection of 13 Z-stack images (3.86 µm in thickness) from (a), starting at the substrate plane (left, z=3, 7.72 um) and moving to more upward planes (middle, z=9, 30.88 µm; right, z=12, 42.46 µm). Individual small neurons and large astrocytes are observed on the surface of the substrate. Both cell types are clearly visible within the neurosphere. (e-g) SEM images of neurospheres adhering to the MEA. (e) Overview of the 3D organization of the primary cell culture. Multiple large neurospheres are formed on the substrate. The red dashed box shows the array section that is further visualized in (f-g). (f) Top and (g) tilted view on neurospheres tightly adhered to the MEA. Neurons above the MEA plane extended processes down to the MEA, thereby connecting to neighboring neurospheres, individual cells and the microelectrodes.

3.4 Patterning PEGDA to control positioning of neurospheres

UV-photocrosslinking has been used extensively for in-vitro studies as an effective approach for the formation of polymeric structures for cell patterning [93], [94]. In contrast to other photopolymerization patterning techniques, laser writing is a direct process which offers great versatility and the capability to precisely create microscale features on various surfaces. Given the success of recording from neurons when neurospheres were proximal to electrodes, attempts were made to control the placement of the neurospheres on the MEA with an anti-fouling region around the electrode sites. To achieve this, a polyethylene glycol diacrylate (PEGDA) solution was deposited on top of the MEA through doctor blading and subsequently irradiated by a UV (343 nm) laser beam. The resulting topographic pattern consisted of separate PEGDA lines with a width of approximately 12 μm and an interspacing of 40 μm, as shown in Fig. 5a. It should be noted that the dimensions and the characteristics of the pattern were chosen in relation to the size of the neurosphere and the position of the electrodes in our MEA design.

PEGDA is known to exhibit poor adhesion properties for the cells due to the limited protein adsorption on its surface [95], [96]. Figure 5b-c depicts a neurosphere at DIV21 being confined within the region defined by the PEGDA lines, which is successfully patterned on top of the microelectrode. The laser patterned PEGDA structures not only allowed us to place the neurospheres on top of the electrode sites, it also provided guidance of neurite outgrowth towards neighboring electrodes and neurospheres (Figure 5d-f). The orientation of the neurites was observed along the pattern and deviated only from these lines once other neurospheres were in close proximity (Figure 4d). On the contrary, the astrocytes seemed to not have a particular distribution induced by the PEGDA-pattern (Figure 5e).

The laser-patterned PEGDA structures contributed to the formation of large neurospheres, which consequently enabled the tracking of single unit activity on neighboring electrodes (Figure 6). Figure 6a shows a neurosphere located in the bottom right corner of the fluorescence image, almost fully covering two electrode sites (E2 and E3) and reaching out to a third electrode (E3) with its neurite network. Single unit activity of three different neurons was detected on all three electrodes (Figure 6b-c). The corresponding recordings (Figure 6c) and single unit waveforms from one neuron (Figure 6d) show a clear increase in amplitude from E1 to E3. This means that the neuron in question must be located in closer proximity to E3, while its electrical signal is simultaneously also recorded up to almost 200 μm further. This is in line with previously reported recording limit of well-isolated extracellular spikes [73]. We thus show that we can reach similar electrophysiological recording limits with this PEGDA-induced neurosphere in vitro culture compared to those of actual in vivo recordings.

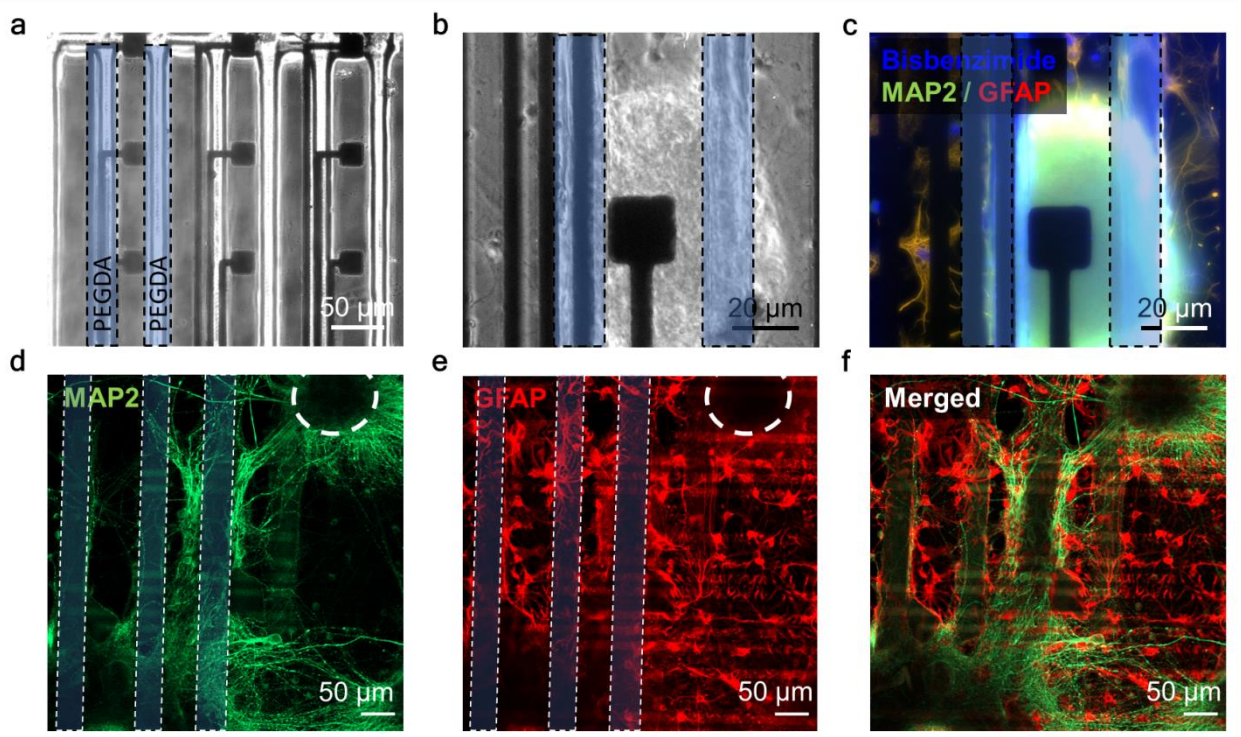

Figure 5. PEGDA patterning for more accurate control on neurosphere placement and neurite outgrowth. (a) Phase contrast image of 9 microelectrodes surrounded by a PEGDA pattern to confine cell adhesion. For clarification purposes, two PEGDA lines are shown in blue. (b) Phase contrast image and (c) fluorescence image of a neurosphere restricted by the PEGDA lines. Neurons, astrocytes and cell nuclei are stained for MAP2 (green), GFAP (orange) and bisbenzimide (blue), respectively. (d)-(f) Confocal images of neurons (MAP2), astrocytes (GFAP) and its overlay showing the guidance of PEGDA lines for neurite outgrowth. PEGDA lines are shown in blue, lines perpendicular to those are part of the metal MEA pattern observed due to autofluorescence and the boundaries of the neurospheres are illustrated with bold white dashed lines.

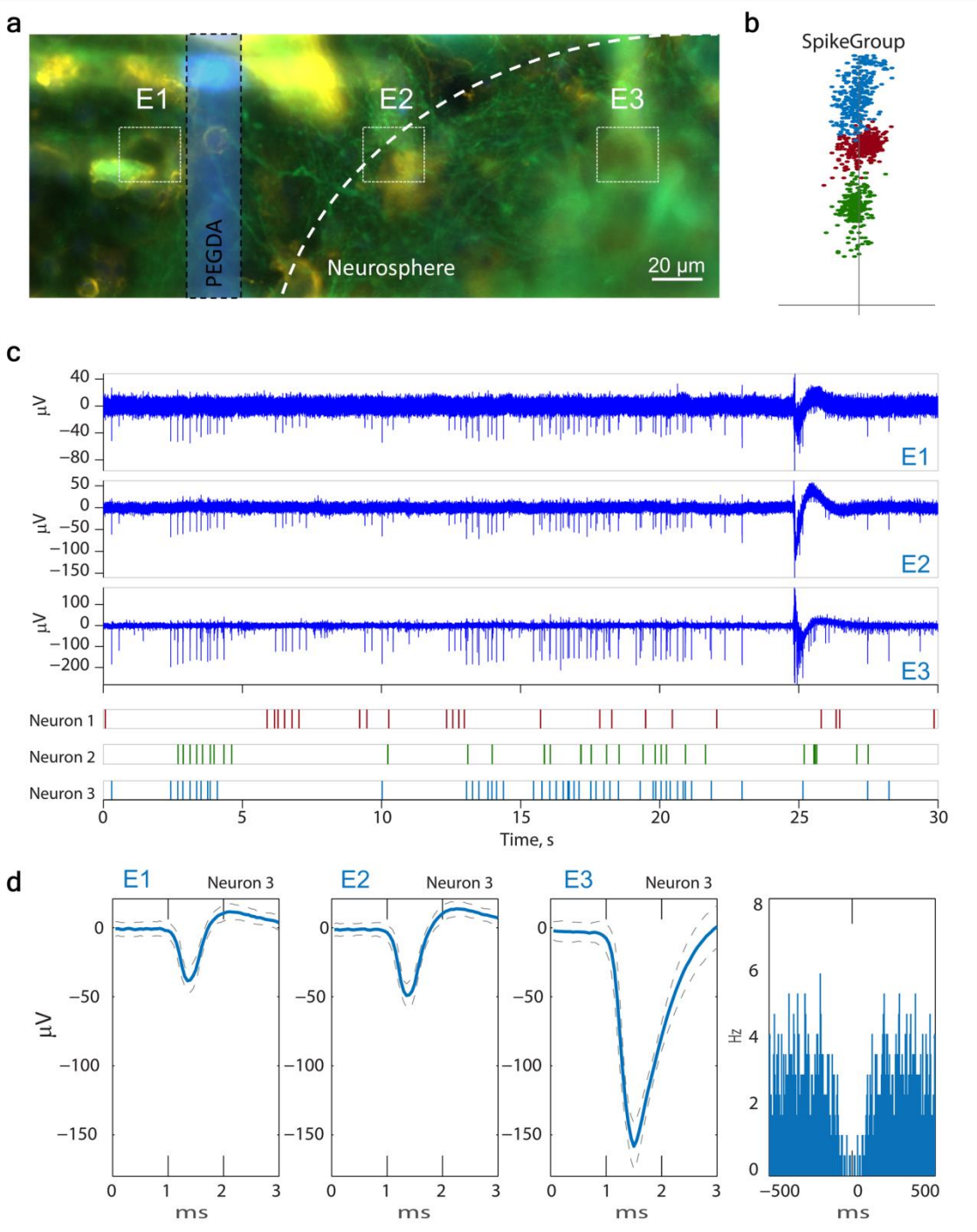

Figure 6. PEGDA patterning to track single unit activity on neighboring electrodes. (a) Fluorescence image of a neurosphere covering almost three electrodes (E1-E3). The dashed white line illustrates the boundary of the neurosphere and the dashed white boxes indicate the location of the electrodes. (b) PCA-based scatter plot, showing the detection of 3 different neurons from the recorded signals. (c) Recordings of E1-E3 with corresponding raster plot of the detected neurons, showing an increase in voltage amplitude from E1 to E3. Recorded neurons are consequently in closer proximity to E3. (d) Single unit waveforms of Neuron 3 recorded with E1-3 and the corresponding ACG.

3.5 Conclusions

Overall, we showed successful in vitro MEA recordings with 48 electrodes out of a total of 224 (n=7 MEAs). This is a recording yield of 21.4% from which 93.75% was obtained from electrodes with neurospheres and 6.25% from single cells on and around the microelectrodes. The 3D conformation of E18 rat primary cortical cells in neurospheres resulted in a significant improvement of MEA recording success. Through spike sorting algorithms, we showed how unit activity per microelectrode increased with HCD and with neurospheres. The presence of neurospheres on the MEA resulted in multi-neuron detection with a single microelectrode and allowed for simultaneous recording of single unit activity with neighboring electrodes. This enhanced recording yield on planar MEAs using a 3D neural in vitro model will facilitate pharmacology-based studies providing more electrophysiological data. The engineering of these highly local clusters of neurons and their processes by substrate patterning, is not unlike the organization of nuclei and their tracts in the brain, and shows promise for the potential of construction of mini-brain structures on MEA devices.

3.6 Experimental section

MEA fabrication

The MEAs were fabricated as previously reported [47], containing 64 electrodes each with a 12 x 12 μm^2 recording area (See Supplementary Figure 1a). The fabrication includes the deposition and patterning of gold, parylene-C and PEDOT:PSS on glass substrates. Substrates (25 x 75 mm^2) were thoroughly cleaned by sonication steps of 10 minutes in a soap bath followed by bath mixture of acetone/isopropanol (1:1). The clean substrates were spin coated with S1813 photoresist (Shipley) and exposed to UV light with a SUSS MBJ4 contact aligner. A paper mask (Selba S.A.) was used during exposure, after which the samples were developed in MF-26 developer. Chromium and gold were deposited in a metal evaporator with a final thickness of 10 nm and 100 nm, respectively. Lift-off was done in a solvent bath of acetone/isopropanol (1:1). Then, two layers of parylene were deposited with a SCS Labcoater each with thickness of approximately 2 μm. During the first deposition, 3-(trimethoxysilyl)propyl methacrylate (A-174 Silane) was added to the deposition chamber as an adhesion promoter. Before the second parylene deposition, a sacrificial layer of soap (1% in deionized water, Micro-90) was spin coated. This created an anti-adhesive layer to facilitate peel-off at a later stage. Photoresist AZ 9260 (Microchem) was then spin coated on the substrates, followed by another photolithography and development step using AZ Developer. The parylene was etched to open the microelectrode areas through reactive ion etching using O_2 plasma (Oxford 80 Plasmalab plus). A PEDOT:PSS dispersion, including Clevios PH 1000 (Heraeus Holding GmbH), 5 wt% ethylene glycol, 0.1 wt% dodecyl benzene

sulfonic acid (DBSA) and 1 wt% of (3-glycidyloxypropyl)trimethoxysilane) (GOPS), was spin coated on the devices and the sacrificial second parylene layer was peeled-off. Finally, the devices were hard baked at 140°C for 1h and immersed in deionized (D.I.) water over night. This last step removed any excess of low molecular weight compounds inside the PEDOT:PSS dispersion.

MEA preparation for cell culture

Protein coating. Glass wells with an inner diameter of 3 cm^2 were attached to the MEAs using PDMS as glue. The devices were plasma treated at 25W for 1 min to make the surface hydrophilic for cell culture. The inside of the well was kept wet from this point on with deionized (DI) water. The devices were entirely sterilized for 30 minutes in 70% ethanol and rinsed with Dulbecco's Phosphate Buffered-Saline (DPBS). The devices were then coated with 50 μg/ml poly-D-lysine (PDL) (70 kDa, Sigma Aldrich) in DI water for 2h at 37°C, rinsed 3 times with DPBS and left overnight in DPBS at 37°C. Next, the devices were coated with 20 μg/ml of laminin (Sigma Aldrich) in DPBS for again 2h at 37°C, rinsed 3 times with DPBS and were placed in the incubator with fresh DPBS until cell seeding.

Laser patterning PEGDA via photopolymerization

Prior to the laser writing process, the substrates were functionalized for the covalent bonding of poly(ethylene glycol) diacrylate (PEGDA, M_n=575). 3-(Trimethoxysilyl)propyl methacrylate (A-174 Silane, Sigma Aldrich) was deposited by chemical vapor deposition under vacuum for 2 hours at 90-100°C to provide C=C moieties for efficient PEGDA adhesion. 2-Hydroxy-2-methylpropiophenone (MPP, >98%, Sigma Aldrich) was incorporated as a photoinitiator and mixed with PEGDA:water solution (1:1) at a concentration of 0.5 wt%. The solution was spread onto the substrates using a handheld doctor blade and placed in the substrate holder for laser processing. The system used for the direct laser writing of PEGDA was based on a sub-picosecond laser source coupled to a laser scanning head. A femtosecond-diode-pumped ytterbium amplified laser (Amplitudes Systems S-Pulse HP) was used with a fundamental wavelength of 1030 nm, while for the present experiments the third harmonic of 343 nm was used, after frequency conversion in nonlinear crystals. The pulse duration was set to 500 fs FWHM (full width at half maximum), estimated from single-shot autocorrelation trace. The laser power was adjusted externally with a set of half waveplate and polarizer for each wavelength. The beam was focused on the sample after passing through galvomirrors (Thorlabs GVS12) and an *f*-Theta-lens that depends on the wavelength: focal length of 254 mm (Thorlabs FTH254-1064) for the infrared and 100 mm for the UV (63-312, Edmund Optics). For the described experiments, the repetition rate of the laser was operated at 400 Hz and the galvomirrors were synchronized

with the laser, meaning that only one shot per location was done in case of a single pass. Home-made software was used for the control of beam displacements on the sample for a particular pattern. At 343 nm, the step size was found to be 8 μm, resulting in a beam overlap of more than 80%. A calibration of the energy in the sample plane was done with a calibrated pyroelectric sensor (OPHIR PE9-C) so that the local fluence can be estimated. After the laser irradiation the samples were immersed into water for 5 min in order to remove the non-crosslinked parts from the surface and a protein coating was performed, as previously described.

Electrical characterization

Impedance measurements were performed with a potentiostat (Autolab PGSTAT128N) in a three electrode configuration. An Ag/AgCl electrode was used as the reference electrode, a Pt electrode was the counter electrode with the recoding electrode of the MEA was the working electrode. The characterization was performed in DPBS solution.

Cortical cell culture

Embryonic day 18 rat cortical tissues were purchased from Brainbits (Brainbits, LLC). The cells were dissociated with a 2 mg/mL papain solution (Hibernate E-Ca without B27, Brainbits LLC) for 10 minutes in a water bath at 30 °C. They were then triturated in Hibernate E containing 2% B27 and 0.5 mM Glutamax (Hibernate EB media, Brainbits LLC) to disperse most of the tissue, spun at 200G for 1 min and resuspended in NbActiv1 media (Brainbits, LLC). Cells were plated at two cell densities, a low cell density of 500 cells/mm^2 (LCD) and a high cell density of 900 cells/mm^2 (HCD). Cell counting was performed using an aliquot of the cell suspension in a hemocytometer. The cells were cultured in NbActiv1^R media, a serum-free Neurobasal™/B27™ media (Brainbits^R), at 37 °C in 5% CO_2 humidified incubators. Every 3 to 4 days, half of the media was replaced by fresh media. For the formation of neurospheres, NbActiv1^R was replaced by NbActiv4^R (Brainbits^R) which additionally contains creatine, cholesterol, and estrogen [82].

SEM and Focused Ion Beam-SEM

All the cell cultures on the MEAs were washed 3 times with pre-warmed DPBS and fixed with 3.5% glutaraldehyde overnight after DIV23. For the cross-sectional images, the cells were further processed with a ROTO staining, uranyl acetate, dehydrated and embedded as presented in [66]. Cross sections were made and polished, fixing a voltage at 30 kV and current at 80 pA. A more detailed description of the Focused Ion Beam-SEM procedure is

given in [66]. Image acquisition of the cross section was performed with a backscattered detector at 3-10 kV and at variable currents. For the neurosphere SEM images, the neurosphere cultures were dried in air and gold was sputtered with a final thickness of 10 nm. The prepared arrays were then mounted on SEM stubs with colloidal silver paste (TED PELLA). Images were acquired fixing a voltage from 3 to 15 kV with variable currents (secondary electrons detector).

Immunofluorescence staining

Neurons were stained for the neuronal marker MAP2 (green), astrocytes for the glial marker GFAP (orange) and all cell nuclei with Bisbenzimide (blue). The cells were fixed for 10 min in 4% paraformaldehyde(PFA)/0.12 M sucrose with 0.1 % glutaraldehyde, followed by 2 rinsing steps with DPBS (without $CaCl_2$ and $MgCl_2$). The blocking/permeabilization step was done with 0.5% TritonX-100 and 5% BSA in DPBS for 5 min at room temperature. Mouse monoclonal antibody MAP2 (Life Technologies SAS) and rabbit monoclonal antibody GFAP (Millipore) were added at a 1:400 dilution in DPBS with 0.05% TritonX-100 and 5% BSA, for overnight at 4 °C. After 4 washing steps with DPBS, Alexa Fluor 488 donkey anti-mouse IgG (Abcam) and Alexa Fluor 568 donkey anti-rabbit IgG (Abcam) were added at a 1:500 dilution in DPBS with 0.05% TritonX-100 and 5% BSA for 1h at room temperature. One wash with DPBS was followed by nuclear staining with a 1 ug/mL bisbenzamide (Sigma Aldrich, 14533) solution. After washing, samples were examined with a fluorescent microscope (Zeiss Axio Observer Z1 Carl) and a confocal microscope (Zeis SLM 800). All acquisition and processing is performed using ZEN Blue 2.3 lite software.

Live/dead staining

Live/dead assays were performed to examine cell viability on the different substrates. Cells were incubated in DPBS with approximately 0.2 μg Calcein AM and 0.3 μg propidium Iodide for 10 min. Living cells were stained with green fluorescent calcein, due to the enzymatic cleavage by esterase of non-fluorescent calcein-AM. Metabolic activity is required to enable this conversion, which is only possible in living cells. Dead cells were stained with a cell-impermeable propidium iodide, which binds to nucleic acids in the nucleus if the cell is dead.

Electrophysiological recordings

Extracellular recordings were performed in a Faraday cage at high room temperature DIV23. All data were recorded with a 32-channel amplifier board (RHD2132, Intan technologies

US). This board was connected to MEAs via pogo pins held in place in a custom-made 3D printed holder, as previously reported [47]. The sampling rate was 20 kHz.

Spike sorting analysis

Single unit activity was identified and isolated using the Neurosuite software package of Neuroscope, NDManager and Klusters [83]. First, spikes groups were defined by grouping a maximum of 8 electrodes, since a single neuron can potentially be seen by several electrodes [83], [97]. Then, for each spike group, the wide-band signals were high-pass filtered at 300 Hz. The detection parameters were primarily optimized for the measured recordings and kept constant for all shown data. Single units were subsequently extracted at a threshold factor of 1.8 with a refractory period of 16 samples. After extracting the spikes from the raw signal, PCA allowed to extract the relevant components (3 principal components per electrode) that retained most of the spike information. Then, the automatic spike sorting algorithm KlustaKwik (http://klustakwik.sourceforge.net; [85]) was used to tentatively assign the detected spikes to individual neurons. Finally, all the spike clusters were manually refined with Klusters [83]. The spike separation quality was determined to be high when the isolated unit clusters showed a clear refractory period (Figure 2c). Data was subsequently plotted using custom-written tools in Matlab (Mathworks) and is presented herein as mean ± SD.

3.7 Supplementary Figures

The MEAs were coated with PDL and laminin to enable the growth of the primary cortical cells for more than 3 weeks. Without the coating, only few cells showed to adhere to the substrate, yet, did not survive past DIV 5 (*Supp. Figure 1a*). Hence, the entire area within the well on top of the MEA was coated first with PDL and then with laminin (*Supp. Figure 1b*). Without PDL, laminin did not seem to have any effect on cell growth (data not shown). The addition of the coating, showed a significant difference with cells staying adhered past DIV 5 and growing a complex network of neurites during three weeks of culture (*Supp. Figure 1c-d*). Cells clearly survived past DIV28, as shown with the live/dead staining in *Supp. Figure 1e.*

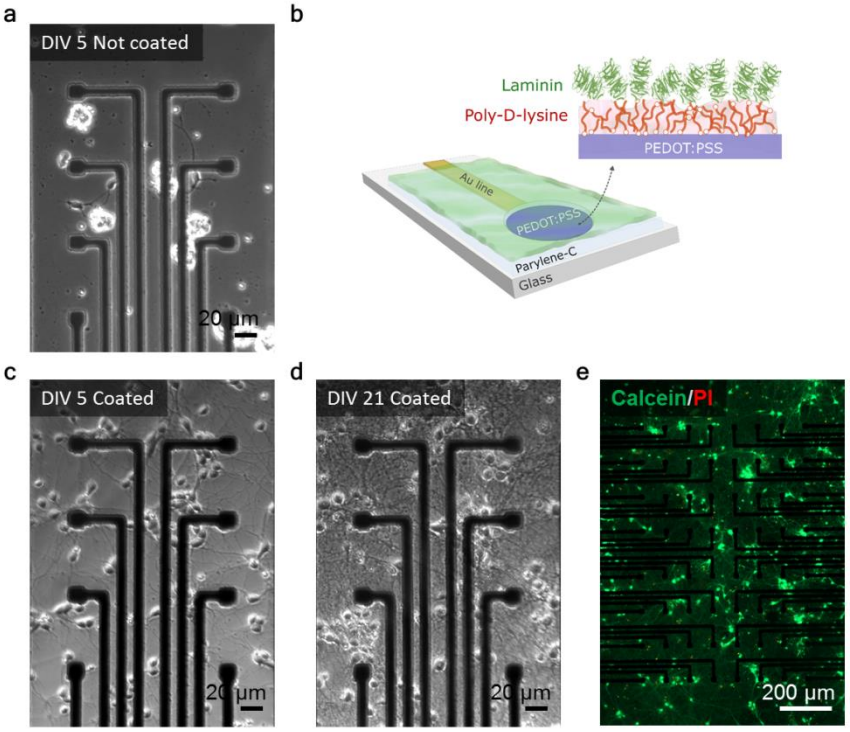

Supplementary Figure 1. (a) Bright field image of the cell culture on a MEA without coating on DIV5. No coating resulted in cell death past DIV5. (b) Schematic drawing of the protein coating, PDL and laminin, on PEDOT:PSS electrodes. (c-d) Bright field images the cell culture on a MEA with coating on DIV5 (c) and DIV21 (d). (f) Fluorescence image of live/dead staining on DIV21. Green cells are alive (Calcein) and dead cells are orange (Propidium Iodide). PDL and laminin as coating layers enabled cell surviving past DIV21.

During MEA recordings, an Intan graphical interface is used to investigate the cell activity at real-time (*Supp. Figure 2a*). The interface shows the simultaneous recording from 32 electrodes (*Right*) and there is an option to open a Spike Scope window to visualize threshold-passed single unit activity (*Left*). Although we did not discuss this matter in close detail the main manuscript above, the number of neurons that were recorded from at LCD and HCD were investigated (F*igure 2b*, with data of 2 MEAs per group). It is very clear that more single unit activity was observed at HCD, yet a further analysis was performed on the individual recorded single cell activity. The mean, maximum and minimum values of the detected single unit amplitudes were investigated after the extraction from the semi-

automated PCA (*Figure 2c*). A boxplot was chosen to demonstrate the distribution of the data, as this is a more accurate representation than solely showing the average and outliers. In the plot, individual data points (i.e. the values of the single cell activity per neuron) are shown in green with a blue distribution curve and the corresponding boxplot. In general and on average, higher amplitudes (i.e. the lowest values) were detected at HCD (Averages: **-45.7 µV** at HCD vs **-34.4 µV** at LCD (**Mean**); **-74.1 µV** at HCD vs. **-44.8 µV** at LCD (**Maximum**); **+7.5 µV** at HCD vs. **-19.0 µV** at LCD (**Minimim**)). The average values do not differentiate between up- and downward units. For this reason, also the maximum values and minimum values of individual units were investigated. The lowest observed amplitudes originate from the HCD group, seen in both the Maximum plot **(-259.0 µV** at HCD vs. **-87.0 µV** at LCD) and the Minimim plot **(-38.0 µV** at HCD vs. **-22.0 µV** at LCD). Interestingly, upwards unit activity was only observed at HCD. Although most activity is downwards, 20.4 % of the units were upwards, which is a similar value as reported by others [74]. Consequently, the highest amplitude values were also observed at HCD with **+34.0 µV** and **+95.0 µV**, as shown in the Maximum and Minimum boxplots (vs. **-26.0 µV** and **-16.0 µV** at LCD, respectively).

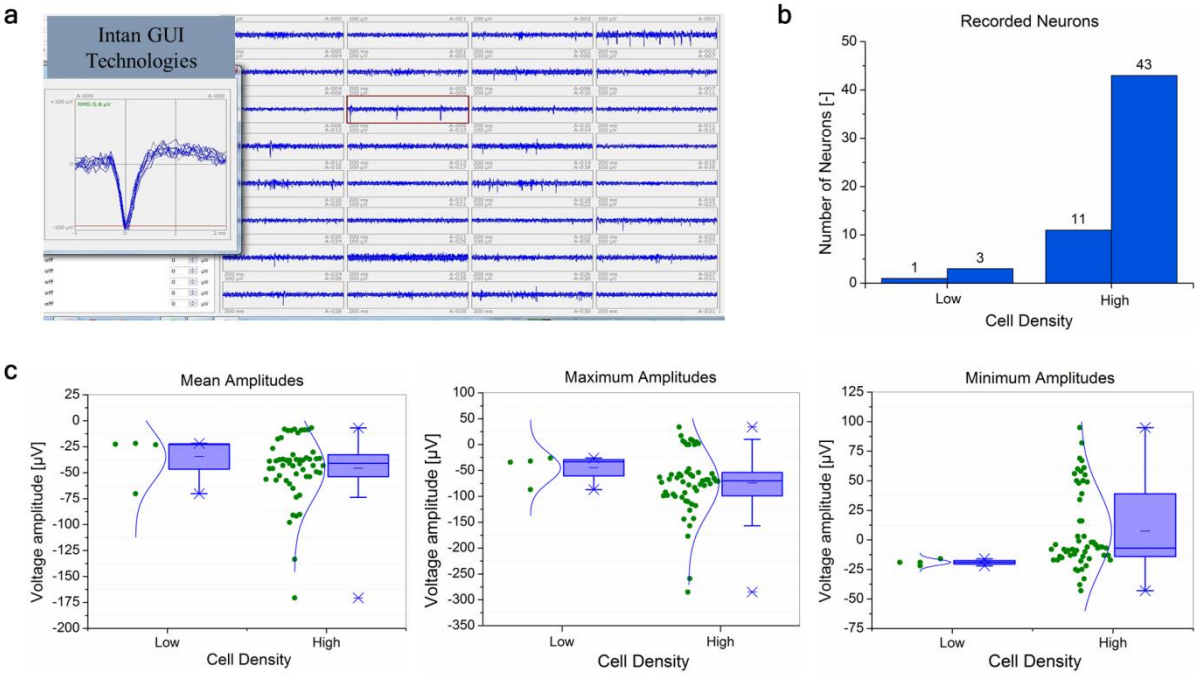

Supplementary Figure 2. Quantification of the recorded single unit amplitudes the from the LCD and HCD experimental groups. (a) Presentation of the Intan graphical interface used during MEA recordings, with an open Spike Scope window (Left). (b) Number of recorded neurons at LCD and HCD. More single unit activity was observed at HCD. (c) The mean, maximum and minimum values of the detected single unit amplitudes. Individual data points are shown in green with a blue distribution curve and the corresponding boxplot. In general, higher (absolute) amplitudes were detected at HCD and upwards unit activity was only observed at HCD.

Chapter 4. A bioresorbable shuttle for penetration of a flexible depth probe *in vivo*

This Chapter will be part of the publication:

"A PVA/PLGA bioresorbable shuttle for implantation of flexible depth probes into the mice brain." J. Pas, A. Rutz, A. Slezia , A. Williamson, A. Kaszas, P. Quilichini, A. Ghestem, M. Donahue, V. Curto, C. Bernard and G.G. Malliaras (paper in preparation, October 2017).

4.1 A Materials Challenge: Inserting Compliant Neural Probes

Irreversible brain damage and complete loss of recording function are unpreventable results when using traditional depth probes. Such probes are neural interfaces designed to understand the complex electrochemical mechanisms deep inside the brain with the ultimate goal to achieve long-term, stable single unit recordings. However, the rigidity of the probes (consisting of silicon or metal micro-wires) causes failure just a few months after implantation **[6], [19]**. The problems pile up after some time and mainly include mechanical failure of interconnects, corrosion of electrical contacts, chronic inflammation due to the severe foreign body response, neuronal death and eventually electrical isolation of the probes **[19]**.

To improve long-term function of depth probes, more compliant materials have been investigated and provide to date very promising results **[3], [6]**. The reasoning behind the use of softer materials is that more compliant probes would cause less damage inside the brain and reduce foreign body response on a long-term basis. Traditional depth probes are made with materials that have elastic moduli above 100 GPa, while the brain is a soft tissue with a modulus ranging from 0.1-10 kPa [3]. Mechanical mismatch as large as 7 orders of magnitude is strongly believed to lead to irreversible tissue damage and eventual electrode failure **[3], [20]**. More compliant devices are fabricated through the use of softer materials, like polyimide parylene-C, SU-8 and polydimethylsiloxane (PDMS) or by making the rigid material thinner, like silicon nanomembranes **[98], [99]** *(Chapter 1, Section 1.3)*.

However, the use of more compliant materials results in a more complicated surgical insertion of the depth probe **[20]**. Most flexible probes are unable to penetrate the brain without buckling and a temporary insertion system is necessary to place the probe at the desired location inside the brain. Solutions to tackle this include either (1) using a stiff

temporary shuttle which is removed after implantation (needle, wire, silicon shank) **[100]–[102]** or (2) a stiff shuttle that degrades or dissolves within in the brain (*Section 4.1.2*). Due to the tissue trauma caused when implanting needles, wires or silicon shanks, our work was focused on the more promising bioresorbable shuttles. Such shuttles are made of bioresorbable polymers (BP) which do not require any surgical removal as they are broken down and excreted or resorbed in the body. The use of a BP is thus a very promising solution to improve the long-term function of flexible neural interfaces leaving behind the flexible probe while diminishing on its own.

4.1.1 Bioresorbable polymers

Although natural bioresorbable polymers have been used for ages, there is still much to discover about synthetic BPs for biomedical applications [103]. Due to the large variety in natural polymers (like collagen, poly(amino acids), elastin, albumin, polysaccharides,…) and the growing catalogue of synthetic polymers (like polyesters, polyglycolide, polycaprolactone,…), there is a great potential to develop new applications with these biomaterials. Every application requires a particular set of properties, which need to be fine-tuned and tested to achieve the desired degradation and physical properties.

The degradation of a BP is dependent upon many factors, such as polymer composition, crystallinity, molecular weight, size and shape of the matrix and the environmental conditions, like pH and local enzyme concentration [104], [105]. For example, a hydrolytically degradable polymer with high crystallinity has a well-organized chain structure, which makes it more difficult for water to diffuse through the bulk material and in most cases decreases the degradation rate. On the contrary, an increase in degradation rate is observed for BPs with lower molecular weights, with small and hydrophilic side chains on the polymer and in strong acidic environments [105].

Biodegradation is not a simple process, not only due to the interplay of so many factors, yet also due to the different types and mechanisms of degradation which can additionally change during the degradation process itself. There is a difference made between surface and bulk degradation. *Surface degradation* involves the degradation from the exposed surface, i.e. the surrounding material should be degraded before inner layers can degrade. This is not the case during *bulk degradation*, when the degradation occurs throughout the entire material, i.e. the inside and the surface degrade simultaneously. Then, there are the different mechanisms which play a role. BPs with hydrolytically labile chemical bonds (esters, anhydrides, carbonates, amides, urethanes and phosphates) undergo hydrolytic degradation, while also *enzymatic* degradation is possible, during which enzymes are responsible for the cleavage of the chemical bonds. While most naturally occurring polymers undergo enzymatic degradation, synthetic polymers can be designed in such a way that both degradations are possible [106].

Another very important consideration is the biocompatibility of the material during its presence in the body. While the initial BP should not evoke any toxic response upon implantation, the degradation products should also be non-toxic. The products need to get metabolized and cleared from the body. Both *in vitro* and *in vivo* assessment is necessary to make sure that the material is acceptable for use in living organisms [106].

4.1.2 Review on the current state-of-art

BPs have been explored for many biomedical applications, however, the use of these materials to facilitate brain penetration for flexible substrates is a very recent research field. While there have been reports on the use of BP as adhesive layer between a neural probe and a rigid insertion support, these will not be discussed in this work. Our work is limited to rigid shuttle made solely from BPs, which is a more promising yet challenging approach as it damages less brain tissue. Here, we briefly discuss on the efforts made and present an overview of reported depth probe parameters with successful penetration *(Table 1)*.

Polyethylene glycol (PEG) is a well-known biodegradable polymer mainly used for drug delivery and soft tissue engineering [103] and it has been reported as one of the first BPs to function as stiffening material for depth probes [53], [107]. In 2005, *Takeuchi et al.* reported on a parylene-based microfluidic system which was filled with PEG [53]. PEG (2700 – 3500 g mol^{-1}) was liquefied on a hotplate at 50 °C, pumped up through suction with a glass pipet into the parylene channel and solidified at room temperature. Once the probe was placed inside the brain, the PEG would dissolve within 200 seconds and leave the parylene probe behind for recording *(Figure 1a)*. Despite this promising invention, this seems like a difficult procedure especially with the risk of rupturing the parylene channel during suction.

Lecomte et al. showed that PEG-coated parylene probes were not as promising as silk-coated parylene probes *(Figure 1b)*. A much higher molecular weight of PEG was used in this work (100 000 g mol^{-1}), which was chosen for being less brittle and, thus, less likely to break during insertion compared to lower molecular weights (3000, 6000, 8000 and 10 000 g mol^{-1}). PEG was diluted in water at 30% w/v, drop casted on top of the flexible probe in a mold and dried at room temperature. While PEG shuttles are able to penetrate brain phantoms, the shuttle did not withstand as high of compression forces as silk (47 mN vs. 300 mN), was not as stiff as silk (120 MPa vs. 2.2 GPa) and could not be used more than twice during insertion due to its fast degradation rate, unlike silk.

Silk was first reported to function as bioresorbable substrate for a brain interface by the combined efforts of Omenetto's and Rogers' group in 2009 [98]. Silk is, from a biological point of view, a very attractive material. Not only does it provide good mechanical stiffness (reported young's moduli of 2 to 6 GPa [107], [108]), its biodegradation time can largely vary from hours to beyond a year and the degradation products are amino acids which can directly be used in cell metabolism [109].

Rogers' and colleagues have published multiple papers using silk as substrate for brain sensors [98], [99], [110] and recent work reports on the use of silk as shuttle material for depth probes [107], [108], [111]. The difference between these papers is mainly the shuttle's fabrication methods, which has either been done through dip-coating or by using a polydimethylsiloxane (PDMS) mold. The use of a mold showed more promising results for shaping the shuttle [107], [108], especially compared to the limited control over the final shape and dimensions of the probe during dip-coating [111]. Furthermore, the exact degradation time of the silk shuttles were not mentioned in the papers. *Wu et al.* did state an immediate dissolution of the silk coating after implantation, however, they did not provide the necessary details on the used silk concentration or other relevant impact factors [108]. The others did perform enzymatic degradation tests on molded and dried silk fibroin sheets, which resulted in degradation times of a few hours (without a mentioned silk formulation) [111] to a few days to even a few weeks (using 7% w/v silk sheets with 5 x 5 x 2 mm^3 dimensions) [107]. While this long degradation time could be problematic for this neural application, the main shortcoming of silk remains the uncertainty on its biocompatibility, especially long-term [109].

Other natural occurring polymers, like cellulose and maltose, have also been used for neural interfaces [112], [113]. Moreover, besides the use of a single BP to function as brain shuttle, there has also been looked at the combination of multiple polymers. *Agorelius et al.* embedded for example parylene-covered golden leads in a thick layer of a gelatin mixture for brain penetration *(Figure 1c)* [114]. The polymer mixture included gelatin, PEG and glycerol, which were shaped into a needle-like tip and were additionally coated with a Kollicoat™ solution. This last coating was necessary to delay the dissolution of the matrix material until the implant was fully implanted. Implantation was successful and the brain surface seemed to contract around the implant. *Harris et al.* demonstrated the possibility of creating nanocomposite implants using poly (vinyl acetate) and cellulose nanocrystals, which would mechanically reduce in tensile moduli from 5 GPa to 12 MPa minutes upon exposure to cerebral spinal fluid at 37°C [115]. The mechanically adaptive implant has also shown much promise to function as drug release system, locally delivering resveratrol to reduce the tissue response at the interface [116].

A major drawback of natural materials is that the material properties are generally harder to manipulate. Consequently, efforts towards the use of synthetic BPs have most recently been reported for this application. For example, *Lo et al.* demonstrated how a fast degrading tyrosine-derived polycarbonate coating improved insertion of a flexible dummy probe into the brain [28]. The promising polymer provided sufficient stiffness (E=1,6 GPa) for insertion into a brain model (1% agarose gel) and showed complete degradation within 2 hours. The polymer degradation is based on hydrolysis and is expected to go even faster *in vivo*, due to the expected larger water content inside a real brain. Moreover, this coating showed 100%

insertion success (n=12) combined with a thin SU8 dummy probe into a fresh rat brain and shows thereby much promise for neural probe applications.

To summarize the work on BP shuttles for neural probes, an overview is provided on implantation relevant characteristics of the above mentioned flexible depth probes (*Table 1)*. The dimensions of the device and coating, along with the mechanical properties and dissolution rates are given. Note that a stiffer material will resist larger buckling forces (*Chapter 1, Section 1.3.1*), which is illustrated by comparing for example a PEG coating and a silk coating. Using both polymers as shuttles with the same dimensions, silk improves the coating strength almost 6-fold [107]. When comparing a silk-coated probe with a tyrosine-based coated probe which mainly differ in shuttle dimensions (a tip length twice as short, yet almost half as thick), makes the tyrosine-based probe almost 30 times less strong compared to the silk coating (300 mN for silk vs. 10 mN for tyrosine-based shuttle). Hence, it must be kept in mind that not only the material characteristics, yet also the coating dimensions, play a role in the success of flexible probe implantation.

To conclude, various BPs have been used to enable insertion of flexible depth probes into the brain. While the polymer PEG initially showed sufficient stiffness and fast degradation rates for this application, silk showed a more promising stiffness, potentially enabling fabrication of smaller devices which consequently induce less brain damage. However, the slow degradation and uninvestigated long-term biocompatibility of silk are concerning drawbacks. While other natural polymers have shown to successfully penetrate the brain, these polymers cannot be as easily tuned as synthetic polymers. Thus, in our opinion, synthetically made polymers are the future for BP-shuttled neural probes.

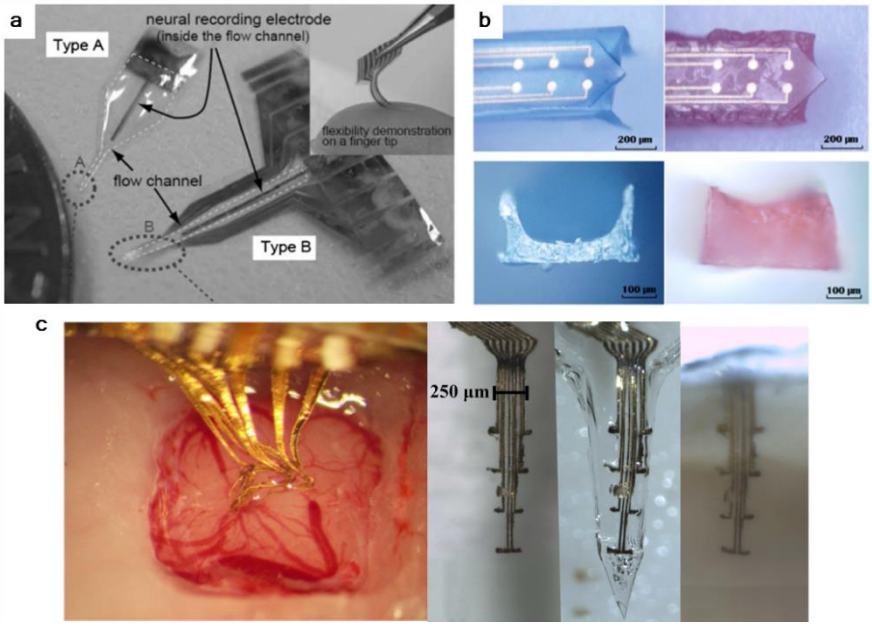

Figure 1. Bioresorbable-shuttled depth probes. (a) Parylene flexible probes with a microfluidic channel containing the BP polyethylene glycol (PEG). Adapted from [25]. (b) Parylene backed-probe with PEG (left) and silk (right) from the front and side view. Adapted from [18]. (c) A gelatin embedded probe with golden leads along which the brain contracts (left) with pictures of the golden leads, the golden leads embedded in the gelatin mixture and the complex inside a brain tissue, respectively (right). Adapted from [31].

Table 1. Overview of reported BP used for brain penetration of depth probes.

Coating Material	Coating method	Substrate material	Dimensions			Mechanical properties			Dissolution	Byproducts	In vivo Rec	Ref
			Probe (L x W x T)	Coating (T)	Total Device	Youngs-modulus	Buckling study	Note	Rate			
PEG	Suction with glass pipet of PEG in microchannel	Parylene	10 µm (T)	10 µm	**20 µm** (T)	-	No coating 1 mN; **12 mN** with PEG	Volume in channel approximately 7 x 10-6 µm^3 PEG	7 x 10-6 µm^3 PEG dissolved in 200 s	-	Acute recording with gold electrode inside microchannel (no direct contact)	Takeuchi et al. (2005)
PEG	PDMS molding	Parylene	**6.25 mm** x 350 µm x 24 µm	236 µm	**250 µm** (T)	120 Mpa	No coating 2.6 mN; **47 mN** with PEG	-	Not exactly determined - too fast dissolved	Unknown	Not performed.	Lecomte et al. (2015)
Silk	PDMS molding	Parylene	**2 mm** x 36 µm x 8 µm	30-65 µm	8 shanks per device; **73 µm** (est. T)	-	-	100 % succes with 65 µm silk coating (n=3)		-	Recording up to 6 weeks.	Wu et al. (2015)
Silk	PDMS molding	Parylene	**6.25 mm** x 350 µm x 24 µm	110 µm bottom - 240 µm walls (u-Beam)	**250 µm** (T)	2.2 Gpa	No coating 2.6 mN; **300 mN** with silk	-	Depends on annealing time. Few days up to 2 weeks (1-6h annealing)	-	Acute recordings. 250 um thick. No buckling.	Lecomte et al. (2015)
Gelatin & PEG & glycerol (Kollicoat)	PMMA molding	Parylene with gold leads	**? mm** X 4 x 10 µm	75, 100 or 125 µm	400 µm (W) x **130 µm** (T)	-	Deformation force: **373 mN**	Buckled: 75 - 100 µm. No Buckling: 125 µm.	In vivo: gelatin dissolved after 3.5h and brain contracted around implant.	Gelatin is degrades by collagenase	Recording up to 3 weeks. Depth 1800 µm achieved.	Agorelius et al. (2015)
Carboxy-methyl-cellulose	Silicon and polyvinyl siloxane molding	Meandering platinum wires insulated with parylene	**1.5 mm** x 10 µm x 2.5 µm	100 - 300 µm (W)	**135 µm** (est. T)	-	-	Insertion succeeded in vivo.	Becomes a gel <3min. Does not completely dissolve.	Monosaccharides	-	Gilgunn et al. (2012)
Maltose	Drawing lithography	Polyimide (PI)	**3.5 mm** x 200 µm x 10 µm	30 - 300 µm (T)	**310 µm** (est. T)	-	Exp. increase with increase in T: **500 mN** or less (T<100 µm); **3.8 N** (T=300 µm)	-	<20 s for T <180 µm. >100 s for T= 300 µm	monosaccharides	2.2 mm deep. Acute recordings.	Xiang et al. (2014)
Tyrosine and PEG derived polycarbonate (E5005(2k))	Dip coating	Polyimide (PI) / Pt-Ir microwire	PI: **? mm** (L) x 60 µm x 7.5 µm	Not mentioned	Not mentioned	862 Mpa (E5005(2k) fibers without PI or µwires)	-	Insertion of coated PI substrate in agarose succeeded.	Recordings with coated µwire possible within 60 min in vivo.	Dissolution and hydrolitic cleavage	60 min after insertion. 1 week long.	Lewitus et al. (2011)
Tyrosine and PEG derived polycarbonate (E5005(2k))	PDMS molding	SU8	**3 mm** x 30 µm x 10 µm	100 or 250 µm	3.5 mm x 100 µm x **110 µm** (L x W x est. T)	1.64 Gpa	**10 mN** (T=110 µm); **90 mN** (T=260 µm)	In vivo: SU8 without coating (6 succes, 5 failed). With coating 100 % succes insertion (n=12).	60min in PBS. 60% dissolved directly after insertion and 2h completely dissolved in 1% agarose model.	Dissolution and hydrolitic cleavage	Dummy probe without microelectrodes	Lo et al. (2015)

4.1.3 Research approach

In this chapter, we will discuss the fabrication of a BP shuttle based on poly(vinyl alcohol) (PVA) and poly(lactic-co-glycolic) (PLGA, 65:35) as solution to enable the penetration of a flexible parylene probe into the brain. Both polymers are synthetic and were chosen due to their biocompatible, the option of chemically tune the polymers further for the desired application and most importantly, have FDA approved uses **[106]**.

Before the evaluation of the PVA-shuttled flexible probe in vivo, a fabrication method was developed to shape PVA into the designed probe format. Then, the dissolution time, stiffness and electrical influence were investigated. The dissolution of the polymer was examined using artificial cerebrospinal fluid (ACSF) at 37 °C to mimic in vivo degradation and the

shuttle stiffness was tested using a 0.6% w/w agarose brain model. A successful penetration into this brain model provides a decent insight into the penetration of an in vivo brain, as the insertion forces of a silicon probe have shown to be similar in the agarose model and a rat's brain with dura (43 mN vs. 41 mN) [33]. Evaluation of the exact mechanical strength was not possible, due to the lack of the necessary equipment to measure the nano-scaled buckling or insertion forces exerted on the probe. The electrical properties of the probe were investigated through electrochemical impedance spectroscopy (EIS) to make sure that the BP would not affect the electrical recordings. Finally, the optimized BP-shuttled probes were tested both in toto and in vivo in collaboration with the Neuroscience Institute of Aix-Marseille University.

4.2 Development of the bioresorbable shuttle

In this work, the use of a simple and cheap, synthetic BP *poly(vinyl alcohol) (PVA)* was investigated to enable brain penetration of a flexible parylene probe. PVA was chosen due to its characteristics of being water soluble, biocompatible and most importantly, already having FDA approved uses [117]. The use of hydrolytic degradable polymers was desired for the ease of shuttle dissolution inside the brain. Moreover, hydrolytically degradable polymers are generally preferred for implants as these do not vary as much per batch or do not elicit variable results once inside patients [106].

PVA is known for its water-soluble character and has been employed in a surprisingly large variety of products in our society [118]. The polymer is obtained via hydrolysis of polyvinyl acetate, which results in fully or partially hydrolyzed PVA *(Figure 2).* The molecular weight of the polymer can variate from 9,000 – 400,000 g mol^{-1}. Practical applications containing PVA include paper and textiles, dissolvable foils for agriculture to deliver fertilizers, dissolvable films for laundry detergents, support structure for 3D printing to dissolve away after fabrication, etc [118], [119].

The BP has been used in many medical applications, such as the first absorbable surgery threads in the 1930's [120], hydrogels for tissue engineering of cartilage and bone [117] and artificial organs [121]. Despite this wide range of applications, little information was found regarding its BP characteristics as stand-alone PVA film. Yet, a promising 0.4 GPa in young's modulus was reported on PVA [122], which is not as stiff as silicon yet remains multiple orders of magnitude higher than brain tissue to enable insertion. Moreover, as the polymer can be converted into a hydrogel, it has the possibility to absorb water and therefor swell, depending on the degree of cross linking [123]. The polymer has mostly been characterized for medical applications when used in combination with other BPs [117]. Regarding its degradation, the excretion of intravenously injected PVA showed that most of the polymer is directly excreted by the kidneys [124]. Accumulation of PVA in other organs was hardly observed and especially the lower molecular weights (15,000 g mol^{-1}) were most rapidly cleared from the blood (compared to higher molecular weights of 70,000-430,000 g $mol^{-1)}$.

Although new research will have to be performed to investigate the excretion from the brain, lower molecular weights of the polymer seem promising.

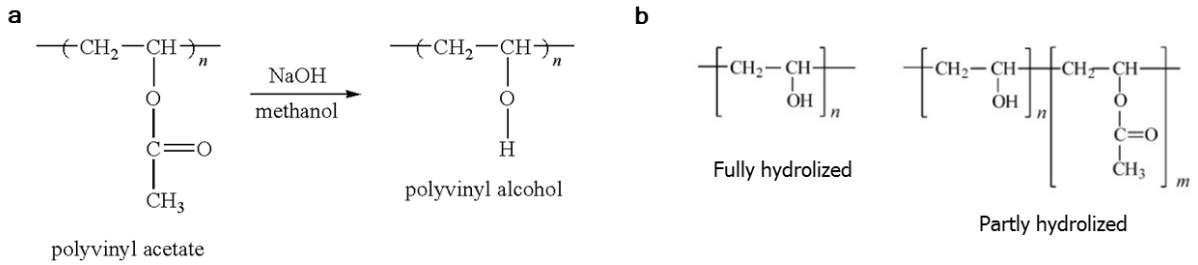

Figure 2. Presentation of PVA. (a) Synthesis of PVA from polyvinyl acetate. (b) The chemical structures of fully and partly hydrolyzed PVA. At high degree of hydrolysis and polymerization, PVA becomes less soluble in water unless heated up to 80 °C [125].

4.2.1 Fabrication of the bioresorbable shuttle

The BP shuttles were prepared after the fabrication of flexible parylene probes connected to ZIF cables (*Chapter 2*). A custom-made polydimethylsiloxane (PDMS) mold is used in which the probe is first aligned with water and a paint brush (*Figure 3*). Then, a 20% w/v PVA solution is deposited on top of the probe and blade-casted. The device and mold are subsequently placed in the oven to homogenously remove the solvent from the polymer solution, unlike leaving it to dry at room temperature as others [107], [126]. This is repeated twice and once dried, the probe easily removed from the mold with tweezers. An alternative fabrication approach was also investigated (*Supp. Figures 1-2, Section 4.6*), however, did not show the desired outcome yet.

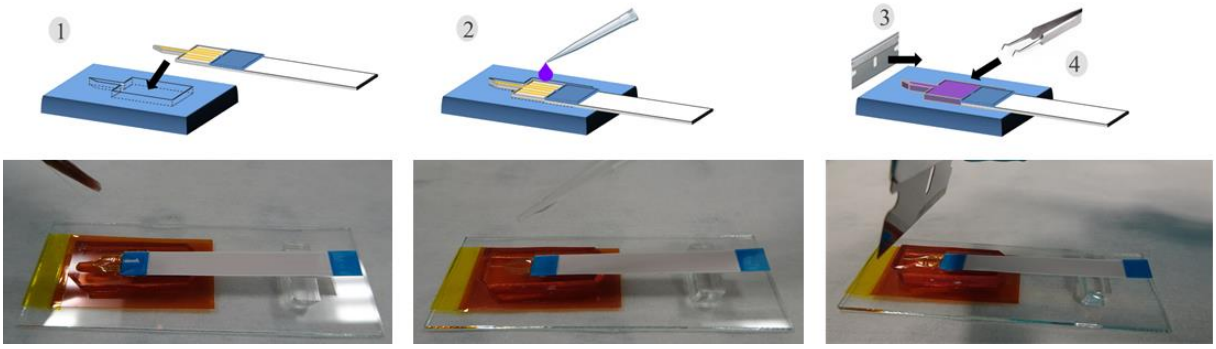

Figure 3. Demonstration on the fabrication of the PVA shuttle. First, the probe is aligned in a PDMS mold using a paint brush and water. Next, a PVA solution is deposited on top, blade casted and placed in the oven at 70°C. After a second deposition run, the probe is removed from the mold.

The molding approach results in a stiff flexible depth probe. While the uncoated probe curls and is very easily damaged, the BP coated probe is not *(Figure 4a)*. The BP does make the probe slightly larger to facilitate alignment in the PDMS mold. The probe is 180 μm wide and 4 μm thick and with the addition of the shuttle, the final dimensions are 280 μm in width and 90 μm in thickness. The probe can be observed with a simple optical microscope since the coating is transparent. The coating was further examined using scanning electron

microscopy (SEM) *(Figures 4b-e)*. The device has a sharp angle of 20°, which is important for penetration, as observed during a preliminary study using SU8 shanks with different tip angles and showed similar results as reported by others [31] (*data not provided*).

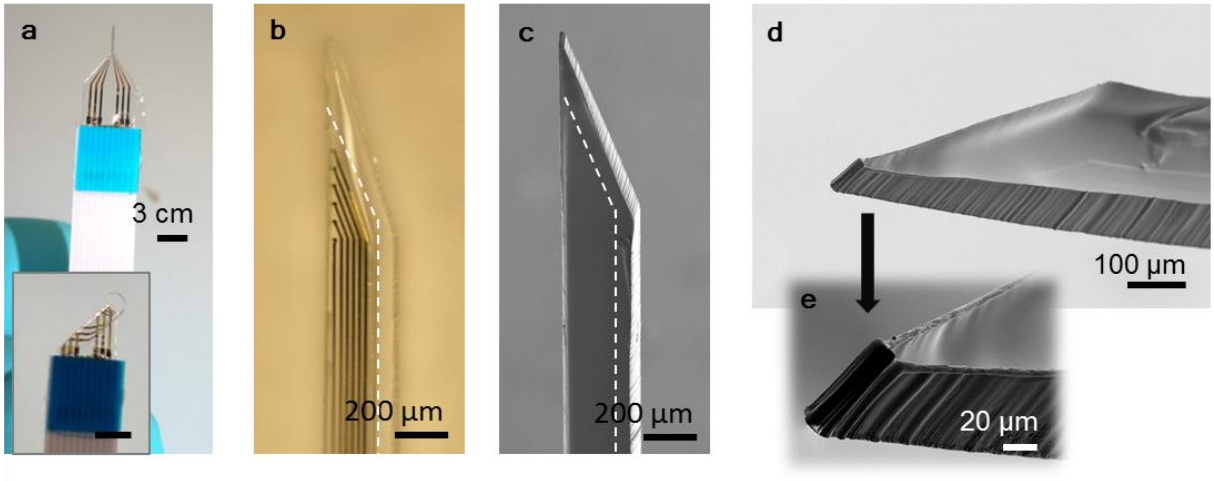

Figure 4. PVA shuttled flexible neural probe. (a) Picture of the probe held up by the PVA shuttle. Inset: a probe without the shuttle. (b) Microscope image of a PVA shuttled probe. The white dashed lines illustrate the boundary of the actual parylene probe, which is smaller than the actual PVA shuttle (probe: 180 µm wide vs. shuttle: 280 µm wide). (c-e) SEM pictures of a PVA shuttled probe, demonstrating a sharp tip angle of 20° and enabling the estimation of the device thickness of 90 µm.

Three molecular weights of PVA were used to evaluate the differences in degradation rates of the shuttles. Dummy shuttles with PVA of 10 000 (10k) and 90 000 g mol^{-1} (90k) dissolved at 20% w/v in deionized water (DI) were made. This was however not possible for shuttles of PVA at the highest molecular weight of 150 000 g mol^{-1} (150k). The polymer did not homogenously dissolve in water at 20% w/v after 3 days of stirring at 90 °C and was thus not further evaluated. In any case, the use of lower molecular weights is favorable for the degradation and excretion of the bioresorbable polymer [124].

Moreover, due to the fast dissoluble character of PVA, additional coatings around the shuttles were evaluated to decrease the BP dissolution rate for *in vivo* penetration. Approaches involved the addition of a hydrophobic coating using fluorinated liquids, the addition of an ultrathin parylene layer around the PVA shuttles and addition of another BP coating known for its very slow degradation rate, poly(lactic-co-glycolic acid) (PLGA). The last option was a great success and will be further elaborated in this chapter.

Why was PLGA chosen? PLGA has been shown to be a very practical polymer for tissue engineering and drug delivery due to its largely tunable mechanical and degradation characteristics [105]. The polymer is a co-polymer of poly lactic acid (PLA) and poly glycolic acid (PGA) and has extensively been studied to understand the release of drug from BP matrices. The physical appearance mainly depends on the initial molecular weight, the ratio of lactide to glycolide, the storage temperature and the overall size of the application. Generally, a higher content of PLA leads to a decreased crystallinity and a slower degradation rate due to the presence of the methyl group. The use of a higher molecular

weight also decreases the degradation time and the material is considered 'fairly rigid' due to its T_g above physiological temperature of 37 °C. The degradation (bulk degradation) of PLGA was demonstrated both *in vitro* and *in vivo* through hydrolysis *(Figure 5)*, which cleaves the ester linkage first into oligomers and then into monomers [105].

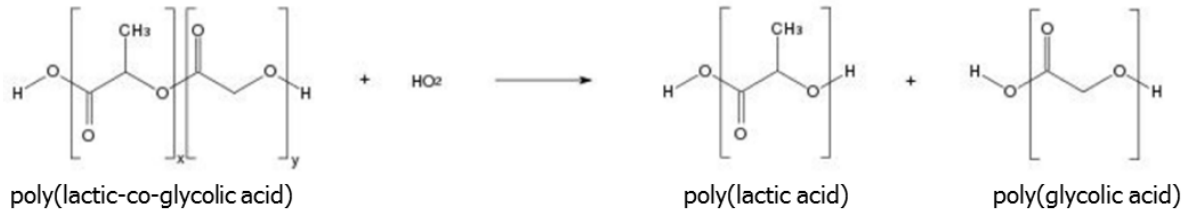

Figure 5. Degradation in vitro and in vivo of PLGA into polylactic acide (PLA) and polyglycolic acid (PGA) through hydolysis. Adapted from [105].

4.2.2 Mechanical characterization

The use of the two different BPs, PVA and PLGA, as shuttle materials was the solution to enable the insertion of the flexible depth probe into a wet brain. Although various concentrations of the BPs for shuttle fabrication were evaluated, shuttles of 20% w/v PVA combined with 25% w/v PLGA were used during the mentioned characterizations here as these showed the most promising results. The other data can be found in *Section 4.6 (Supp. Figures 3-6)*. Dissolution tests were performed at 37 °C using ACSF and the mechanical stiffness was evaluated using a wet 0.6% agarose brain model.

As shown in *Figure 6*, PVA shuttles (10k) dissolved within 30 seconds. Although the use of a higher molecular weight of PVA (90k) changed the dissolution rate compared to the 10k PVA shuttles, it did not have any significant impact on its loss of rigidity in solution: the tip started 'moving' in the solution shown with the curled position (a displacement due to dissolution). The swelling of the shuttle was not investigated. This should nevertheless not be neglected, as this could affect brain tissue during in vivo experiments. Future work

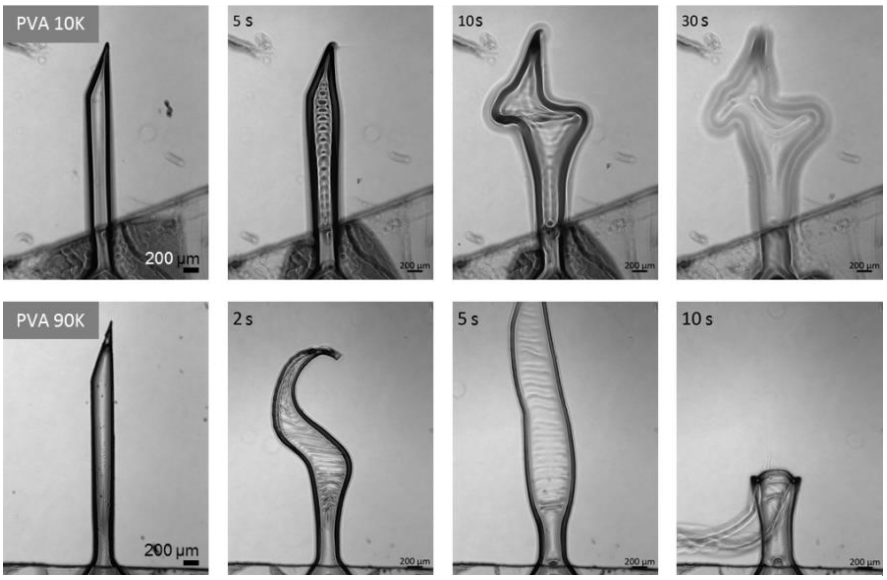

Figure 6. Dissolution of 10k and 90k PVA shuttles. PVA10k shuttles dissolve within 30 min when immersed in warm ACFS. PVA90k shuttles did not dissolve that fast, yet lost their rigidity almost instantaneously.

should focus on this. This experiment showed that both molecular weights seemed to be affected only 10 seconds after immersion. Thus, the lowest molecular weight of 10k was used during the rest of this work.

Different coatings for the PVA shuttle were investigated to prevent the fast dissolution rate. A PLGA coating prevented the shuttle from dissolving as fast and kept the probe intact for at least more than 3 minutes *(Figure 7)*. *Figure 7a* shows an overview of the observed dissolution range of the PVA shuttles without and with PLGA coating around. Three stages were defined to evaluate the dissolution a dummy shuttle (i.e. just the BP shuttle without a flexible probe):

- Stage 1: The shuttle starts to deform, due to the immersion into warm ACSF.
- Stage 2: The shuttle starts to significantly move due to dissolution, which means that it has lost its rigidity.
- Stage 3: Borders of the BP shuttle are almost not visible anymore and/or a thin layer is observed.

The addition of a PLGA coating through dip coating significantly decreased the dissolution time *(Figure 7a)*. The deformation of the PVA/PLGA shuttle is postponed by almost a minute and the loss of rigidity (based on stage 2) is generally observed after more than 2 minutes, which is significantly longer than the 7 seconds of the PVA shuttle. Furthermore, while the PVA shuttle appears to be completely gone after 30 seconds, a thin layer remains of the PVA/PLGA shuttle for more than 1 month. Crucial time points for the different shuttles with a flexible probe are illustrated in *Figure 7b*. Clearly, the PVA/PLGA shuttle provides a more promising BR interface for brain penetration.

a

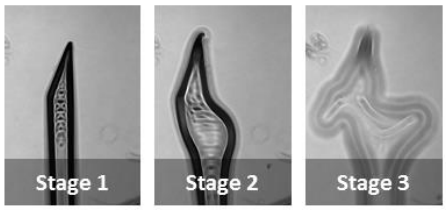

Probe	Stage 1 Start deformation	Stage 2 Start movement	stage 3 Limited borders
PVA			
p1	7 s	7 s	30 s
p2	2 s	5 s	30 s
p3	1 s	2 s	30 s
Range	1 - 7 s	2 - 7 s	30 s
PVA/PLGA			
p1	60 s	> 200 s	> 1 month
p2	60 s	> 200 s	> 1 month
p3	45 s	120 s	> 1 month
Range	45 - 60 s	120 s - >200 s	> 1 month

b

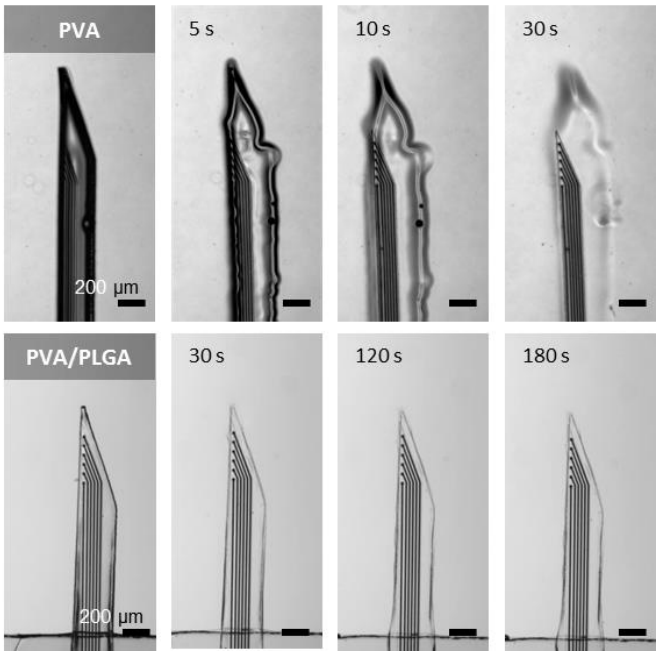

Figure 7. Dissolution of PVA and PVA/PLGA shuttles. (a) The difference between both shuttle types were evaluated based on three stages: the time during which (1) deformation starts, (2) movement is observed and (3) the borders are almost gone. PVA/PLGA shuttles deform and lose their rigidity much later than

PVA shuttles, which dissolve after only 30s while PVA/PLGA shuttles remain present for more than a month. (b) Example of the dissolution of PVA and PVA/PLGA shuttled probes in ACSF at 37 °C. The PVA shuttle completely dissolves within 30 seconds, while the PVA/PLGA shuttle only starts dissolving around a minute and remains present for more than a month.

The exact dissolubility rate of the PVA/PLGA shuttle was difficult to estimate. Unlike PVA, PLGA degrades very slow through bulk erosion, as shown both *in vitro* and *in vivo* [105], [117]. During the performed experiments, PVA appeared to dissolve most probably through defects in the PLGA layer. Along with the dissolution of the PVA, the probes stiffness is lost. Although PLGA coatings seem to remain present for at least a month at 37 °C in ACSF (*Figure 8*), a flexible substrate is consequently expected several minutes after *in vivo* implantation. Although PLGA primarily degrades through hydrolytic degradation, there are conflicting results suggesting the occurrence of additional enzymatic degradation [105]. This will nevertheless not have any significant influence on the implantation of the flexible probe.

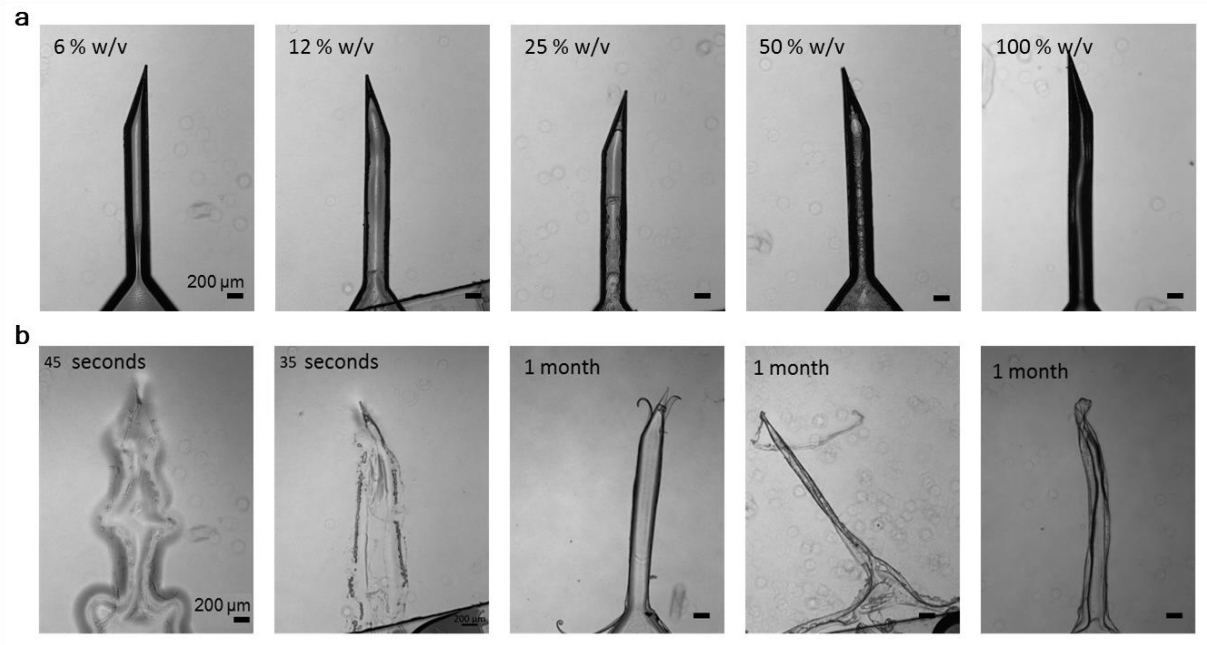

Figure 8. PVA shuttles coated with various PLGA concentrated solutions. (a) Images of the shuttles before immersion in ACSF. (b) Dissolved or still immersed PVA/PLGA shuttles in ACSF at 37° during the mentioned times. Low PLGA concentrations do not decrease the total dissolution time, while concentrations above 25% w/v of PLGA in acetone remain relatively well intact past 1 month.

There were two limiting factors for *in vivo* brain penetration with a PVA shuttled probe, mainly the fast dissolution rate and the straightness of the probe tip. The PVA shuttle showed sufficient strength to penetrate the agarose brain model without a PLGA coating, as shown in *Figure 9a*. The PVA shuttle does dissolve within one minute inside the wet brain model, making multiple penetrations impossible. Moreover, the PVA shuttles need to be straight to ensure a deep penetration *(Figure 9b-c)*. The PVA shuttles were sensitive to the humid air and occasionally bent when not used directly. Although a bent probe could enter, a deviation inside the brain was consequently more likely which would not be desired during *in vivo* experiments. While the first factor was solved by adding a PLGA coating, the

second was dealt with by keeping the probe with PVA shuttle inside the mold till just before the surgery.

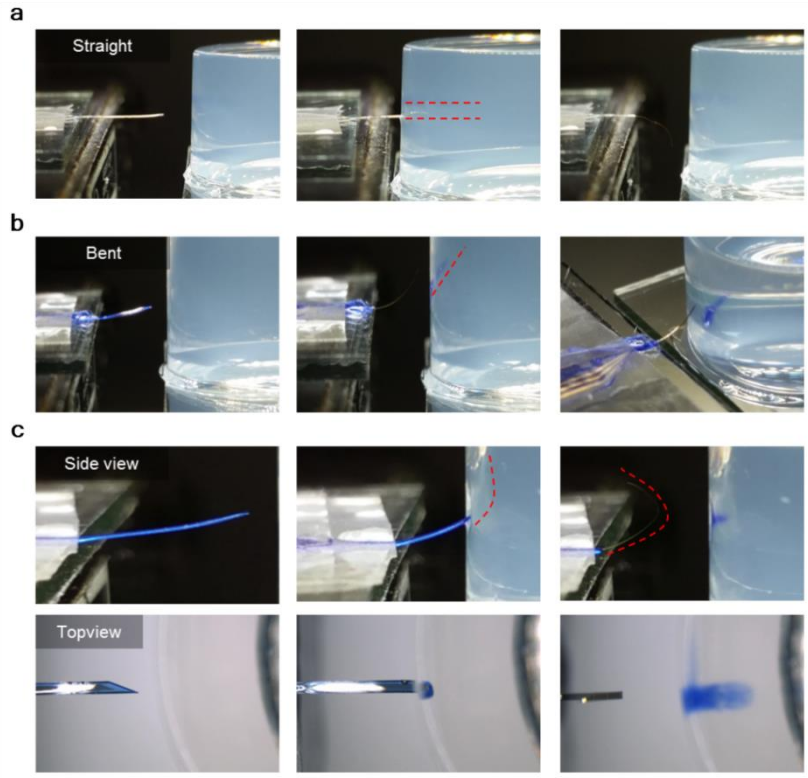

Figure 9. Penetration of PVA shuttled probes into an agarose brain model. (a) Successful penetration of a straight probe into the brain. The PVA shuttle is dissolved after penetration. (b) A bent probe can penetrate the brain. (c) Side and top view of a brain penetration with a bent probe. Despite the fact that the probe enters, it remains at the surface of the brain.

Besides the decreased dissolution of the shuttle with, the addition of PLGA also enabled multiple penetrations of the brain with the same probe (*Figure 10*). While PVA shuttles dissolved inside the wet agarose and almost nothing of the probe tip would remain, this was not the case with PLGA/PVA shuttles. The shuttle would slowly degrade in time, and up to five penetrations were observed twice with PLGA coated shuttles (n=6). One must however take in mind that the mechanical penetrations were performed in room temperature brain model. The higher body temperature has additional effect on the shuttle's dissolution.

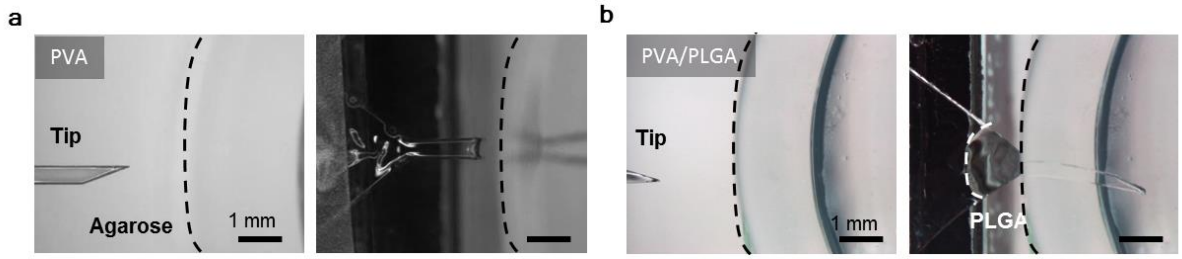

Figure 10. Top view penetrations of BP shuttles. A PVA shuttle (a) dissolves during the penetration while a PVA/PLGA shuttle (b) remains intact and allows multiple penetrations.

To summarize, although PVA showed sufficient stiffness to penetrate the brain model, its dissolution rate of ~70 μm per minute made it almost impossible to get the probe deep into

the brain model before it would dissolve. The additional PLGA coating showed its benefit by allowing not only deep penetration, also enabling multiple penetrations of the same probe. And finally, a straight probe tip is required to insert the probe deep into the brain without deviation.

4.2.3 Electrical characterization

Two type of shuttles were made based on the fabrication procedure: a *'front side-coated' (FSC)* probe and a *'back-side-coated' (BSC) probe*. A FSC probe had the electrodes upwards in the PDMS mold before PVA coating and its tip was completely immersed in a PLGA solution. On the contrary, a BCS probe had the electrodes downwards in the mold before PVA coating and only the back side of the BSC probe would be placed in contact with the PLGA solution. A schematic is shown in *Figure 11a* to illustrate the depositions of both polymers. A difference between both probes was made to evaluate whether the BPs would influence the electrical properties of the probe. While the FSC probe would have polymer covering the electrodes, this was not expected for the BSC probes.

However, both deposition methods seemed to cover the probes microelectrodes in PVA despite the different coating procedures (*Figure 11b*). The electrode sites are clearly not visible in both cases, while they were both upwards during the SEM imaging. This means that the PVA solution does go below the parylene probe in the PDMS mold during shuttle fabrication. The majority of the polymer did remain on top of the device, which is seen by the different depth profiles of the parylene edge in the pictures. Moreover, while the FSC probe shows homogeneous BP layers around the tip, this is not observed with the BSC probe. Despite only dipping the back side of the probe in the PLGA solution, also a part of the front side of the BS probe tip seems to be coated with PLGA (green part, *Figure 11b*). This is almost unpreventable, as the micrometer tip is manually dip-coated into the PLGA solution.

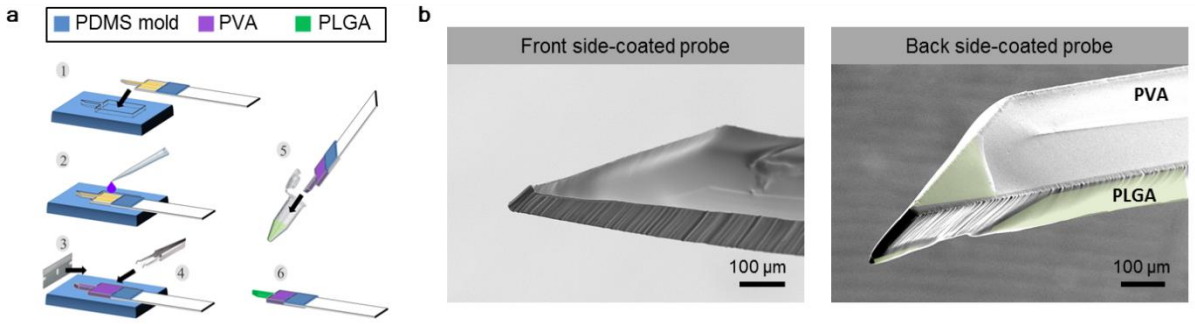

Figure 11. (a) Fabrication of a PVA/PLGA shuttled probes. (b) Front side coated (FSc) and back side-coated (BSc) probes with the microelectrodes covered in BPs. PLGA (greenish areas) is also observed on the front side of the BSc probes, due to the challenging manual dip-coating.

The BP shuttles did not seem to greatly affect the electrical impedance of the flexible probes at the biologically relevant 1 kHz (*Figure 12*). As mentioned in *Chapter 2*, impedance was measured through a three-electrode set-up during electrochemical impedance spectroscopy (EIS) in DPBS. A gradual change in impedance is observed during the immersion of the PVA

FCS probe in the saline solution (*Figure 12a*). The impedance of the electrode restored to its original value after 10 minutes. This seemed to be the case for the large majority of the measured PVA FSC coated electrodes, as shown with the 13 different evaluated electrodes in *Figure 12d* (E1-E13). An average impedance of 41.5 ± 6.4 kΩ (before) and 33.2 ± 16.8 kΩ (after) were observed, excluding in this average electrode 5 (*E5*) which showed an impedance of 46.7 kΩ (before) and 551.1 kΩ (after).

Surprisingly, a slightly more abrupt and faster decrease in impedance was observed for PVA/PLGA shuttled probes (*Figure 12c*). The original value was restored after only 3 minutes for both FCS and BSC probes. This was not expected, as the PVA/PLGA shuttle is much slower dissolved than a PVA shuttle. This consequently shows that the presence of the polymers do not obstruct the electrical measurements, which makes both the FCS and BSC probes suitable for *in vivo* recordings. Similar average impedances were observed, more specifically 42.6 ± 5.9 kΩ (before) and 30.8 ± 14.7 kΩ (after), excluding the exceptionally high impedances above 100 kOhm of E11 (before) and E8, E12 (after). Further research with the PVA/PLGA shuttled probe will be performed to understand this observed trend.

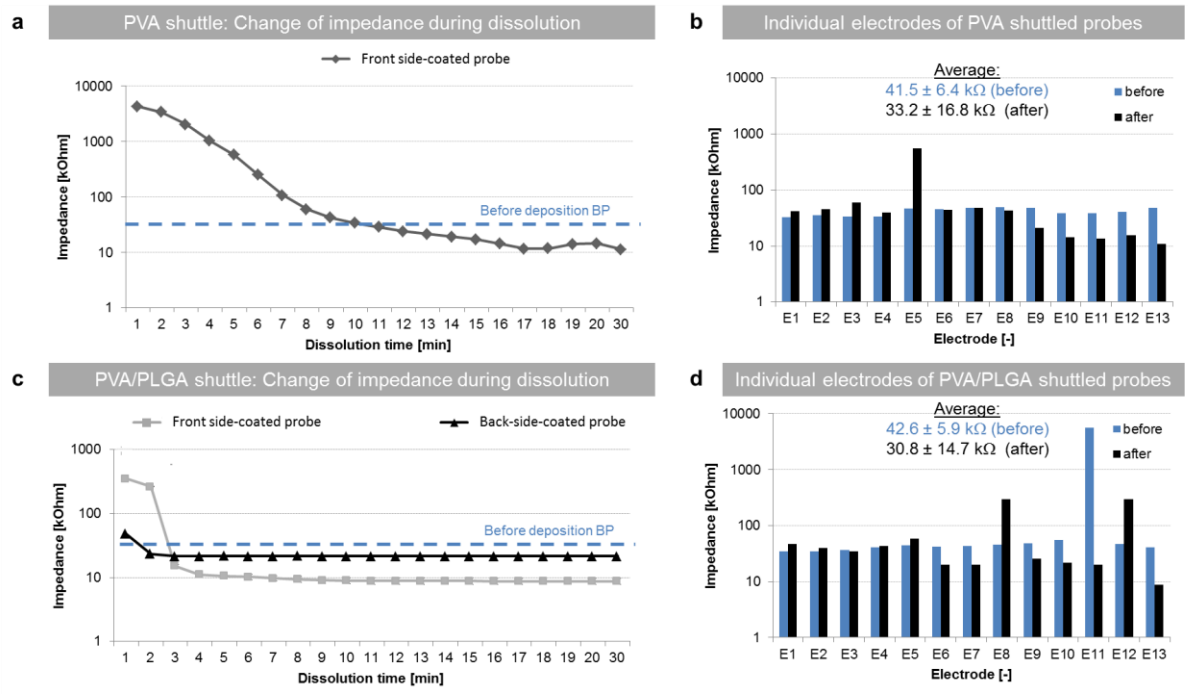

Figure 12. Effect of BP shuttles on electrode impedance. Comparison of PVA (a and b) and PVA/PLGA (c and d) probes. (a) and (c) show a change of impedance in time of a single electrode during dissolution in DPBS at room temperature is shown for both. (b) and (d) show an overview of the individual change in electrode impedances before BP deposition and after 10 min dissolution of the BP shuttle (n=13 electrodes per plot, E1-E13).

The change in impedance over several weeks was also investigated during a continuous storage of the probes in DPBS at 37°C to mimic *in vivo* environment (*Figure 13*). The average impedance of this batch was 32.3 ± 13.2 kΩ before the deposition of the BPs (shown in blue).

This value was lower during the weekly measuring times of the experiment (overview of all the measured impedances are found in *Supp. Figure 7, Section 4.6*). Exceptionally, an increase in impedance during the 4 weeks of evaluation was observed (*Figure 13b*, 3 electrodes are 'exceptions', n=27). No particular difference was observed with SEM between the different electrodes, apart from the electrode which reached an impedance of 600 kΩ as it seemed mechanically damaged. A paint brush is occasionally used to place the tip in decent position for measurements. Overall, the low impedance and stable measurement show great promise for chronic *in vivo* recordings.

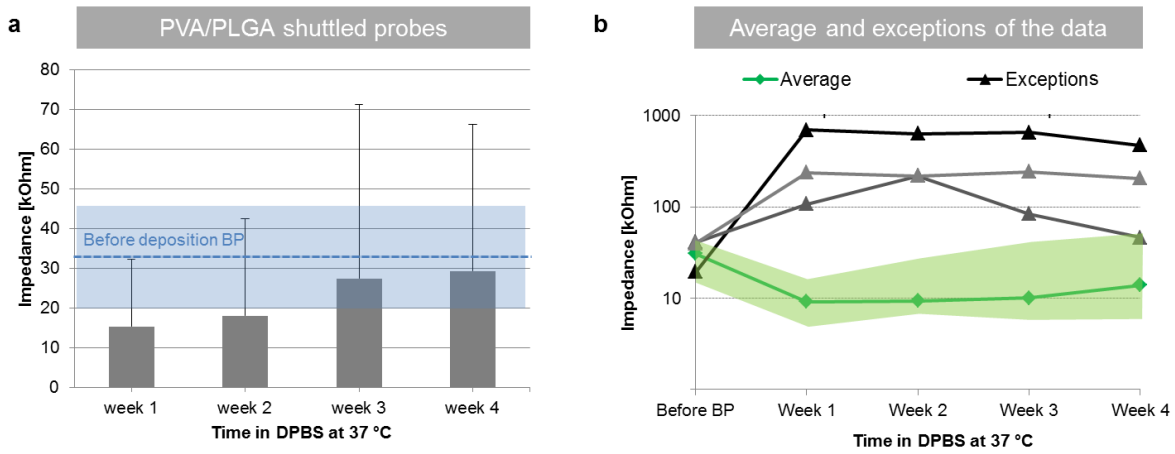

Figure 13. Change in impedance during a month of immersion in DPBS at 37 °C. (a) The average impedance and standard deviation of 24 electrodes on 4 different PVA/PLGA shuttled probes are shown in function of the amount of weeks immersed in the saline solution (n=24). The impedance is overall lower during immersion of probes in the saline solution compared to the initial value before deposition of the BPs. Data is presented as mean ± SD. (b) The average impedances per week on logarithmic scale. The measured averages (green line) and the area between the minimum and maximum observed values (green are) are shown (n=24). The exceptional impedances of 3 excluded electrodes (n=3) are plotted in the same graph, each with a different line, to illustrate that occasionally the impedance did increase after weeks in saline solution.

4.3 In vivo experiments

The PVA/PLGA shuttled flexible probes were easily inserted into the brain without dura of *in vivo* anaesthetized mice. Successful penetration was observed with 7 out of 7 straight probes and 1 out of the 6 bent probes during 7 separate experiments. Only the bended probes did not penetrate the brain, which was to be expected after characterization. The penetration of only 1 bent probe was made possible by additionally using tweezers to try and keep it straight. *Figure 14* shows histology results from three probe penetrations, showing the straight trajectory for a straight probe and a more deviated and failed penetration for two bent probes. Hence, it is not only necessary to have a sufficiently stiff shuttle, it must also be very straight to ensure a successful penetration.

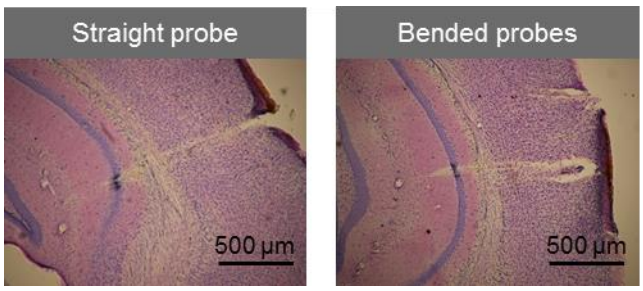

Figure 14. Histology with Nissl staining after brain penetration with a straight (left) and two bended probes (right).

Acute in vivo measurements were performed with PVA/PLGA-shuttled probes and resulted in the recording of local field potentials (LFPs) and single cell activity. Figure 15a shows a picture of one of the penetrated probes inside a mice brain along with a microscope picture of that same probe below. An example of the recorded LFP signals with a single probe is shown in Figure 15b. Four out of the six electrodes measured activity. The tip of the probe reached up to the sixth cortical layer *(Figure 15c)*. Cell nuclei and neural cells were stained from the extracted brain with DAPI and Nissl during histology. The trace of the probe is clearly visible with similar dimensions as the BP-shuttled probe. The microelectrodes of the probe were located at least 150 µm above the end of the tip, with a spacing of 90 um in between the electrodes. Most electrodes were thus located in the fifth cortical layer during the recordings.

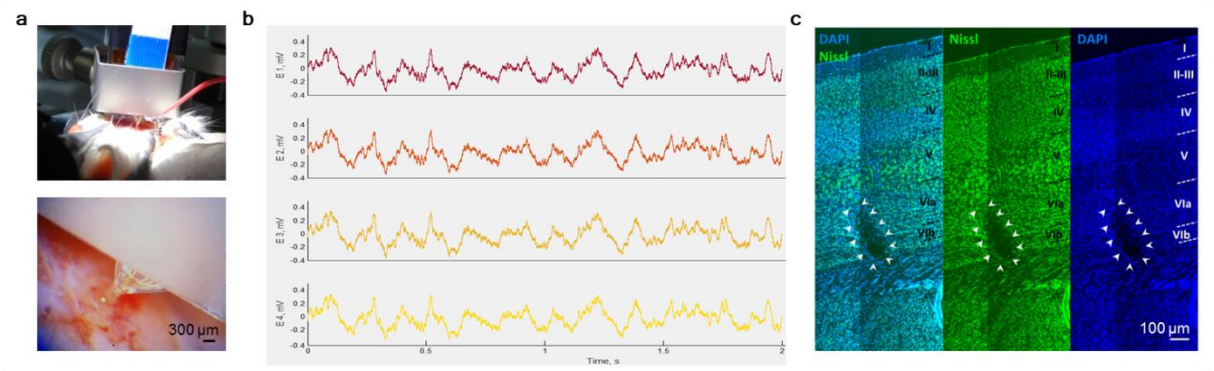

Figure 15. Acute single cell recording of a putative cortical layer V pyramidal neuron with a bioresorbable flexible depth probe in an *in vivo* anaesthetized mouse. (a) Pictures of a PVA/PLGA probe inside a mouse brain. (b) LFP recordings from 4 electrodes on a single probe. (c) Histology with Nissl and DAPI after recording, showing a perpendicular view on the trajectory of the implanted probe.

A first chronic *in vivo* experiments was performed to investigate the potential of the PVA/PLGA BS flexible probe. The probe penetrated despite the slightly bent form (*Figure 16a-b)* and recordings were performed for 30 minutes to 1.5 hours every 2-3 days for a month. During the recordings, the mouse was placed in an arena containing only animal litter *(Figure 16c)*. Four out of the six electrodes recorded LFP signals during the entire period. The quality of the recording was evaluated based on the baseline value of the recordings *(Figure 16d)*. At first, a high signal-to-noise ratio (SNR) was observed with a baseline between 40 to 50 µV. However, this SNR rapidly decreased and almost the double

value was observed after 20 days. An EEG screw was added during the experiment as control. *Figure 16d* also shows data from a silicon probe and a tungsten wire which were used in a separate rat experiment (data from INSERM, Aix-Marseille Université). The controls did not show as much decay in SNR as our probes. The noise level of the electrodes clearly increases chronically *in vivo (Figure 16e)*, which definitely needs to be prevented in the future to allow for single cell recordings during long-term experiments.

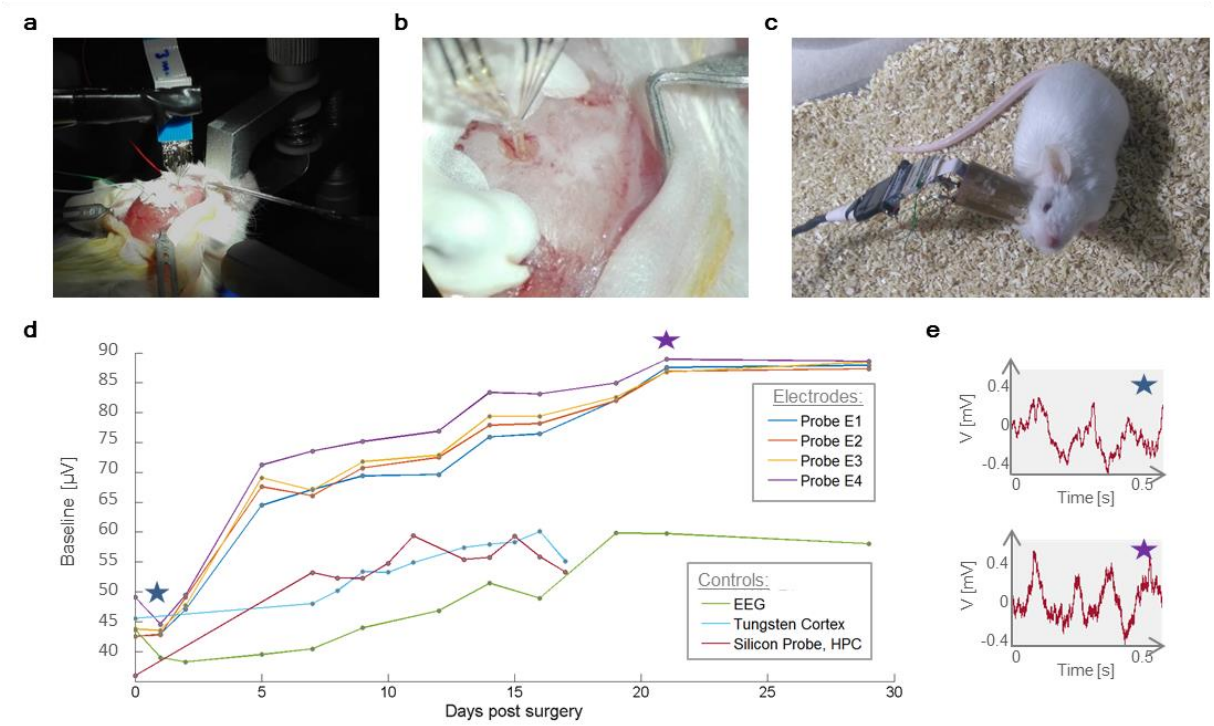

Figure 16. Results of a chronic experiment with a PVA/PLGA flexible neural probe. (a) and (b) Pictures of a PVA/PLGA probe inside a mouse brain. (c) Picture of the mouse during recordings on day 20. The probe is attached to the head with dental glue and protected from the mouse with a little surrounding hat. The black cable and omnetic connection are only attached during recordings. (d) Baseline amplitude in function of time. The amplitude is the median value of the computed baseline width from a 500 second recording window. (e) Example of the recordings from probe electrode 1 at day 1 (blue star) and at day 21 (purple star). The noise level clearly increases in time.

The PVA/PLGA shuttled flexible probe showed a significantly larger scar compared to a silicon probe after a month of recording. An example of a silicon probe is shown in *Figure 17a* and our probe is shown in *Figure 17b*. The surface of the brain seemed much more damaged compared to the brain which contained the silicon probe. A large vacant space is observed near the brain surface. This severe damage is however explained by the fact that the probe was initially not completely straight. The probe did not reach the desired location of the hippocampus, but reached until the fourth layer of the cortex. The lack of single cell activity is most probably due to the large scar made by the shuttle, which does not provide a favorable condition for surrounding neurons to fire action potentials. Hence, the first chronic

in vivo results showed that there is still more work to be done to improve our flexible neural interface.

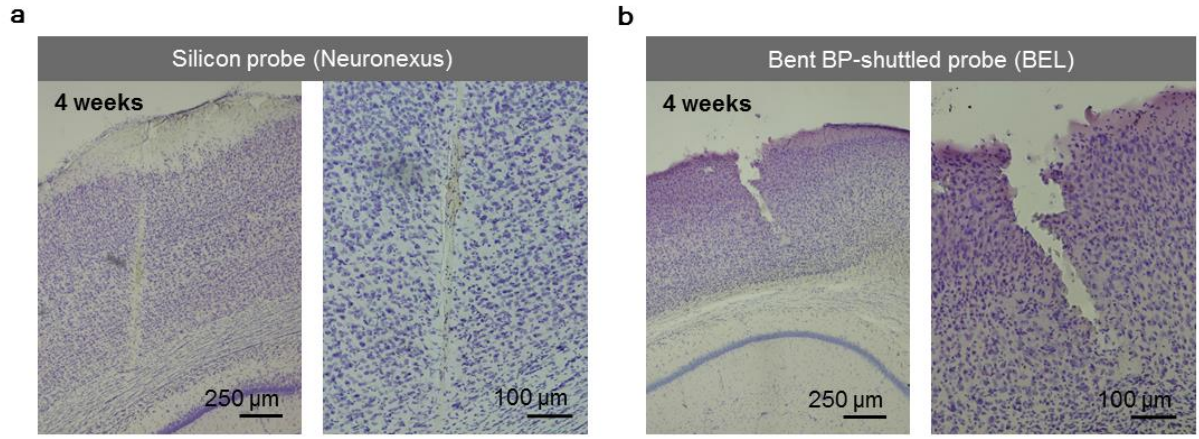

Figure 17. Histology of brain slices after chronic *in vivo* recordings with a silicon probe (a) and our PVA/PLGA shuttled probe (b). More severe brain damage is observed with our probe, despite its flexible nature.

4.4 Conclusion

The efforts made towards developing a flexible, yet sufficiently stiff and therefore implantable, depth probe through the use of a bioresorbable polymer shuttle on our parylene-based devices were discussed in this chapter. PVA was initially chosen due to its synthetic nature, its well-known biocompatibility and the already reported FDA approved uses. The polymer was shaped into the desired micrometer probe scale through PDMS molding. A sharp and sufficiently stiff shuttle was formed in this manner, which showed successful penetration into agarose brain models. The fast dissolution of the polymer, however, prevented deep brain penetration, which was resolved by adding a thin coating of PLGA around it. The final PVA/PLGA bioresorbable shuttle was characterized before *in vivo* experiments and showed to lose its stiffness and recover to its initial low impedance within 3 minutes when completely immersed into a warm saline solution.

As expected, the penetration of a straight PVA/PLGA shuttled probe was also very successful *in vivo*. Probe were inserted deep into the cortex of mice (layer VI) and recorded LFPs and single cell activity during acute measurements. The first chronic experiment did show that more experiments are necessary to evaluate the long-term function of this bioresorbable shuttled probe. The probe penetrated successfully despite being slightly bent, yet consequently led to more brain damage than desired. This will most likely improve when using straight probes during future experiments, as shown with the smaller damaged tissue during acute measurements. Another issue which requires further attention is the observed decrease in SNR in time. While the initial noise level was only ~40 µV, this doubled to almost 80 µV within three weeks, which means that the capturing of single cell activity would be

limited past that time frame. This decrease needs to be explored and understood. Nevertheless, this chronic data is based on solely one probe during one experiment. Further investigation is required to actually validate this observation. To conclude, the bioresorbable shuttle does perform its main function of inserting the flexible probe deep into the brain and shows therefore much promise for the future state-of-the art flexible depth probes.

4.5 Experimental section

The experiments described below were performed in accordance with experimental guidelines approved by Aix-Marseille University Animal Care and Use Committee and by the French Ministry of Education and Research Protocol #01451-02.

Probe fabrication

The depth probe fabrication process includes the deposition and patterning of parylene-C, chromium, gold and PEDOT:PSS films, as previously reported [54]. Briefly, parylene was deposited on a glass wafer with an approximate thickness of 2 μm using an SCS Labcoater 2. Two layers of photoresist, LOR (MicroChemicals) and S1813 (Shipley), were spin-coated on the parylene film. LOR was spun at 3000 rpm for 40s and baked at 200 °C for 1 min. S1813 was spun at 5000 rmp for 40 s and baked at 115 °C for 2 min. The layers were exposed to UV light (96 mJ cm^{-2}) using an SUSS MJB4 contact aligner and developed using MF 26 developer. The wafer was plasma treated for 1 min at 100W with O_2 using a reactive ion etcher (Oxford 80 plus plasma etcher). Then, a thin layer of 10 nm of chromium was deposited in a metal evaporator (Alliance Concept EVA450) to improve the adhesion of gold, which was deposited next with a final thickness of 100 nm. Lift-off was performed leaving the wafer overnight in NMP (Sigma-Aldrich). Two layers of parylene were subsequently deposited, one as insulation layer and one as sacrificial layer during a later peel-off technique. A layer of 2% soap was added in between. The insulation layer was patterned with the probe outline, using AZ9260 spun at 3000 rpm for 40s, baked at 110 °C for 2 min, exposed (65-90 $mJ.cm^{-2}$), developed in AZ developer for 4 min and etched for 8 min at 400 W with 50 sccm O_2 and 5 sccm CHF_3. The same was done after the sacrificial parylene layer was added to etch away the parylene at the microelectrode sites. Next, the PEDOT:PSS solution was prepared adding 5% (v/v) of ethylene glycol, 0.5 μL mL^{-1} of dodecyl benzene sulfonic acid (DBSA) and 1 wt% of 3-glycidoxypropyltrimethoxysilane (GOPS) to the aqueous dispersion (PH 1000 from H.C. Stark). This PEDOT:PSS solution was spin-coated twice, once at 3000 rpm and once at 1500 rpm. A baking of 1 min was done in between both steps at 90 °C. The sacrificial parylene layer was peeled-off and the films were baked at 140 °C for 1 h. Before the packaging, the probes were immersed in deionized water to remove any excess low molecular weight compounds inside the PEDOT:PSS film. Finally, the probes were removed from the wafer and ZIF cables (Mouser Electronics)

were attached with anisotropic conductive film (ACF) using an APR-5000-DZ soldering machine.

Bioresorbable PVA/PLGA shuttle fabrication

The fabrication of the PVA/PLGA shuttle involves the fabrication of a PDMS mold and the alignment and deposition of both BPs. First, a PDMS mold was made using epoxy-based negative photoresist SU8. SU8 2075 (Microchemicals) was deposited on a cleaned glass wafer and spun at 500 rpm for 10 s and 1000 rpm for 30 s for a final SU8 thickness of ~200 μm. Next, a soft bake at 65 °C and 95 °C for 7 and 45 min was performed, followed by UV exposure (SUSS MJB4 contact aligner, i-line filter, 350 mJ cm^{-2}) and a post exposure bake of 5 and 15 min. After development in SU8 developer (Microchemicals) for 17 min, the glass wafer was wrapped in aluminum to form a dish and PDMS (1:10 of base:curing agent, Sigma-Aldrich) was deposited and cured in the oven at 70 °C overnight. The PDMS mold was gently peeled-off and the SU8 features were printed into the mold.

Next, the PVA/PLGA shuttle is made. The flexible parylene probe with attached ZIF cable was first aligned into the PDMS mold. The mold was 100 μm wider than the actual probe, to facilitate the alignment. PVA (Sigma Aldrich, CAS number: 26780-50-7; 10,000 g mol^{-1}) was dissolved at 20 w/v in water by heating up the mixture for 1h at 90 °C. The dissolved PVA was drop-casted and blade coated in the mold and left in the oven for 10 min at 70 °C to slowly evaporate the water. A second PVA coating was done and left in the oven for another half an hour. Next, the probe with PVA shuttle were removed from the mold with tweezers and dipped into a 25 wv% PLGA (Sigma aldrich, CAS number: 9002-89-5; with a lactide:glycolide ratio of 65:35) acetone solution to coat the tip with PLGA. The solvent evaporated fast at RT and the PVA/PLGA parylene probe was ready for use.

Electrical characterization

Impedance measurements were performed with a potentiostat (Autolab PGSTAT128N) in a three electrode configuration. The reference, counter and working electrode were a Ag/AgCl electrode, a Pt electrode and the depth probe, respectively. Measurements were performed in DPBS by applying a 10 mV root mean square sinus wave with frequencies varied logarithmically from 1 Hz to 100 kHz. Data is presented as mean ± SD throughout this work, unless noted different.

Mechanical characterization

In agarose brain models

Agarose gels were prepared at 0.6% w/w agarose in water and autoclaved at 121 °C for 20 min in 24 well-plates (Falcon™). The agarose gels were used as brain models and were kept wet with a few drops of water while stored in the fridge at 4 °C. During penetration tests, a microscope (Axio Zeiss) was used to visualize and record the horizontal penetration of the PVA/PLGA probe into the agarose models. The probe was manually inserted at the estimated speed of 1 cm min^{-1} using a micromanipulator stage to which the probe was attached.

Acute electrophysiological recordings

Mouse surgery for acute recordings

Adult male *OF1* mice were used for the experiments. Mice were entrained to a 12 h light/dark cycle with food and water available *ad libitum*. Surgeries and experiments were done under ketamine/xylazine anesthesia (ketamine, 83 mg/kg; xylazine, 3.3 mg/kg), body weight) was used as anesthetic. Mice were fixed in a mouse stereotaxic frame (Stoelting). After a subcutaneous injection of a local pain killer, ropivacaine craniotomy was made from bregma: anteroposterior 1.0 mm and mediolateral 1.2 mm; dorsoventral 2.8 mm from the surface). Skull was opened, dura was removed, and flexible, bioresorbable microelectrodes were lowered into the parietal cortex.

Acute recordings and data analysis

Recordings were made with Ampliplex amplifier (Ampliplex KJE-1001). Extracellular signals were high-passed filtered (0.3 Hz), amplified (2,000 times) by a 32-channel amplifier, and digitized at Ampliplex. Single spike activity was identified using the Neurosuite software package of Neuroscope, NDManager and Klusters [83]. During spike analysis, the measured signals were high-pass filtered at 300 Hz and single units were extracted at a threshold factor of 1.7 with a refractory period of 16 samples. Through a three principal component analysis (PCA), the relevant components were extracted and automatically sorted using the spike sorting algorithm KlustaKwik [85]. The obtained spike cluster was at the end manually refined with Klusters and subsequently presented here.

Histology and immunocytochemistry

Animals were transcardially perfused first with saline, then with 150 ml of fixative solution containing 4% PFA in 0.1 M phosphate buffer (PB). Tissue blocks were cut on a Vibratome (Leica VT1200S) into 50 μm coronal sections. After extensive washes in PB, Nissl staining was performed (NeuroTrace 500/525 Green Fluorescent Nissl Stain, Thermofisher). Sections

were mounted on SuperFrost slides and covered with a mounting medium containing 2-(4-amidinophenyl)-1H -indole-6-carboxamidine (DAPI) (Flouromount Mounting Medium with DAPI, Abcam).

Chronic electrophysiological recordings

Three chronic experiments were initially set up to test the long-term performance of our devices. However, due to unforeseen adverse events, only one experiment was successfully performed till the end.

Mouse surgery

A male adult FVB/N mouse (28g) was anesthetized with a Ketamine/Xylazine mix (25 mg/kg and 2.5 mg/kg, respectively, in NaCl 9‰, IP). Additional boost (20 µl of ketamine/xylazine mix (100mg/kg and 10mg/kg, respectively) were given every hour. Once asleep, the head was then secured in a stereotaxic frame. The body temperature was constantly monitored and maintained at 37.5 ºC with a rectal probe and heating pad. Some ophthalmic gel was placed on the eyes to prevent desiccation. Before cutting the skin, some ropivacaine (0.2%, 2mg/kg) was injected sub-cutaneous. The skull was then exposed, cleaned and dried. All the instruments were sterilized beforehand. Two miniature stainless-steel screws were inserted in the bone above the cerebellum and served as ground and reference for the electrophysiological recordings. A third screw was driven above the left somatosensory cortex (above the durra matter) to serve as anchor and as EEG recording, since it was connected to a microwire to the connector. Some C&B Metabond cement covered the three screws and formed a pedestal circling the top of the skull for the copper-mesh hat. A 1mm^2 craniotomy was then drilled at 2mm posterior and 1.5mm lateral to bregma, the durra matter was opened and the brain surface washed with sterile NaCl 9‰. The probe XX was mounted on a holder and secured on one arm of the stereotaxic frame, and lowered quickly to -1.5mm from the brain surface with a motorized drive. Once in place, a drop of dexamethasone (4mg/ml) was used to rinse the craniotomy and prevent inflammation. Some paraffin was used as a first sealant and Metabond as the last sealant of the craniotomy. The probe's holder was then dismounted from the stereotaxic arm and the flex cable folded into a compact shape. A hat of copper-mesh was finally sealed with Metabond on the skull, and served as physical and electrical (the mesh was connected to the ground screw) shielding of the probe and screws. The ground, reference and EEG connector pins as well as the probe flex cable were finally secured at the top of the hat. The mouse received an injection of antibiotics (Baytril 5%, 5mg/kg, i.p.) and some ibuprofen (7.5mg/kg) was given in the drinking water for the 3 following days. The mouse was then placed back in its home cage, with food and water ad libitum. The home cage was stored in a dedicated animal facility room where temperature and hygrometry were monitored and kept constant, and with 12-12h day/night cycles. Any

sign of pain or discomfort was monitored during the following days and eventually tended to.

Chronic recordings

The recordings were performed for 30 minutes to 1.5 hours every 2-3 days for 3 weeks. For this purpose, the mouse was placed in an arena containing only animal litter. The probe and the three pins were connected to the Plexon headstage, which conveyed the electrophysiological signals to the Neuralynx amplifier. The extracellular signals were amplified (1000x), bandpass filtered (1 Hz to 5 kHz) and acquired continuously at 32 kHz with a Digital Lynx (Neuralynx) at 16-bit resolution. Raw data were preprocessed using NEUROSUITE and only segment without movement artifacts were kept for the analysis. Between 300 and 500 seconds were used to compute the baseline value on each channel of the probe and the EEG channel: 10,000 randomly chosen epochs of 100 samples were extracted and the baseline value measured. Their median value was used as the daily value of baseline for each site.

Histology and immunocytochemistry

After a month of recording, the mouse was injected with a lethal dose of Pentothal (150mk/kg, i.p.) and perfused intracardially with 4% paraformaldehyde solution in 0.12 M phosphate buffer (PB), pH 7.4. The brain was extracted and post-fixed at 4°C overnight. After extensive washes in PB, Nissl staining was performed on slice of 60 µm-thick coronal sections (Vibratome).

4.6 Supplementary Figures

Fabrication remarks

Shaping bioresorbable polymers was the most challenging task of this work due to the its sensitivity to water and other solvents. Although the presented solution with a PDMS mold is simple and showed good results, a more efficient way was initially targeted. Fabrication troubles and the initial fabrication process are briefly discussed below.

The fabrication of the PVA/PLGA shuttle through the use of a PDMS mold is a time consuming approach. It requires the creation of a homogeneously thick shuttle layer along the entire length of the tip. A steady hand (or patience for the many trials) and precision is needed to achieve a perfect alignment of the probe inside the PDMS mold. Then, once in place, the PVA polymer solution should be dropped on top without creating any air bubbles. A 20% w/v PVA solution was used for this reason, as the solution was not too viscous yet would contain sufficient polymer to stiffen the device after two coatings. It was however almost impossible not to trap air bubbles at the sharp tip of the probe (Supp. *Figure 1a*). These were mostly carefully removed with a pipet tip or paint brush, which did sometimes damage the tip of the probe with the microelectrodes. If bubbles were however not removed, it created a weak point at the tip and did not provide the necessary stiffness to insert deep into the brain (Supp. *Figure 1b*). Moreover, if not careful during the removal of bubbles, the probe tip could easily be displaced, thereby entrapping more air bubbles and messing up the alignment (Supp. *Figure 1c*). Hence, air bubbles were to be removed or the bioresorbable shuttle was unusable.

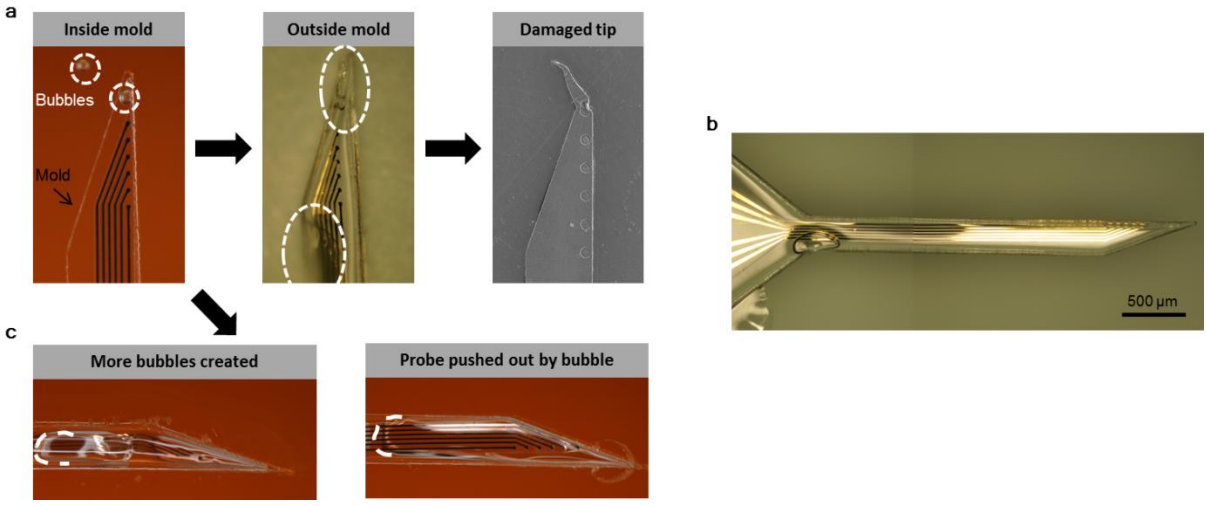

Supplementary Figure 1. Fabrication issues when using a molding approach. (a) Air bubbles are entrapped by the PVA solution inside the PDMS mold (*left*). The mold is placed on a sheet of kapton, making the image orange for better contrast. Bubbles are encircled with white dashed lines. After oven treatment, the probe is removed from the mold and vacancies are created in the tip in case bubbles had remained inside

the mold (*middle*). The removal of air bubbles can sometimes mechanically damage the tip (right). (b) The air bubble at the base of the tip creates a weak point, which makes brain penetration impossible. (c) Huge bubbles can be created during attempts to remove other air bubbles (left) with probe displacement as result (right). Air bubbles are partly emphasized with white dashed lines.

The ability to fabricate of multiple probes at the same time would significantly decrease fabrication time. Initially, the idea was to develop an efficient *all-in-one* fabrication method, which would enable the entire fabrication of the bioresorbable shuttle without the removal of the probes from the production wafer. This would thus enable the fabrication of multiple bioresorbable shuttled flexible probes at the same time, unlike probe per probe as presented in this work. Despite the initially promising results using a so-called "Orthogonal resist" (SL1) to enable lift-off of SU8 molds patterned around all the probes on the glass wafer, the method did not succeed after adding the bioresorbable polymer before the final lift-off step (*Supp. Figure 2a-b).* Although the probes eventually could lift-off from the wafer with the bioresorbable PVA on top, the mold would remain firmly stuck to the entire device (*Supp. Figure 2c*). Various methods were investigated to prevent this from happening, including for example the addition of hydrofobic coatings on the SU8 molds, it did not yet seemed to work. Either the interaction of the SU8 mold to the PVA was too strong, or the PVA did not shape properly in the mold due to the hydrophobic surrounding. The fabrication of multiple bioresorbable shuttled probes would nevertheless be a great addition as probe per probe fabrication remains time consuming.

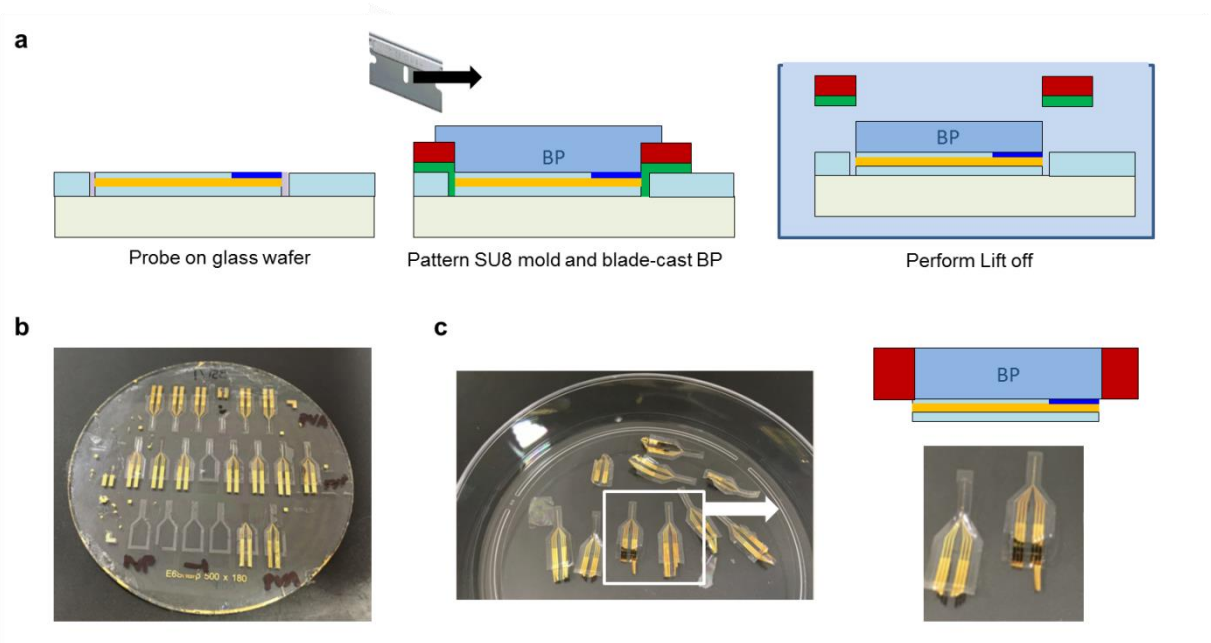

Supplementary Figure 2. Alternative *all-in-one* fabrication method of PVA shuttles. (a) Schematic of the approach. 1) A single probe on a glass wafer. 2) The patterned result using orthogonal resist (green) and an SU8 mold (red) around the probe, followed by blade-casting the bioresorbable polymer (BP). 3) Lift-off in a solvent bath to remove the mold and ultimately shape the BP. (b) Failed lift-off result. The empty molds were controls to test lift-off. (c) Successful lift-off with the molds still stuck to the probes in a petri dish, including a zoom in and the schematic of the observed device.

If an *all-in-one* fabrication method were to be successful, a new method would have to be developed to connect the probes to the recording set up. Since the flexible probe is only 4 μm thin, the addition of a ZIF cable ensured a fixed and good electrical connection to the recording set ups, such as Neuraneuxus™ or Ampliplex™. This addition would not be possible with the bioresorbable shuttle already on the probe, as it would not resist the required high temperatures to connect the cable. Without such ZIF cable, two sheets of kapton could be used to obtain the necessary thickness and pressure for a decent connection. Yet, repeated attachments to electrical connections in this manner does damage the thin parylene at the connector pads, with complete loss of contact as plausible outcome. The addition of a reliable electrical connection to the flexible probe will most definitely be required for chronic.

Mechanical charaterization remarks

The addition of hydrophobic coatings were considered in order to decrease the degradation rate of the fast dissolvable PVA shuttles. This was not a success as shown in *Supp. Figure 3*. Even after perfluorodecyltrichlorosilane (FDTS) coatings, without and with fluorinated solvents of perfluoroperhydrophenanthrene (FS) and Flombin (Fb) deposited on top, the shuttles started to dissolve within 20 seconds after immersion in ACSF at 37 °C.

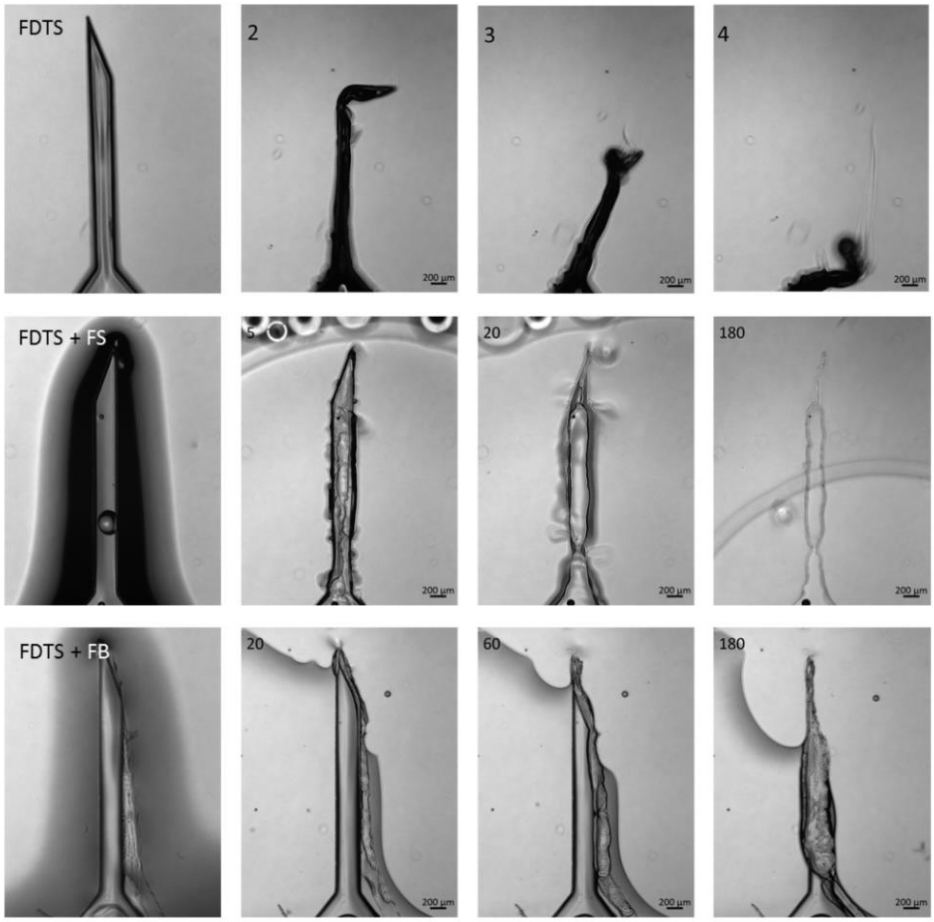

Supplementary Figure 3. Hydrophobic coatings on PVA shuttles. Crucial time point of dissolution are shown and the time in seconds is written in the top left corner. Shuttle dissolution started after only 20 seconds (at the latest).

The addition of a poly(lactic-co-glycolic) (PLGA) coating was successful to decrease the dissolution time of a PVA shuttle. Dip-coating solutions with various PLGA concentrations were made to evaluate the difference in dissolution of the shuttles. *Supp. Figure 4* shows the various coating concentrations evaluated and *Supp. Figure 5-6* show representative images of PLGA/PVA shuttle dissolutions.

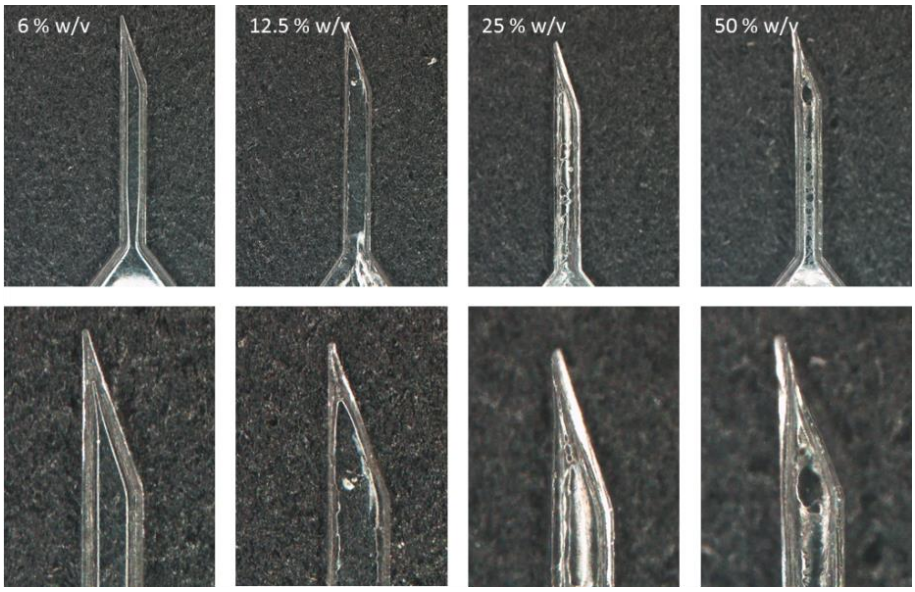

Supplementary Figure 4. PVA shuttles dipcoated in different concentrations of PLGA solutions. Low concentrations provided a more homogeneous layer than the 50 % w/v concentration.

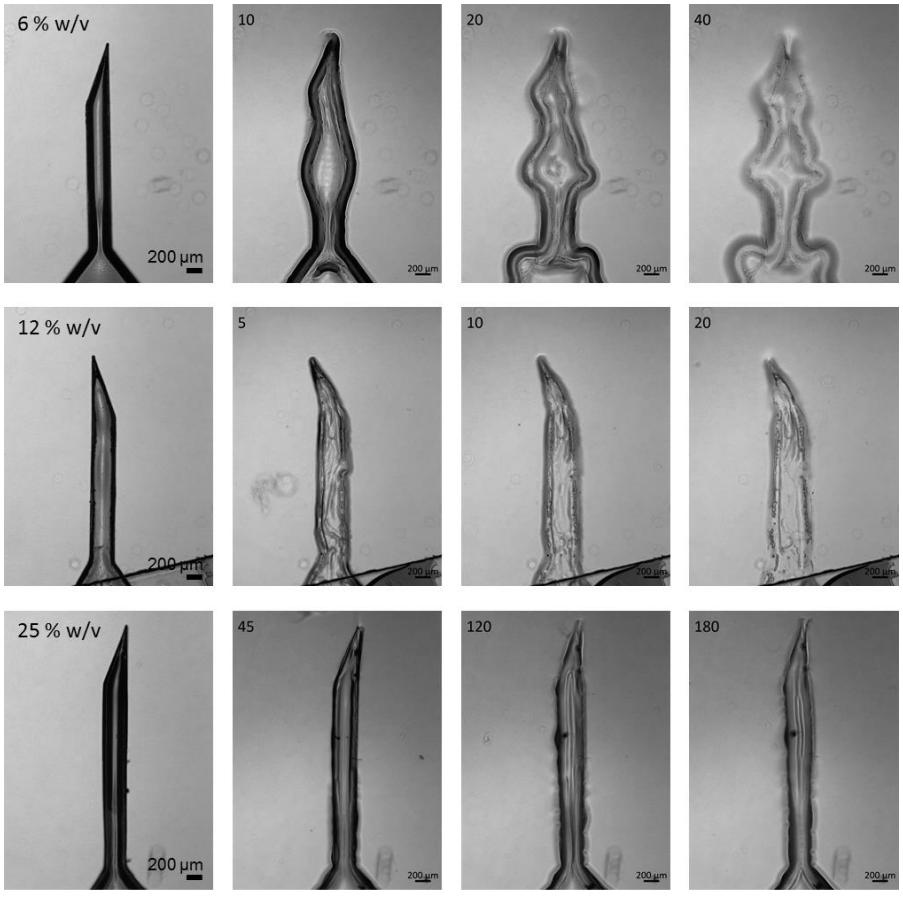

Supplementary Figure 5. Dissolution of PLGA-coated PVA shuttles, made from solutions with low PLGA concentrations. Crucial time points (in seconds) are shown. Only 25 % w/v remains present after 3 minutes (180 seconds).

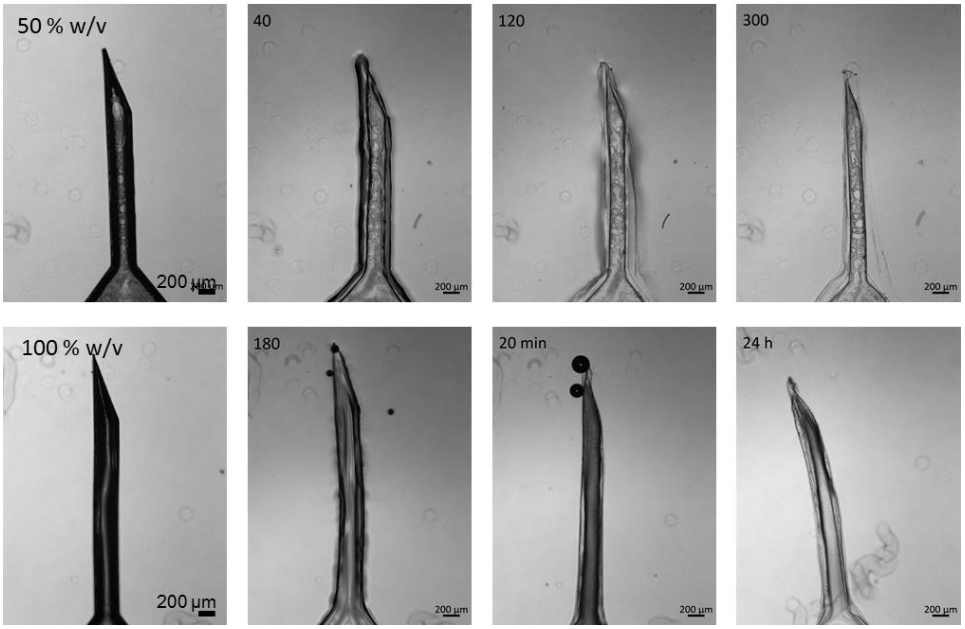

Supplementary Figure 6. Dissolution of PLGA-coated PVA shuttles, made from solutions with high PLGA concentrations. Crucial time points (in seconds) are shown. A 50 % w/v concentration did not show homogeneous coverage of the PVA shuttle, unlike the other concentrations, yet remained relatively intact for the shown time. The 100% w/v PLGA coatings showed even more dissolution resistance. The shuttle had shown to be displaced 24h after immersion in ACSF.

Electrical characterization remarks

During chronic characterization of the electrical impedance, the average values of the weekly measured impedances were lower than the average initial value of the electrodes before the deposition of the BPs (*Supp. Figure 7a*). This data contained impedances as low as sometimes 5 kHz (*Supp. Figure 7b*), which raised a doubt on whether the electrodes were shorted during the experiment. The standard deviations were therefore calculated for every probe at every time point *(Supp. Figure 7c)*. A standard deviation lower than 10 was marked red. Although probe 3 and 4 show a low standard deviation, the values are as expected and are reliable. The values of probe 1 are however relatively low. Although the initial values before BP addition are also low, the values below 10 kΩ are a concern. It might be possible that the electrodes are somehow shorted due to the uptake of saline solution in between the ZIF cable and the connector pads. This is to be excluded with future experiments which prevent this from happening.

a

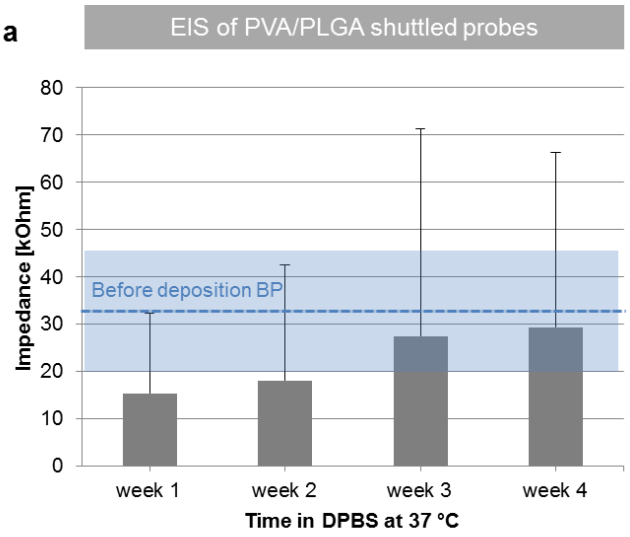

b

Table of EIS values at & kHz [kΩ]

Electrode Nr	before BP	week 1	week 2	week 3	week 4
	Probe 1				
1	18,5	5,7	10,0	3,7	10,4
2	13,9	15,1	21,8	281,8	36,0
3	14,6	14,9	28,7	49,3	67,3
4	14,1	7,1	8,6	7,4	9,3
5	13,2	5,2	4,5	5,4	6,6
6	14,0	3,8	5,7	4,7	9,3
	Probe 2				
8	21,8	6,9	7,3	6,8	7,7
9 ('exc. 1')	19,4	692,7	635,8	651,8	471,0
10	25,6	9,2	9,1	8,3	47,0
11	36,8	76,1	80,4	77,5	140,8
12	50,0	3,8	6,2	5,0	6,7
13	28,8	3,0	4,9	3,7	7,3
	Probe 3				
15	45,9	13,3	7,9	5,3	4,9
16	42,1	13,0	7,6	4,9	4,5
17	40,7	54,6	101,6	133,3	78,1
18	41,6	13,6	8,7	5,7	5,3
19 ('exc. 2')	41,4	107,5	217,7	83,7	46,4
20	43,7	10,6	6,0	4,5	4,0
	Probe 4				
22	39,2	12,8	11,8	14,2	9,1
23	40,3	12,0	11,3	13,7	9,2
24	39,1	11,8	10,9	18,8	14,9
25 ('exc. 3')	40,0	238,9	219,4	242,1	204,9
26	40,8	14,8	12,9	161,1	11,1
27	54,5	14,4	12,7	15,4	108,8
Average	32,5	56,7	60,5	75,3	55,0
Stdev	15,9	141,8	134,1	142,5	100,0

c

Table of standard deviations of EIS values

	before BP	week 1	week 2	week 3	week 4
probe 1	1,9	5,0	9,8	110,7	24,2
probe 2	11,4	276,2	252,5	259,4	182,7
probe 3	1,9	39,1	86,7	55,7	31,4
probe 4	6,0	92,2	84,7	99,5	81,2

Supplementary Figure 7. Change in impedances at 1 kHz during immersion of PVA/PLGA shuttled probes in DPBS at 37 °C (n=27). (a) The average values and standard deviation of the measured data. The average values and standard deviation of the electrodes before deposition of BP are shown with the blue dashed line and blue area's around it. (b) The individually measured data points to show the variations between the electrodes on 4 different probes. Electrode 9, 19 and 25 are the 'Exceptions' (from *Figure 13b*). (c) Overview of the standard deviations per time point from electrodes on the same probe. The red boxes show data with standard deviation below 10 kΩ.

Chapter 5. Conclusion and outlook

5.1 Conclusion

Implantable neural interfaces are designed to bridge the human brain with the outside world through state-of-the art microelectronics. However, today's state-of-the-art devices do not allow long-term use *in vivo*. The foremost limiting factor discovered to date is the mechanical mismatch between implant and brain tissue, which imminently leads to rejection and complete functional loss of the neural interface. The main challenge in this neuroengineering field is thus to design a mechanically flexible interface, notwithstanding that this same device should provide the necessary stiffness to be placed deep inside the brain.

In this thesis, the aim was to develop soft neural interfaces to improve the long-term performance for both *in vitro* and *in vivo* applications. In *Chapter 1*, neural interfaces were introduced along with their shortcomings, which led to the conclusion that more compliant materials are necessary to improve signal quality. In *Chapter 2*, focus was placed on the fabrication of flexible devices. Organic materials were used to interface with neural tissue: parylene-C was used as insulating layer, due to its high dielectric strength, biocompatibility and most importantly, flexibility and PEDOT:PSS was used to lower the impedance and improve the signal-to-noise ratio. MEAs and depth probes were made through photolithography and the devices showed the required low impedances to allow single cell recording.

In *Chapter 3*, the enhancement of single cell recordings on our PEDOT:PSS-coated MEAs was shown. An important factor in this study was the primary cortical cell density, which showed to significantly increase the chance of measuring activity from individual neurons if kept relatively high (900 cells/mm^2). The recorded spikes were analyzed and clustered per neuron through semi-automated spike sorting programs to show that high cell density did result in more single cell recordings per MEA. The enhancement was further increased through the formation of 3D neurospheres on the MEAs. With the presence of such neurospheres on our MEAs, the success rate of recording single cell activity rose to more than 40%. Moreover, confinement of the neurospheres on top of the microelectrodes was achieved through laser patterning of PEGDA. This is of utmost importance as the neurospheres should be present on top of a microelectrode in order to enable the single cell recording. Overall, successful in vitro MEA recordings was shown with 48 electrodes out of a total of 224 (n=7 MEAs). This is a recording yield of 21.4% from which 93.75% was obtained from electrodes with neurospheres and 6.25% from 2D cultures. This hereby not only showed that our PEDOT:PSS coated MEAs successfully performed their function of recording single cell activity, yet a valuable *in vitro* model was also developed which shows great potential to improve pharmacology-based studies by providing significantly more electrophysiological data per device.

Finally, in *Chapter 4* the efforts made towards developing a flexible and implantable depth probe through the use of a bioresorbable polymer shuttle on our parylene-based devices were discussed. PVA was initially chosen due to its tunable properties as synthetic polymer, its well-known biocompatibility and the already reported FDA approved uses. The polymer was shaped into the desired micrometer probe size through PDMS molding. A sharp and sufficiently stiff shuttle was formed in this manner, which showed successful penetration into agarose brain models. The fast dissolubility of the polymer however prevented deep brain penetration, which was resolved by adding a thin coating of PLGA around it. The final PVA/PLGA bioresorbable shuttle was characterized before *in vivo* experiment and showed to lose its stiffness and recover to its initial low impedance within 3 minutes when completely immersed into a warm saline solution. As expected, the penetration of a straight PVA/PLGA shuttled probe was also successful *in vivo*. Probes were inserted deep into the brain of mice (layer VI) and recorded both LFP and single cell recordings during acute measurements. Finally, the initial chronic experiments indicated that these devices may be suitable for long term implantations, however, additional experiments are necessary to evaluate the long-term function of this bioresorbable shuttled probe.

5.2 Outlook *in vitro* work

The enhancement of single cell recordings with neurospheres *in* vitro shows much promise and could potentially be taken further by also designing 3D MEAs. Attention is growing to engineer 3D designs to interface with biology [92], [127]. The reasoning behind it is simple: living tissue is 3D so if we are trying to connect with it, *why not also go 3D?* A better interface can be created by doing so, as shown for example by *Hai et al.* [128], [129]. They reported on the fabrication of 3D golden mushroom-shaped microelectrodes (designed to mimic dentritic spines), which are being engulfed by ganglion neural cells to enable co-called 'in-cell recordings' *(Figure 1)*. The additional engulfment-promoting peptide on the microelectrodes triggers cells to tightly surround the microelectrodes with their cell membranes, and consequently results in a significant decreased seal resistance of ~70MΩ (vs. 2 MΩ of 2D microelectrodes) [126] (Section 1.2.2). Surprisingly, this significantly improved the recorded signal amplitudes up to 1-25 mV for action potentials, comparable to amplitudes achieved during intracellular recordings [127]. There is however still work to be done, as this technique has not been successful yet with primary hippocampal neurons or primary cardiomyocytes [17]. Moreover, they state to have a large variability in electrical properties due to the inhomogeneous fabrication methods in their laboratory, based on nanoscale-photolithography and electroplating [127].

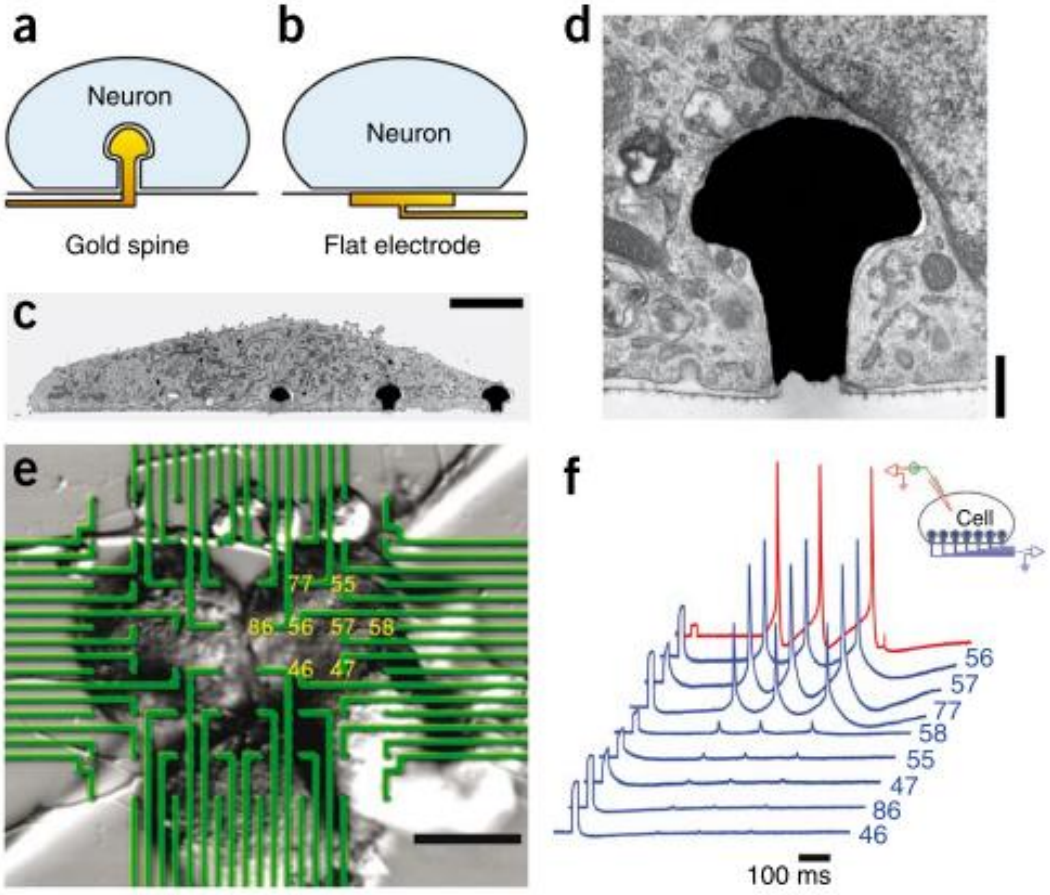

Figure 1. Mushroom-shaped microelectrodes designed for 'in-cell recordings'. (a) Schematic of a neuron engulfing a golden mushroom-shaped (or spine-shaped) microelectrode and (b) a neuron on a flat electrode. (c) An electron micrograph of a cross-section through a PC12 cell engulfing 3 functionalized gold spines. (d) Electron micrograph of a gold spine engulfed by a PC12 cell. (e) Confocal microscopy image of 3 Aplysia neurons cultured on a multi-gold spine electrode array. The conducting lines are depicted in green. (f) Simultaneous action potential recordings (blue) from 8 gold-spine electrodes (indicated by numbers in e) in response to intracellular stimulation of the neurons by a conventional sharp microelectrode. Each trace depicts initially a 5 mV, 20 ms calibration pulse and then, after a delay, 3 action potentials. Inset, schematic of experimental set up. Scale bars, 5 μm (c); 500 nm (d) and 50 μm (e). Adapted from [127].

Besides the improvement of the MEA designs, more effort could be invested in the creation of more physiological representative 'mini-brains'. *Imagine*, designing a 'brain in a dish' which spontaneously grows on 2D or 3D microelectrodes. Reported work towards building such 3D neural structures include the use of a microbead assembly to create a 3D substrate for hippocampal cells [90], the use of PDMS microchambers to create neurospheres with cortical cells [88], or the use of 3D collagen gels to unrestrict the positioning of neurons and neurite outgrowth of hippocampal cells into such a 3D hydrogel [91], [130]. This could be an exciting scientific breakthrough that ultimately leads to better pharmacological testing models thereby reducing the need for animal testing.

5.3 Outlook *in vivo* work

Chronic in vivo validation

The bioresorbable PVA/PLGA shuttled flexible neural probes should be further investigated during more chronic *in vivo* experiments to prove its benefit. Surprisingly, our first chronic *in vivo* results did not seem as promising as we would have hoped. First, more experiments need to follow to verify the decreased SNR of the PEDOT:PSS coated probe, which is in our opinion the most worrying issue. To this end, the flexible probe should primarily be tested chronically without the polymer shuttle and then be compared to data with polymer shuttle. Although the BP did not seem to affect the electrical properties of the probe during characterization, this should clearly also be investigated *in vivo*.

Other applications

The PVA/PLGA shuttle shows great promise to function as a bioresorbable shuttle for flexible neural interfaces. It obtains the required stiffness to penetrate soft brain tissue at small thickness (< 100 µm) and loses this rigidity through simple hydrolytic degradation. Besides functioning as insertion aid of depth probes, this shuttle could also be applied to other neural interfaces, such as more superficial penetrating multi-microelectrode array devices (*Figure 2a*) or on devices for electrocorticography (ECoGs) (*Figure 2b*). The multi-MEA would have the same insertion principle as the depth probe. The ECOG, on the contrary, would be inserted horizontally under the skull and on top of the brain by sliding it in between both tissues. This would be beneficial as only a small craniotomy window would need to be made, minimizing the exposure of brain tissue to the outside world. Both applications are already under investigation in our lab.

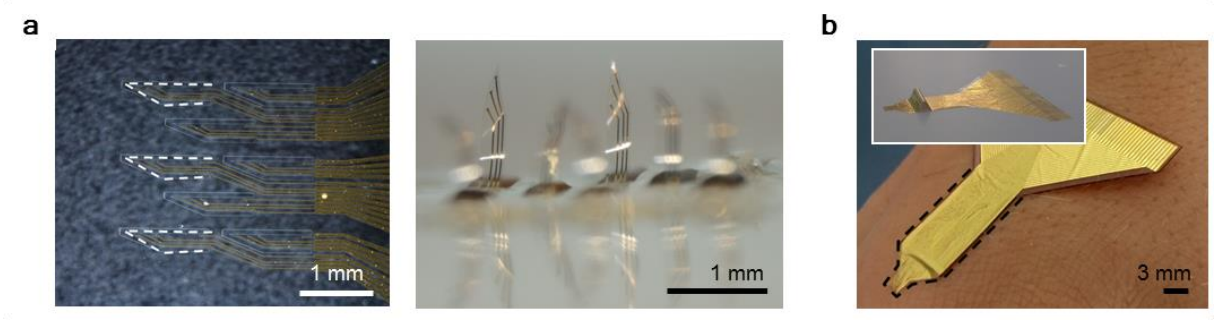

Figure 2. Other flexible neural interfaces for which the PVA/PLGA shuttle could be useful. (a) A parylene-based multi-microelectrode array on a black sub ground (*left*). White dashed lines illustrate the boundary of the shape of the tip which are to be stiffened with bioresorbable polymer. A first result after positioning and stiffening of the flexible tips on the device (*right*). (b) The flexible ECoG which is to be coated with bioresorbable polymer in between the black dashed lines. Inset: demonstration of the flexible nature of the device. With courtesy of C. Proctor for (a) and G.J. Dijk for (b).

Bibliography

[1] World Health Organization, Neurological disorders: Public health challenges. Chapter 2: Global burden of neurological disorders. Estimates and projections. World Health Organization, 2006.

[2] A. Verkhratsky, O. A. Krishtal, and O. H. Petersen, “From Galvani to patch clamp: the development of electrophysiology,” Pflüg. Arch. - Eur. J. Physiol., vol. 453, no. 3, pp. 233–247, Nov. 2006.

[3] S. P. Lacour, G. Courtine, and J. Guck, “Materials and technologies for soft implantable neuroprostheses,” Nat. Rev. Mater., vol. 1, no. 10, p. 16063, Sep. 2016.

[4] “The Meninges.” [Online]. Available: http://teachmeanatomy.info/neuro/structures/meninges/. [Accessed: 11-Oct-2017].

[5] “Blood-Brain Barrier Illustration Stanford.” [Online]. Available: http://web.stanford.edu/group/hopes/cgi-bin/hopes_test/wp-content/uploads/2015/09/Blood-Brain-Barrier-Picture-2-581x383.jpg. [Accessed: 11-Oct-2017].

[6] R. Chen, A. Canales, and P. Anikeeva, “Neural recording and modulation technologies,” Nat. Rev. Mater., vol. 2, no. 2, p. 16093, Jan. 2017.

[7] “Brain Basics: The Life and Death of a Neuron. National Institute of Neurological Disorders and Stroke.” [Online]. Available: https://www.ninds.nih.gov/Disorders/Patient-Caregiver-Education/Life-and-Death-Neuron. [Accessed: 11-Oct-2017].

[8] “Biopsychology: Sensory, Relay and Motor Neurons | tutor2u Psychology.” [Online]. Available: https://www.tutor2u.net/psychology/reference/biopsychology-sensory-relay-and-motor-neurons. [Accessed: 11-Oct-2017].

[9] “Action potential.” [Online]. Available: http://bio1152.nicerweb.com/Locked/media/ch48/action_potential.html. [Accessed: 11-Oct-2017].

[10] “Neurotransmitter. Encyclopedia Britannica.” [Online]. Available: https://www.britannica.com/science/neurotransmitter#ref784691. [Accessed: 11-Oct-2017].

[11] N. G. Hatsopoulos and J. P. Donoghue, “The Science of Neural Interface Systems,” Annu. Rev. Neurosci., vol. 32, no. 1, pp. 249–266, Jun. 2009.

[12] L. R. Hochberg et al., “Neuronal ensemble control of prosthetic devices by a human with tetraplegia.,” Nature, vol. 442, pp. 164–71, 2006.

[13] L. R. Hochberg et al., “Reach and grasp by people with tetraplegia using a neurally controlled robotic arm,” Nature, vol. 485, no. 7398, pp. 372–375, May 2012.

[14] J. P. Donoghue, “Bridging the Brain to the World: A Perspective on Neural Interface Systems,” Neuron, vol. 60, no. 3, pp. 511–521, Nov. 2008.

[15] M. E. J. Obien, K. Deligkaris, T. Bullmann, D. J. Bakkum, and U. Frey, “Revealing neuronal function through microelectrode array recordings,” Front. Neurosci., vol. 8, Jan. 2015.

[16] G. Buzsáki, C. A. Anastassiou, and C. Koch, “The origin of extracellular fields and currents — EEG, ECoG, LFP and spikes,” Nat. Rev. Neurosci., vol. 13, no. 6, pp. 407–420, May 2012.

[17] M. E. Spira and A. Hai, “Multi-electrode array technologies for neuroscience and cardiology,” Nat. Nanotechnol., vol. 8, no. 2, pp. 83–94, Feb. 2013.

[18] D. Khodagholy et al., “NeuroGrid: recording action potentials from the surface of the brain,” Nat. Neurosci., vol. 18, no. 2, pp. 310–315, Dec. 2014.

[19] M. Jorfi, J. L. Skousen, C. Weder, and J. R. Capadona, “Progress towards biocompatible intracortical microelectrodes for neural interfacing applications,” J Neural Eng, vol. 12, no. 1, p. 011001, Feb. 2015.

[20] A. Weltman, J. Yoo, and E. Meng, “Flexible, Penetrating Brain Probes Enabled by Advances in Polymer Microfabrication,” Micromachines, vol. 7, no. 10, p. 180, Oct. 2016.

[21] M. P. Ward, P. Rajdev, C. Ellison, and P. P. Irazoqui, “Toward a comparison of microelectrodes for acute and chronic recordings,” Brain Res., vol. 1282, pp. 183–200, Jul. 2009.
[22] K. A. Potter, A. C. Buck, W. K. Self, M. E. Callanan, S. Sunil, and J. R. Capadona, “The effect of resveratrol on neurodegeneration and blood brain barrier stability surrounding intracortical microelectrodes,” Biomaterials, vol. 34, no. 29, pp. 7001–7015, Sep. 2013.
[23] K. A. Potter, A. C. Buck, W. K. Self, and J. R. Capadona, “Stab injury and device implantation within the brain results in inversely multiphasic neuroinflammatory and neurodegenerative responses,” J. Neural Eng., vol. 9, no. 4, p. 046020, Aug. 2012.
[24] J. W. Jeong, G. Shin, S. I. Park, K. J. Yu, L. Xu, and J. A. Rogers, “Soft materials in neuroengineering for hard problems in neuroscience,” Neuron, vol. 86, no. 1, pp. 175–86, Apr. 2015.
[25] J. Subbaroyan, D. C. Martin, and D. R. Kipke, “A finite-element model of the mechanical effects of implantable microelectrodes in the cerebral cortex,” J Neural Eng, vol. 2, no. 4, pp. 103–13, Dec. 2005.
[26] A. Sridharan, S. D. Rajan, and J. Muthuswamy, “Long-term changes in the material properties of brain tissue at the implant-tissue interface,” J Neural Eng, vol. 10, no. 6, p. 066001, Dec. 2013.
[27] G. C. McConnell, H. D. Rees, A. I. Levey, C. A. Gutekunst, R. E. Gross, and R. V. Bellamkonda, “Implanted neural electrodes cause chronic, local inflammation that is correlated with local neurodegeneration.,” J Neural Eng, vol. 6, pp. 1741–2560, 2009.
[28] M. Lo et al., “Coating flexible probes with an ultra fast degrading polymer to aid in tissue insertion,” Biomed. Microdevices, vol. 17, no. 2, Apr. 2015.
[29] C. Tian and J. He, “Monitoring insertion force and electrode impedance during implantation of microwire electrodes,” Cortex, vol. 104, no. 24, pp. 44–4, 2005.
[30] M. Jeon et al., “Partially flexible MEMS neural probe composed of polyimide and sucrose gel for reducing brain damage during and after implantation,” J. Micromechanics Microengineering, vol. 24, no. 2, p. 025010, 2014.
[31] A. A. Sharp, A. M. Ortega, D. Restrepo, D. Curran-Everett, and K. Gall, “In vivo penetration mechanics and mechanical properties of mouse brain tissue at micrometer scales,” IEEE Trans Biomed Eng, vol. 56, no. 1, pp. 45–53, Jan. 2009.
[32] W. Jensen, U. G. Hofmann, and K. Yoshida, “Assessment of subdural insertion force of single-tine microelectrodes in rat cerebral cortex,” in Engineering in Medicine and Biology Society, 2003. Proceedings of the 25th Annual International Conference of the IEEE, 2003, vol. 3, pp. 2168–2171.
[33] N. H. Hosseini, R. Hoffmann, S. Kisban, T. Stieglitz, O. Paul, and P. Ruther, “Comparative study on the insertion behavior of cerebral microprobes,” in Engineering in Medicine and Biology Society, 2007. EMBS 2007. 29th Annual International Conference of the IEEE, 2007, pp. 4711–4714.
[34] J. Thelin et al., “Implant Size and Fixation Mode Strongly Influence Tissue Reactions in the CNS,” PLoS ONE, vol. 6, no. 1, p. e16267, Jan. 2011.
[35] S. R. Goldstein and M. Salcman, “Mechanical factors in the design of chronic recording intracortical microelectrodes,” Biomed. Eng. IEEE Trans. On, no. 4, pp. 260–269, 1973.
[36] W. Jensen, K. Yoshida, and U. G. Hofmann, “In-vivo implant mechanics of flexible, silicon-based ACREO microelectrode arrays in rat cerebral cortex,” IEEE Trans. Biomed. Eng., vol. 53, no. 5, pp. 934–940, May 2006.
[37] J. Muthuswamy, A. Gilletti, T. Jain, and M. Okandan, “Microactuated neural probes to compensate for brain micromotion,” in Engineering in Medicine and Biology Society, 2003. Proceedings of the 25th Annual International Conference of the IEEE, 2003, vol. 2, pp. 1941–1943.
[38] R. M. Owens and G. G. Malliaras, “Organic electronics at the interface with biology,” MRS Bull., vol. 35, no. 6, pp. 449–456, 2010.

[39] H. Shirakawa, E. J. Louis, A. G. MacDiarmid, C. K. Chiang, and A. J. Heeger, “Synthesis of electrically conducting organic polymers: Halogen derivatives of polyacetylene (CH)x.,” JCS Chem. Commun., 1977.
[40] B. Nordén and E. Krutmeijer, “Conductive polymers,” R. Swed. Acad. Sci. Nobel Prize Chem., 2000.
[41] K. Cobb, “The Dawn of Brain-Machine Interfaces. Biomedical Computation Review.” [Online]. Available: http://biomedicalcomputationreview.org/content/dawn-brain-machine-interfaces. [Accessed: 23-Oct-2017].
[42] X. Cui, J. F. Hetke, J. A. Wiler, D. J. Anderson, and D. C. Martin, “Electrochemical deposition and characterization of conducting polymer polypyrrole/PSS on multichannel neural probes,” Sens. Actuators Phys., vol. 93, no. 1, pp. 8–18, Aug. 2001.
[43] D.-H. Kim, M. Abidian, and D. C. Martin, “Conducting polymers grown in hydrogel scaffolds coated on neural prosthetic devices,” J. Biomed. Mater. Res., vol. 71A, no. 4, pp. 577–585, Dec. 2004.
[44] K. A. Ludwig, N. B. Langhals, M. D. Joseph, S. M. Richardson-Burns, J. L. Hendricks, and D. R. Kipke, “Poly(3,4-ethylenedioxythiophene) (PEDOT) polymer coatings facilitate smaller neural recording electrodes,” J Neural Eng, vol. 8, no. 1, p. 014001, Feb. 2011.
[45] P. G. Taylor et al., “Orthogonal Patterning of PEDOT:PSS for Organic Electronics using Hydrofluoroether Solvents,” Adv. Mater., vol. 21, no. 22, pp. 2314–2317, Jun. 2009.
[46] D. Khodagholy et al., “Highly conformable conducting polymer electrodes for in vivo recordings,” Adv Mater, vol. 23, no. 36, pp. H268–72, Sep. 2011.
[47] D. A. Koutsouras et al., “PEDOT:PSS microelectrode arrays for hippocampal cell culture electrophysiological recordings,” MRS Commun., vol. 7, no. 02, pp. 259–265, Jun. 2017.
[48] G. E. Loeb, M. J. Bak, M. Salcman, and E. M. Schmidt, “Parylene as a chronically stable, reproducible microelectrode insulator,” IEEE Trans. Biomed. Eng., no. 2, pp. 121–128, 1977.
[49] J. A. DeFranco, B. S. Schmidt, M. Lipson, and G. G. Malliaras, “Photolithographic patterning of organic electronic materials,” Org. Electron., vol. 7, no. 1, pp. 22–28, Feb. 2006.
[50] M. Sessolo et al., “Easy-to-fabricate conducting polymer microelectrode arrays,” Adv Mater, vol. 25, no. 15, pp. 2135–9, Apr. 2013.
[51] K. Fukuda et al., “Fully-printed high-performance organic thin-film transistors and circuitry on one-micron-thick polymer films,” Nat. Commun., vol. 5, Jun. 2014.
[52] B. A. Wester, R. H. Lee, and M. C. LaPlaca, “Development and characterization of in vivo flexible electrodes compatible with large tissue displacements,” J. Neural Eng., vol. 6, no. 2, p. 024002, Apr. 2009.
[53] S. Takeuchi, D. Ziegler, Y. Yoshida, K. Mabuchi, and T. Suzuki, “Parylene flexible neural probes integrated with microfluidic channels,” Lab Chip, vol. 5, no. 5, pp. 519–23, May 2005.
[54] A. Williamson et al., “Localized Neuron Stimulation with Organic Electrochemical Transistors on Delaminating Depth Probes,” Adv. Mater., vol. 27, no. 30, pp. 4405–4410, Aug. 2015.
[55] S. Venkatraman et al., “In Vitro and In Vivo Evaluation of PEDOT Microelectrodes for Neural Stimulation and Recording,” IEEE Trans. Neural Syst. Rehabil. Eng., vol. 19, no. 3, pp. 307–316, Jun. 2011.
[56] D. Martin and G. Malliaras, “Interfacing Electronic and Ionic Charge Transport in Bioelectronics,” ChemElectroChem, p. n/a–n/a, Jan. 2016.
[57] U. A. Aregueta-Robles, A. J. Woolley, L. A. Poole-Warren, N. H. Lovell, and R. A. Green, “Organic electrode coatings for next-generation neural interfaces,” Front Neuroeng, vol. 7, p. 15, 2014.
[58] J. Rivnay et al., “Structural control of mixed ionic and electronic transport in conducting polymers,” Nat. Commun., vol. 7, p. 11287, Apr. 2016.
[59] E. M. Thaning, M. L. M. Asplund, T. A. Nyberg, O. W. Inganäs, and H. von Holst, “Stability of poly(3,4-ethylene dioxythiophene) materials intended for implants,” J. Biomed. Mater. Res. B Appl. Biomater., vol. 93B, no. 2, pp. 407–415, May 2010.

[60] R. A. Green et al., “Substrate dependent stability of conducting polymer coatings on medical electrodes,” Biomaterials, vol. 33, no. 25, pp. 5875–5886, Sep. 2012.
[61] D. A. Koutsouras, P. Gkoupidenis, C. Stolz, V. Subramanian, G. G. Malliaras, and D. C. Martin, “Impedance Spectroscopy of Spin-Cast and Electrochemically Deposited PEDOT:PSS Films on Microfabricated Electrodes with Various Areas,” ChemElectroChem, vol. 4, no. 9, pp. 2321–2327, Sep. 2017.
[62] X. Cui and D. C. Martin, “Electrochemical deposition and characterization of poly(3,4-ethylenedioxythiophene) on neural microelectrode arrays,” Sens. Actuators B Chem., vol. 89, no. 1–2, pp. 92–102, Mar. 2003.
[63] S. Zhang, P. Kumar, A. S. Nouas, L. Fontaine, H. Tang, and F. Cicoira, “Solvent-induced changes in PEDOT:PSS films for organic electrochemical transistors,” APL Mater., vol. 3, no. 1, p. 014911, Jan. 2015.
[64] J. Rivnay et al., “High-performance transistors for bioelectronics through tuning of channel thickness,” Sci. Adv., vol. 1, no. 4, pp. e1400251–e1400251, May 2015.
[65] C. M. Proctor, J. Rivnay, and G. G. Malliaras, “Understanding volumetric capacitance in conducting polymers,” J. Polym. Sci. Part B Polym. Phys., vol. 54, no. 15, pp. 1433–1436, Aug. 2016.
[66] F. Santoro et al., “Revealing the Cell–Material Interface with Nanometer Resolution by Focused Ion Beam/Scanning Electron Microscopy,” ACS Nano, Jul. 2017.
[67] A. R. Harris, P. J. Molino, R. M. I. Kapsa, G. M. Clark, A. G. Paolini, and G. G. Wallace, “Correlation of the impedance and effective electrode area of doped PEDOT modified electrodes for brain–machine interfaces,” The Analyst, vol. 140, no. 9, pp. 3164–3174, 2015.
[68] M. J. Yim and K. P. Paik, “Design and Understanding of anisotropic Conductive Films (ACF’s) for LCD Packaging,” IEEE Trans. Compon. Packag. Manuf. Technol., vol. 21 (2), 1998.
[69] A. D. Gilmour, A. J. Woolley, L. A. Poole-Warren, C. E. Thomson, and R. A. Green, “A critical review of cell culture strategies for modelling intracortical brain implant material reactions,” Biomaterials, vol. 91, pp. 23–43, Jun. 2016.
[70] J. Pine, “Recording action potentials from cultures neurons with extracellular microcircuit electrodes,” Journal of Neuroscience Methods, pp. 19–31, 1980.
[71] R. Kim, S. Joo, H. Jung, N. Hong, and Y. Nam, “Recent trends in microelectrode array technology for in vitro neural interface platform,” Biomed. Eng. Lett., vol. 4, no. 2, pp. 129–141, Jun. 2014.
[72] Y. Furukawa, A. Shimada, K. Kato, H. Iwata, and K. Torimitsu, “Monitoring neural stem cell differentiation using PEDOT–PSS based MEA,” Biochim. Biophys. Acta BBA - Gen. Subj., vol. 1830, no. 9, pp. 4329–4333, Sep. 2013.
[73] G. Buzsáki, “Large-scale recording of neuronal ensembles,” Nat. Neurosci., vol. 7, no. 5, pp. 446–451, May 2004.
[74] Y. Nam and B. C. Wheeler, “In vitro microelectrode array technology and neural recordings,” Crit. Rev. Biomed. Eng., vol. 39, no. 1, 2011.
[75] Y. Nam and B. C. Wheeler, “Imaging locations of neurons vs. glia in low density culture,” in Neural Engineering, 2005. Conference Proceedings. 2nd International IEEE EMBS Conference on, 2005, pp. 325–327.
[76] S. B. Achour and O. Pascual, “Astrocyte–Neuron Communication: Functional Consequences,” Neurochem. Res., vol. 37, no. 11, pp. 2464–2473, Nov. 2012.
[77] B. C. Wheeler and G. J. Brewer, “Designing Neural Networks in Culture,” Proc. IEEE, vol. 98, no. 3, pp. 398–406, Mar. 2010.
[78] W. L. C. Rutten, T. G. Ruardij, E. Marani, and B. H. Roelofsen, “Cultured neural networks: Optimization of patterned network adhesiveness and characterization of their neural activity,” Appl. Bionics Biomech., vol. 3, no. 1, pp. 1–7, Jan. 2006.
[79] A. Blau, “Cell adhesion promotion strategies for signal transduction enhancement in microelectrode array in vitro electrophysiology: An introductory overview and critical discussion,” Curr. Opin. Colloid Interface Sci., vol. 18, no. 5, pp. 481–492, Oct. 2013.

[80] S. M. Ojovan et al., “Nanocrystalline diamond surfaces for adhesion and growth of primary neurons, conflicting results and rational explanation,” Front. Neuroengineering, vol. 7, Jun. 2014.
[81] S. G. Turney and P. C. Bridgman, “Laminin stimulates and guides axonal outgrowth via growth cone myosin II activity,” Nat. Neurosci., vol. 8, pp. 717 – 719, 2005.
[82] G. J. Brewer, T. T. Jones, M. D. Boehler, and B. C. Wheeler, “NbActiv4 medium improvement to Neurobasal/B27 increases neuron synapse densities and network spike rates on multielectrode arrays,” J. Neurosci. Methods, vol. 170, no. 2, pp. 181–187, May 2008.
[83] L. Hazan, M. Zugaro, and G. Buzsáki, “Klusters, NeuroScope, NDManager: A free software suite for neurophysiological data processing and visualization,” J. Neurosci. Methods, vol. 155, no. 2, pp. 207–216, Sep. 2006.
[84] R. Quian Quiroga, “Spike sorting,” Scholarpedia, vol. 2, no. 12, p. 3583, 2007.
[85] K. D. Harris, D. A. Henze, J. Csicsvari, H. Hirase, and G. Buzsáki, “Accuracy of tetrode spike separation as determined by simultaneous intracellular and extracellular measurements,” J. Neurophysiol., vol. 84, no. 1, pp. 401–414, 2000.
[86] G. Buzsáki et al., “Tools for Probing Local Circuits: High-Density Silicon Probes Combined with Optogenetics,” Neuron, vol. 86, no. 1, pp. 92–105, Apr. 2015.
[87] L. Hoelting et al., “A 3-dimensional human embryonic stem cell (hESC)-derived model to detect developmental neurotoxicity of nanoparticles,” Arch. Toxicol., vol. 87, no. 4, pp. 721–733, Apr. 2013.
[88] K. Okita, M. Kato-Negishi, H. Onoe, and S. Takeuchi, “Neurospheroid array on a flexible substrate for cortical microstimulation,” in Micro Electro Mechanical Systems (MEMS), 2013 IEEE 26th International Conference on, 2013, pp. 221–224.
[89] M. Mayer, B. Müller, S. Kadereit, S. Ritter, and C. Thielemann, “Human neurospheres on microelectrode arrays: a model to investigate ionizing radiation effects on neuronal network communication.”
[90] M. Frega, M. Tedesco, P. Massobrio, M. Pesce, and S. Martinoia, “Network dynamics of 3D engineered neuronal cultures: a new experimental model for in-vitro electrophysiology,” Sci. Rep., vol. 4, no. 1, May 2015.
[91] J. L. Bourke et al., “Three-dimensional neural cultures produce networks that mimic native brain activity,” J. Tissue Eng. Regen. Med., Jul. 2017.
[92] X. M. Ma and J. Elisseeff, Scaffolding In Tissue Engineering. CRC Press, 2005.
[93] Y. Wang, G. T. Salazar, J.-H. Pai, H. Shadpour, C. E. Sims, and N. L. Allbritton, “Micropallet arrays with poly(ethylene glycol) walls,” Lab. Chip, vol. 8, no. 5, p. 734, 2008.
[94] Y. Gao, J. Broussard, A. Haque, A. Revzin, and T. Lin, “Functional imaging of neuron?astrocyte interactions in a compartmentalized microfluidic device,” Microsyst. Nanoeng., vol. 2, p. 15045, Feb. 2016.
[95] E. K. er U. Larsen, M. B. L. Mikkelsen, and N. B. Larsen, “Protein and cell patterning in closed polymer channels by photoimmobilizing proteins on photografted poly (ethylene glycol) diacrylate,” Biomicrofluidics, vol. 8, no. 6, p. 064127, 2014.
[96] M. Peter and P. Tayalia, “An alternative technique for patterning cells on poly(ethylene glycol) diacrylate hydrogels,” RSC Adv, vol. 6, no. 47, pp. 40878–40885, 2016.
[97] P. Bartho, H. Hirase, L. Monconduit, M. Zugaro, K. D. Harris, and G. Buzsáki, “Characterization of Neocortical Principal Cells and Interneurons by Network Interactions and Extracellular Features,” J. Neurophysiol., vol. 92, no. 1, pp. 600–608, Mar. 2004.
[98] D. H. Kim et al., “Silicon electronics on silk as a path to bioresorbable, implantable devices,” Appl Phys Lett, vol. 95, no. 13, p. 133701, Sep. 2009.
[99] S. W. Hwang et al., “A physically transient form of silicon electronics with integrated sensors, actuators and power supply,” Science, vol. 337, no. 6102, pp. 1640–4, Sep. 2012.
[100] S. Felix et al., “Removable silicon insertion stiffeners for neural probes using polyethylene glycol as a biodissolvable adhesive.,” Conf Proc IEEE Eng Med Biol Soc, 2012.

[101] J. Liu et al., “Syringe-injectable electronics,” Nat. Nanotechnol., vol. 10, no. 7, pp. 629–636, Jun. 2015.
[102] L. Luan et al., “Ultraflexible nanoelectronic probes form reliable, glial scar–free neural integration,” Sci. Adv., vol. 3, no. 2, p. e1601966, 2017.
[103] B. D. Ulery, L. S. Nair, and C. T. Laurencin, “Biomedical applications of biodegradable polymers,” J. Polym. Sci. Part B Polym. Phys., vol. 49, no. 12, pp. 832–864, Jun. 2011.
[104] D. Y. Kwon et al., “Biodegradable stent,” J. Biomed. Sci. Eng., vol. 05, no. 04, pp. 208–216, 2012.
[105] H. K. Makadia and S. J. Siegel, “Poly Lactic-co-Glycolic Acid (PLGA) as Biodegradable Controlled Drug Delivery Carrier,” Polymers, vol. 3, no. 4, pp. 1377–1397, Aug. 2011.
[106] L. S. Nair and C. T. Laurencin, “Biodegradable polymers as biomaterials,” Prog. Polym. Sci., vol. 32, no. 8–9, pp. 762–798, 2007.
[107] A. Lecomte et al., “Silk and PEG as means to stiffen a parylene probe for insertion in the brain: toward a double time-scale tool for local drug delivery,” J. Micromechanics Microengineering, vol. 25, no. 12, p. 125003, Dec. 2015.
[108] F. Wu, L. W. Tien, F. Chen, J. D. Berke, D. L. Kaplan, and E. Yoon, “Silk-Backed Structural Optimization of high density flexible intracortical neural probes - from Javier,” J. Microelectromechanical Syst., vol. 24, no. 1, 2015.
[109] Y. Wang et al., “In vivo degradation of three-dimensional silk fibroin scaffolds,” Biomaterials, vol. 29, no. 24–25, pp. 3415–3428, Aug. 2008.
[110] S.-K. Kang et al., “Bioresorbable silicon electronic sensors for the brain,” Nature, Jan. 2016.
[111] F. Wu, M. Im, and E. Yoon, “A flexible fish-bone-shaped neural probe strengthened by biodegradable silk coating for enhanced biocompatibility,” in Solid-State Sensors, Actuators and Microsystems Conference (TRANSDUCERS), 2011 16th International, 2011, pp. 966–969.
[112] P. J. Gilgunn et al., “An ultra-compliant, scalable neural probe with molded biodissolvable delivery vehicle,” in Micro electro mechanical systems (MEMS), 2012 IEEE 25th international conference on, 2012, pp. 56–59.
[113] Z. Xiang et al., “Ultra-thin flexible polyimide neural probe embedded in a dissolvable maltose-coated microneedle,” J. Micromechanics Microengineering, vol. 24, no. 6, p. 065015, Jun. 2014.
[114] J. Agorelius, F. Tsanakalis, A. Friberg, P. T. Thorbergsson, L. M. E. Pettersson, and J. Schouenborg, “An array of highly flexible electrodes with a tailored configuration locked by gelatin during implantation—initial evaluation in cortex cerebri of awake rats,” Front. Neurosci., vol. 9, Sep. 2015.
[115] J. P. Harris et al., “In vivo deployment of mechanically adaptive nanocomposites for intracortical microelectrodes,” J Neural Eng, vol. 8, no. 4, p. 046010, Aug. 2011.
[116] J. K. Nguyen et al., “Influence of resveratrol release on the tissue response to mechanically adaptive cortical implants,” Acta Biomater., vol. 29, pp. 81–93, Jan. 2016.
[117] E. A. Kamoun, X. Chen, M. S. Mohy Eldin, and E.-R. S. Kenawy, “Crosslinked poly(vinyl alcohol) hydrogels for wound dressing applications: A review of remarkably blended polymers,” Arab. J. Chem., vol. 8, no. 1, pp. 1–14, Jan. 2015.
[118] N. Ben Halima, “Poly(vinyl alcohol): review of its promising applications and insights into biodegradation,” RSC Adv, vol. 6, no. 46, pp. 39823–39832, 2016.
[119] P. Pajak, M. Ziemski, and B. Nowak, “Poly(vinyl alcohol) - biodegradable vinyl material,” Chemik, vol. 64, pp. 523–530, 2010.
[120] L. L. Razumova, A. A. Veretennikova, G. Y. Zaikov, and L. A. Vol’f, “Degradation of polyvinyl alcohol surgical thread,” Polym. Sci. USSR, vol. 25, no. 10, pp. 2418–2425, 1983.
[121] A. Hasan, Tissue Engineering for Artificial Organs. 2017.
[122] K. Yamaura, M. Tada, T. Tanigami, and S. Matsuzawa, “Mechanical properties of films of poly (vinyl alcohol) derived from vinyl trifluoroacetate,” J. Appl. Polym. Sci., vol. 31, no. 2, pp. 493–500, 1986.

[123] srinath Muppalaneni, “Polyvinyl Alcohol in Medicine and Pharmacy: A Perspective,” J. Dev. Drugs, vol. 02, no. 03, 2013.
[124] T. Yamaoka, Y. Tabata, and Y. Ikada, “Comparison of Body Distribution of Poly (vinyl alcohol) with Other Water-soluble Polymers after Intravenous Administration,” J. Pharm. Pharmacol., vol. 47, no. 6, pp. 479–486, 1995.
[125] N. A. Peppas, “Turbidimetric studies of aqueous poly (vinyl alcohol) solutions,” Macromol. Chem. Phys., vol. 176, no. 11, pp. 3433–3440, 1975.
[126] M. C. Lo et al., “Coating flexible probes with an ultra fast degrading polymer to aid in tissue insertion,” Biomed Microdevices, vol. 17, no. 2, p. 34, Apr. 2015.
[127] C. A. Van Blitterswijk and J. De Boer, Tissue Engineering, 2nd ed. Elsevier, 2015.
[128] A. Hai et al., “Spine-shaped gold protrusions improve the adherence and electrical coupling of neurons with the surface of micro-electronic devices,” J. R. Soc. Interface, vol. 6, no. 41, pp. 1153–1165, Dec. 2009.
[129] A. Hai, J. Shappir, and M. E. Spira, “In-cell recordings by extracellular microelectrodes,” Nat. Methods, vol. 7, no. 3, pp. 200–202, Mar. 2010.
[130] W. Tonomura, K. Shimizu, and S. Konishi, “Electrophysiological recordings using spatially arranged microelectrode probes embedded into 3-D neuronal cultures,” Proc MicroTAS2010, pp. 265–267, 2010.

Scientific contributions

The work described in this thesis resulted in publications listed here below. Within our *Bioelectronics Department*, research is performed with a multidisciplinary team and PhD candidates are involved in many more projects than described in their thesis manuscript. For this reason, a short description is added to the co-author papers to which the PhD candidate contributed.

Presented work in manuscript

Neurospheres on patterned PEDOT:PSS microelectrode arrays enhance electrophysiology recordings. J. Pas, C. Pitsalidis, D.A. Koutsouras, P. Quilichini, F. Santoro, B. Cui, L. Gallais, R.P. O'Connor, G.G. Malliaras and R.M. Owens (2017) *Adv. Biosystems.* DOI: 10.1002/adbi.201700164.

A PVA/PLGA bioresorbable shuttle for implantation of flexible depth probes into the mice brain. J. Pas, A. Rutz, A. Slezia , A. Williamson, A. Kaszas, P. Quilichini, A. Ghestem, M. Donahue, V. Curto, C. Bernard and G.G. Malliaras (paper in preparation, October 2017).

Other scientific contributions

Polyelectrolyte Layer-by-Layer Assembly on Organic Electrochemical Transistors. A.M. Pappa, S. Inal, K. Roy, Y. Zhang, C. Pitsalidis, A. Hama, J. Pas, G.G. Malliaras and R.M. Owens *(2017) ACS Appl. Mater. Interfaces*, 9 (12), pp 10427–10434.

Abstract Oppositely charged polyelectrolyte multilayers (PEMs) were built up in a layer-by-layer (LbL) assembly on top of the conducting polymer channel of an organic electrochemical transistor (OECT), aiming to combine the advantages of well-established PEMs with a high performance electronic transducer. The multilayered film is a model system to investigate the impact of bio-functionalization on the operation of OECTs comprising a poly(3,4-ethylenedioxythiophene) polystyrenesulfonate (PEDOT:PSS) film as the electrically active layer. Understanding the mechanism of ion injection into the channel that is in direct contact with charged polymer films provides useful insights for novel biosensing applications such as nucleic acid sensing. Moreover, LbL is demonstrated to be a

versatile electrode modification tool enabling tailored surface features in terms of thickness, softness, roughness, and charge. LbL assemblies built up on top of conducting polymers will aid the design of new bioelectronic platforms for drug delivery, tissue engineering, and medical diagnostics.

PEDOT:PSS Microelectrode Arrays for Hippocampal Cell Culture Electrophysiological Recordings. *D.A.* Koutsouras, A. Hama, J. Pas, P. Gkoupidenis, B. Hivert, C. Faivre-Sarrailh, E.Di Pasquale, R.M. Owens, and G.G. Malliaras (2017) *MRS Communications*, 7 , pp 259 – 265.

Abstract In vitro electrophysiology using microelectrode arrays (MEAs) plays an important role in understanding fundamental biologic processes, screening potential drugs and assessing the toxicity of chemicals. Low electrode impedance and ability to sustain viable cultures are the key technology requirements. We show that MEAs consisting of poly(3,4-ethylenedioxythiophene) doped with poly(styrene sulfonate) (PEDOT:PSS) and coated with poly-L-lysine satisfy these requirements. Hippocampal cell cultures, maintained for 3 – 6 weeks on these MEAs, give high quality recordings of neural activity. This enables the observation of drug-induced activity changes, which paves the way for using these devices in in vitro drug screening and toxicology applications.

Infrared neural stimulation induces intracellular Ca2+ release mediated by phospholipase C. D. Moreau, C. Lefort, J. Pas, S.M. Bardet, P. Leveque, R.P. O'Connor (2017) *Journal of Biophotonics* [Epub]. DOI: 10.1002/jbio.201700020

Abstract Nanosecond pulsed electric fields (nsPEFs) have a variety of applications in the biomedical and biotechnology industries. Cancer treatment has been at the forefront of investigations thus far as nsPEFs permeabilize cellular and intracellular membranes leading to apoptosis and necrosis. nsPEFs may also influence ion channel gating and have the potential to modulate cell physiology without poration of the membrane. This phenomenon was explored using live cell imaging and a sensitive fluorescent probe of transmembrane voltage in the human glioblastoma cell line, U87 MG, known to express a number of voltage-gated ion channels. The specific ion channels involved in the nsPEF response were screened using a membrane potential imaging approach and a combination of pharmacological antagonists and ion substitutions. It was found that a single 10ns pulsed electric field of 34 kV/cm depolarizes the transmembrane potential of cells by acting on specific voltage-sensitive ion channels; namely the voltage and Ca2+ gated BK potassium channel, L- and T-type calcium channels, and the TRPM8 transient receptor potential channel.

Acknowledgments

This is it! This is a gathering of all the work I have done in these last three years in the Bioelectronics Department at the Centre Microelectronique de Provence (CMP). It has been a good experience to learn about microfabrication and the (practical) challenges that come along with them, but it was an even great experience to get to know so many people along the way. The work would not have been the same, and definitely not as much fun, without all the people involved in the science and in my daily life at CMP. I would like to thank everyone involved during my PhD time for making this an unforgettable time, each and everyone of you in their own special kind of way. I would not be the person I am now if you were missing. So, I take my time here to thank people in particular and to put some memorable moments on paper.

First, I would like to thank my family, my dad, mother, brother and twin sister. I would have not achieved this without the never ending support of my parents. They gave me a "work hard for it, and you will succeed" attitude. I loved learning about science. Ever since I was young, I enjoyed doing my homework, solving mathematical equations, learning all about the wonders of biology and how chemistry can explain so many things around us. That has brought me to do my research during my Master studies in the lab of Prof. Bert Meijer and Prof. Stephanie Lacour, and now during my PhD in the lab of Prof. George Malliaras. I have been surrounded by great scientists and am very thankful for all the opportunities they have offered me.

George, thank you for making me part of the BEL family. It was a great experience doing research in such a multidisciplinary field with such a diverse team. We were a very international group here in the South of France, had a lot of fun and grew very close. I loved starting my day hearing people chit chatting in the morning in the kitchen. Although I would not always stick around long, I enjoyed having a coffee before going into the lab, talking about food, about the beautiful places in the Provence, the fun skiing in Austria or anywhere else in the world where you allowed us to go for conference. At the end, we would hear you say: "Life is good!" or "Paper…?! CAAAAAKE!!". These were great moments! I would also like to thank you, George and also Roisin, for the mental support you have provided me. You were very kind, open and supportive and put me as a person first, instead of the research. Thank you!

Then, my fellow PhD students and post-docs, you made the lab a special place to hang out!

Let's start with the sunshine in the lab, our Isabel, or lovely Isabellita. You definitely made me laugh with all your funny or provocative comments. You amaze me how you can always get away with it. I guess it's that big smile on your face and the fact that you mean no harm, you just like to tease people. You make work fun! Plus, we had some 'true-happiness' times

with all those tortilla's, jamon's, lasagna's and wines. Thank you for being such a great friend and colleague!

Anna-Maria, you were my PhD-year mate! Remember that you immediately asked me to go to the gym together? That didn't work, but I can really enjoy how you would try to stimulate yourself to do some exercise. You did great! Plus, you showed character when we went hiking up in Parc Mercantour. I really enjoyed our rides to work in the mornings from Aix. Although you are not an early bird, you really did an effort for being on time. I really adored our chats and will miss the 'Ghellooo!' in the mornings. Your managing skills amaze me and I'm sure you will be using them where ever you end up. Good luck! The conference time with you in Boston and the trip in Greece was unforgettable fun. I hope we get to have such a great time again when we work for some fancy business later.

Dear Sahika, it was already in the early years of my research here but we did spent some unforgettable time together. Of course, the shared car rides to work together with Anna-Maria, the shopping for a wedding dress in Aix and Marseille, the many (home-cooked) dinners in Aix, the conferences and trips like MRS in Boston and New York, BioEl in Austria and probably so many more. You were a great friend and I hope that the distance and switch to industry will not create too much of a gap. Good luck with your academic career, I wish you all the best!

Shahab, it was a pleasure to share the office with you. We also started our PhD around the same time, which felt good to not be the only one in that situation. You are a very kind person, greeting everyone in the morning and asking them how they are. Thank you for leaving me in peace when you noticed I was having a bad day and thank you for the interesting chats at the desk.

Thomas, you are such a nice guy and a pleasure to work with. You are helpful and calm, but also enthousiastic at the same time. You always ran up the stairs, and although you said you didn't do that anymore, it is still in you, that fire and wanting to get things done. Thank you for being a great friend and for all the beach-volley ball fun at plage du Prophete in Marseille!

Marcel, it took some time to get to know you. Although we didn't really work together, I appreciated your German approach of having rules. You stuck to them and reminded others of them. That really improved the working space, so thank you! Keep up with the funny and weird jokes, I finally start understanding them. I'm looking forward to working with you in Panaxium next year.

Ilke, dude!! You are a lazy French citizen, but committed to your work and a kind and patient colleague. You are always up for a beer (or Pastis) and became a good friend. Thank you for being around! I hope to still visit you in New York. Have you found a bar that can replace SELECT and have "Pastisssss!", yet?

Dimitris, let's face it: we had a tough time working together. But I do appreciate you spending time to fabricate devices for the cell culture. Plus, we did have some fun times with our Olimpia collegues in Milan, San Sebastian and Bologna.

Magali, my biologist PhD friend in the lab. It was good having you around to discuss a bit on the cell cultures and the problems in the lab. I know it was not easy for you as I was surely somewhat negative about the (southern) French attitude I felt confronted with. But I did get to see many good things as well and am happy I can stay even longer to appreciate it more. Good luck with your research!

Mahmoudy, you are a kind and ambitious guy and I truly hope you succeed with your new business. We didn't get to work together, but you did become my office mate at the end of our PhD. I enjoyed sharing our frustrations and concerns and was glad to see a relieved man after your defense. Stay positive and keep it up. You are smart and know what you want, so do it!

Maryyyyy! You rock, thank you for being so awesome and for opening up these last years. I enjoy discussing about fabrication and projects, but I loved even more playing soccer, beer brewing and drinking at SELECT. Man, you can play and drink! I look very much forward to some more of the fun and hanging out together here in the south.

Bengyyy and Viviiiii. Vincenzo and Viviana. Pappà e mamma. Dear friends. I cannot tell you how much you have meant for me. You are so loving and caring and I am very thankful for all the good times together. Remember the first boat trip to Île Frioul, the picnic at the parc in Marseille, the beach-volleyball games, the lovely dinners and amazing sundried tomatoes,… There is so much to name. You are great and I am so thrilled to got to know your little Nicolo (sorry, French keybord, it doesn't have the required accent on the o). He is soooo beautiful and will grow to be a French/English Italian stallion. I really hope we keep in touch!

Chris, or how I like to call you, Mr. Proctor. You astonished me with your social network that you have built up here. I am very happy we got to do a decent hike in the Parc Queyras and that we had some good BBQ times in Marseille. Keep up the science and the fun, you have a great balance for this!

Babis, together with Anna-Maria you are such a great and funny couple. I was happy for you that you finally succeeded to work in our lab. You were very bussy with all the projects you had started and it was tough getting a hang on you. I really enjoyed the time outside the lab, the fun evenings together with all of us, having delicious dinners or drinks at LeNovo. Or the time that you guided us through Thessaloniki and the island of Skopolos. Man, thank you, that was amazing.

Donatiiii, girl, I hope to talk to you in a few years and hear that you have found your goal in life. You are a wonderful lady with great Italian (vegetarian) cooking skills and much love to give. I really enjoyed the chatting and sharing and the rare but fun times hanging out. Thank

you for being my friend. I hope that we can keep up the occasional chillin' out, even with you being in Cambridge!

Loig, je suis super contente que tu m'as toujours parlé en Français. Ça m'as aidé à améliorer et d'aussi apprécier la langue. Je vais comme même m'engager encore plus dans les années qui viennent et j'espère que tu resteras au sud pour encore profiter de la vie dans le Provence!

Alex (Alexandra), you were a great support to me the last year of my research. I appreciate your help on every aspect, the experiments, the writing, the sharing of experiences in academia, the fun evenings in Marseille and so much more. It's too bad we didn't get to hike together, but I'm sure we can still plan a beautiful trip with Gerwin and Mayo in the Alps. Let's do it!

And Rod (Rodney), thank you for your energy and sharing your passion to do science and find a cure for cancer. I truly hope you will manage to find your way and I'm looking forward to work with you if possible.

There were many more people in our lab and building who I'd like to also briefly name. Jon and Liza, thanks for the delicious dinners and fun evenings. Adel, thank you for your advice on the biology. Pierre and Bahar, thank you for both sharing your knowledge and experiences. I'm looking forward to work with you in the near future! Esma, it must not be easy to be a mum and scientist at the same time. Good luck! Usein, I hope you make it happen here in France. Eloise, it wasn't easy but we survived. I really wish you all the best! Aimie, I look forward to working more together in the future. Ana Sanchez, what about the lasagna times?! David Ohayon, thanks for walking me (great hikes on Sundays!). Bastien, Severine and other FEL people, thanks for the soccer and fun game nights. Agnes and Louise, merci pour les chouettes temps parlent en Néerlandais. J'ai adoré les cours Néerlandais. Gaelle, Thierry, Jessica et tout le team du Salle Blanche, merci pour votre aide et votre gentillesse! Richard, Melodie, Gracien, Johanna et Aurelie, Michelle, Anaïs et Veronique, un grand merci pour votre patience avec moi, la petite Belge. Ça m'as fait beaucoup de plaisir!

I would also like to thank the teams in Latimone in Marseille under the supervision of Chistophe Bernards. They helped me with all the animal experiments, which were not as easy as initially thought.

Pascale and Antoine, merci pour les expériences combiner avec Ilke, Loig ou toute seule. Il y a encore beaucoup à faire, comme vous avez vu, ce n'est malheureusement pas du tout si simple que ça se ressemble. Mais j'ai fait mon meilleur pour y avancé. Merci pour m'avoir forcer de bien analyser les résultats.

Adam, Andrea and Atilla, it was a real pleasure to work with you. You were very helpful and kind and you stood up for me. I enjoyed the many stories you told, Adam and will never

forget the jumping-on-the-chair scene during one of your talks. You do have a special way of presenting, it's entertaining!

The most important person I have kept for the end to thank. Gerwin, my lovely man, ik ben jou zo erg dankbaar voor alle steun en liefde die je me hebt gegeven tijdens mijn onderzoek. You stood by me and kept me together while I was either loving or hating the science. I am very grateful for your positive attitude and your faith in me and my research. You made me feel more confident, less useless and … you made me laugh when I needed it! I feel like I can handle so much more with you by my side, personally and professionally. You are amazing, I could not have done this without you. Thank you with all my heart!

Gardanne, October 2017

Jolien Pas